

# TECHNISCHE UNIVERSITÄT MÜNCHEN

## Lehrstuhl für Humanbiologie

Molecular and proteomic analysis of signaling pathways in  
pancreatic ductal adenocarcinoma using genetically  
engineered mouse models

Barbara Maria Grüner

Vollständiger Abdruck der von der Fakultät Wissenschaftszentrum Weihenstephan für Ernährung, Landnutzung und Umwelt der Technischen Universität München zur Erlangung des akademischen Grades eines

Doktors der Naturwissenschaften

genehmigten Dissertation.

Vorsitzender: Univ.-Prof. Dr. M. Klingenspor

Prüfer der Dissertation: 1. Univ.-Prof. Dr. M. Schemann  
2. Priv.-Doz. Dr. J. T. Siveke  
3. Univ.-Prof. Angelika Schnieke, PhD

Die Dissertation wurde am 03.04.2012 bei der Technischen Universität München eingereicht und durch die Fakultät Wissenschaftszentrum Weihenstephan für Ernährung, Landnutzung und Umwelt am 05.07.2012 angenommen.

## Zusammenfassung

Ziel dieser Arbeit war es verschiedene Aspekte des duktales Adenokarzinoms des Pankreas (PDAC) hinsichtlich Diagnose, Therapie und Entstehung mit Hilfe genetisch veränderter Mausmodelle (GEM) zu untersuchen. PDAC ist eine fatale Erkrankung mit einer sehr geringen medianen Überlebenszeit und einer sehr hohen Sterblichkeitsrate. Dies ist hauptsächlich der sehr späten Diagnose, der sehr frühen Metastasierung und der hohen intrinsischen Resistenz gegen jegliche Chemotherapie zuzuschreiben. Mittels gut etablierter endogener Mausmodelle können alle Stadien des PDAC – frühe präneoplastische Läsionen ebenso wie Karzinome im Endstadium – zu definierten Zeitpunkten untersucht werden.

Im ersten Projekt dieser Arbeit wurden GEM mittels bildgebender Massenspektrometrie (MALDI IMS) untersucht um die mögliche Anwendung zur Detektion potentieller Biomarker für frühere Diagnose und dadurch erhöhte Überlebenschancen der Patienten zu evaluieren. MALDI IMS ermöglicht die markierungsfreie proteomische Analyse von Gewebe in räumlicher Auflösung mit gleichzeitigem Erhalt der morphologischen Information. Pankreasgewebeschnitte von GEM zu verschiedenen Zeitpunkten der Tumorgenese mit präneoplastischen Läsionen ebenso wie Wildtyp- oder Tumorgewebe wurden mittels MALDI IMS gemessen und eine Vielzahl differentiell exprimierter *m/z* Spezies detektiert. Zwei dieser Spezies konnten mittels Flüssigchromatographie und Tandem-Massenspektrometrie identifiziert werden. Die Expression von murinem Serum Albumin (ALB1) wurde durch Western Blot Analyse und Immunhistochemie verifiziert und konnte mit der hepatischen Transdifferenzierung von PDAC Gewebe assoziiert werden. Thymosin beta 4 (TMSB4X) Expression war in pankreatischen intraepithelialen Neoplasien (PanIN) und PDAC erhöht, ebenso wie in Serum von Pankreastumormäusen im Vergleich zu Serum von Wildtypmäusen. Beide Proteine stellen zwar aufgrund ihrer hohen Abundanz keine geeigneten Kandidaten für potentielle Biomarker dar, aber die vorliegenden Resultate und die neuartige Verknüpfung von GEM mit MALDI IMS in einer komplexen Studie

zeigen die prinzipielle Anwendbarkeit von MALDI IMS an GEM zur Untersuchung des Proteoms/Peptidoms von Tumorgewebe.

Im zweiten Projekt dieser Arbeit wurde MALDI IMS benutzt um die Zugänglichkeit und Verteilung von Erlotinib, einem Tyrosinkinase-Inhibitor des epidermalen Wachstumsfaktorrezeptors (EGFR) und dem zur Zeit einzigen zugelassenen Inhibitor für zielgerichtete Therapie des PDAC, im Pankreaskarzinom zu untersuchen. Erlotinib wurde Pankreaskarzinommäusen einmalig oral verabreicht und seine Verteilung sowie die Verteilung seines aktiven Metaboliten wurden mittels MALDI IMS in Pankreasgewebeschnitten gemessen. Beide Massen hatten ihre höchste relative Intensität eine Stunde nach oraler Gabe in Wildtypmäusen und diese war in PDAC Gewebe signifikant niedriger. Die Verteilung und relative Intensität in Tumorregionen korrelierte nicht mit dem prozentualen Anteil CD31-positiver Blutgefäße im Tumor. Stattdessen konnte eine signifikant positive Korrelation der relativen Intensität des aktiven Metaboliten mit dem Anteil duktaler Strukturen oder dem Anteil Ki67-positiver proliferativer Zellen im Tumor festgestellt werden.

Im dritten und wichtigsten Projekt der Arbeit wurde schließlich die Rolle des EGFR während der Entstehung des PDAC im gut-etablierten *Kras*<sup>G12D</sup> Mausmodell untersucht und charakterisiert. Onkogenes KRAS erhöht die Expression und Aktivierung von EGFR. Genetische Ablation oder pharmakologische Inhibierung des EGFR eliminiert effektiv die KRAS-induzierte Tumorgenese *in vivo*, wobei EGFR Aktivität für die Entstehung transformations-sensitiver metaplastischer Gangstrukturen notwendig ist. Zusätzlich ist EGFR für das hohe Aktivitätslevel von ERK verantwortlich, das wiederum unerlässlich für die Tumorgenese des Pankreas, vor allem für die Transdifferenzierung von azinären zu dukталen Zellen, ist. Dies konnte auch im Kontext Pankreatitis-induzierter PanIN Entstehung in *Kras*<sup>G12D</sup> Mäusen bestätigt werden. Diese kontroversen Ergebnisse tragen dazu bei, dass sich die Sichtweise auf lineare Signalwege in der Tumorgenese ändert. Ein konstitutiv aktives Onkogen lässt die Präsenz und Aktivierung eines vorangeschalteten Rezeptors nicht redundant werden. Dies mag dazu beitragen bestehende Therapien zu verbessern und neue Wege in der Tumorthherapie zu eröffnen.

Parts of this thesis were submitted for publication:

**Gruener B.M.**, H. Hahne, P.K. Mazur, M. Trajkovic-Arsic, S. Maier, I. Esposito, C.W. Michalski, J. Kleeff, S. Rauser, R.M. Schmid, B. Kuester, A. Walch, and J.T. Siveke, *MALDI imaging mass spectrometry for in situ proteomic analysis of preneoplastic lesions in pancreatic cancer*. PLoS One. 2012;7(6):e39424.

Ardito C.M\*., **B.M. Gruener\***, C. Lubeseder-Martellato, K.K. Takeuchi, K.E. DelGiorno, E.S. Carpenter, C.J. Halbrook, D. Pal, J.C. Hall, P.K. Mazur, T. Briel, A. Herner, D.W. Threadgill, M. Sibilias, M.K. Washington, C.L. Wilson, R.M. Schmid, E.W. Raines, H.C. Crawford, and J.T. Siveke, *EGF Receptor is Required for Kras-induced Pancreatic Tumorigenesis*. Cancer Cell 2012, <http://dx.doi.org/10.1016/j.ccr.2012.07.024>

*\*both authors contributed equally to this work*

*to my Parents*

*für meine Eltern*

## Table of contents

1	Introduction .....	11
1.1	The Pancreas.....	11
1.1.1	Anatomy and physiology .....	11
1.1.2	Development of the pancreas.....	12
1.2	Pancreatitis and pancreatic cancer .....	13
1.2.1	Acute Pancreatitis.....	14
1.2.2	Chronic pancreatitis.....	14
1.2.3	Pancreatic cancer.....	15
1.2.4	Therapy of pancreatic cancer .....	18
1.2.5	Models of pancreatic cancer.....	19
1.2.6	Signaling pathways in pancreatic cancer.....	23
1.3	The epidermal growth factor receptor (EGFR) .....	27
1.3.1	ERBB family members .....	27
1.3.2	EGFR ligands .....	29
1.3.3	EGFR activation and degradation.....	31
1.3.4	EGFR signaling pathways and its biological function .....	33
1.3.5	EGFR signaling in pancreatic cancer and targeted chemotherapy.....	37
1.4	MALDI IMS.....	40
1.5	Aim of this thesis.....	44
2	Materials and Methods.....	45
2.1	Mice .....	45
2.1.1	Induction of acute pancreatitis in <i>Kras</i> <sup>G12D</sup> mice .....	45
2.1.2	Treatment with BAY 86-9766 .....	46
2.1.3	Treatment of <i>Kras</i> <sup>G12D</sup> ; <i>p53</i> <sup>KO</sup> mice with cetuximab or erlotinib.....	46
2.1.4	Treatment of <i>WT</i> and <i>Kras</i> <sup>G12D</sup> ; <i>p53</i> <sup>KO</sup> mice with erlotinib for MALDI Drug Imaging.....	46
2.2	Histological analyses.....	46

2.2.1	Production of FFPE-tissue samples .....	46
2.2.2	Paraffin sections .....	47
2.2.3	H&E .....	47
2.2.4	Immunohistochemistry.....	47
2.2.5	Immunofluorescence .....	48
2.2.6	Histological quantification .....	49
2.2.7	Statistical analyses of histological quantifications and pancreas to body weight ratios.....	49
2.3	RNA/DNA analyses.....	49
2.3.1	DNA Isolation from mouse tails for genotyping.....	49
2.3.2	Genotyping PCR.....	50
2.3.3	RNA Isolation.....	50
2.3.4	cDNA Synthesis.....	51
2.3.5	Quantitative RT-PCR.....	51
2.3.6	Extraction of pancreatic DNA from FFPE-blocks.....	51
2.3.7	<i>Kras</i> and <i>Egfr</i> deleted PCR .....	52
2.4	Proteinbiochemistry.....	52
2.4.1	Isolation of protein from cells or tissue .....	52
2.4.2	Protein concentration determination .....	53
2.4.3	SDS polyacrylamide gel electrophoresis (SDS PAGE) and Western Blot .....	53
2.4.4	Ras and Rac activity assays.....	55
2.4.5	Immunoprecipitation .....	56
2.4.6	ELISA - Enzyme linked immunosorbent assay - for TMSB4X .....	56
2.5	Cell culture .....	57
2.5.1	Isolation and culture of primary murine tumor cell lines from the pancreas.....	57

2.5.2	Treatment of <i>Kras</i> <sup>G12D</sup> ; <i>p53</i> <sup>KO</sup> and <i>Kras</i> <sup>G12D</sup> ; <i>p53</i> <sup>KO</sup> ; <i>Egfr</i> <sup>KO</sup> cell lines with EGF.....	57
2.5.3	Isolation and culture of acinar epithelial explants .....	58
2.5.4	Quantitation of ductal transdifferentiation of acinar epithelial explants .....	59
2.5.5	Immunofluorescence of acinar epithelial explants .....	59
2.6	Matrix-assisted laser desorption/ionization Imaging mass spectrometry (MALDI-IMS) .....	60
2.6.1	MALDI-IMS on tissue sections from mouse pancreata.....	60
2.6.2	Statistical analysis of MALDI-IMS data.....	60
2.6.3	Peptide and protein identification by liquid chromatography and tandem mass spectrometry (LC-MS/MS) .....	61
2.7	Drug Imaging with MALDI-IMS.....	62
2.7.1	Measurement of erlotinib on pancreatic sections .....	62
2.7.2	Statistical analysis of drug imaging data.....	63
3	Results.....	65
3.1	MALDI imaging mass spectrometry for <i>in situ</i> proteomic analysis of preneoplastic lesions in pancreatic cancer.....	65
3.1.1	MALDI-IMS is a specific method to analyze sections from murine pancreata .....	65
3.1.2	Detection of specific discriminating <i>m/z</i> -species for pancreatic lesions and cancer.....	66
3.1.3	<i>m/z</i> -species 2790, 2812 and 2829 are specifically found in PanIN lesions .....	69
3.1.4	Validation of significant discriminating peaks in an independent sample set .....	72
3.1.5	Protein identification of the three most significant species by LC-MS/MS.....	72
3.1.6	Validation of identified candidates .....	73



3.1.7	ALB1 expression is associated with hepatic transdifferentiation of the pancreas during carcinogenesis .....	74
3.1.8	TMSB4X is specifically upregulated in the murine pancreas during PDAC development .....	76
3.2	Analysis of erlotinib distribution in PDAC <i>in vivo</i> .....	78
3.2.1	Determination of time point for highest drug concentration .....	78
3.2.2	Erlotinib levels are higher in healthy than in tumor bearing pancreatic compartments .....	79
3.2.3	Correlation of relative mass intensity with percentage of CD31-positive vessels in the tumor .....	81
3.2.4	Correlation of mass intensity, proliferation rate and tumor differentiation .....	82
3.3	EGFR is essential for RAS-driven pancreatic carcinogenesis .....	85
3.3.1	EGFR pathway upregulation precedes tumorigenesis in <i>Kras<sup>G12D</sup></i> mice .....	85
3.3.2	EGFR activity is required for pancreatic tumorigenesis .....	87
3.3.3	Pancreatitis-associated tumorigenesis requires EGFR .....	90
3.3.4	EGFR activity is required for the formation of metaplastic ducts ..	91
3.3.5	RAS activity levels and localization are not altered in <i>Kras<sup>G12D</sup>;Egfr<sup>KO</sup></i> pancreata .....	94
3.3.6	EGFR-dependent ERK activation is required for pancreatic tumorigenesis .....	95
4	Discussion .....	101
4.1	MALDI imaging mass spectrometry for <i>in situ</i> proteomic analysis of preneoplastic lesions in pancreatic cancer .....	101
4.2	Analysis of erlotinib distribution in PDAC <i>in vivo</i> .....	106
4.3	EGFR is essential for RAS-driven pancreatic carcinogenesis .....	112
5	Summary .....	116
6	References .....	118
7	Supplementary material .....	133
7.1.1	Supplementary Tables 7-1 to 7-12 .....	133

7.1.2	Annotated MS/MS spectra supporting the identification of ALB1 and TMSB4X.....	148
7.1.3	Sequence coverage of ALB1 and TMSB4X.....	151
8	Appendix.....	152
8.1	List of abbreviations .....	152
8.2	Curriculum vitae .....	154
8.3	Acknowledgements - Danksagungen.....	156

# 1 Introduction

## 1.1 The Pancreas

### 1.1.1 Anatomy and physiology

The pancreas consists of two functionally different compartments, which are spatially not separated but constitute in parallel. First, the exocrine compartment which makes up for up to 90 % of the pancreas. This compartment is comprised of the acinar cells that secrete digestive enzymes and are arranged in buds ending into the ducts. Ducts secrete bicarbonate and mucins and carry the digestive enzymes secreted from the acini to the duodenum. The second compartment is the endocrine that consists of five different cell types: glucagon-secreting  $\alpha$ -cells, insulin-secreting  $\beta$ -cells, somatostatin-releasing  $\delta$ -cells, ghrelin-producing  $\epsilon$ -cells, and the pancreatic polypeptide-secreting PP-cells, which all together group into islets, the islets of Langerhans. The produced hormones are all participating in the regulation of glucose homeostasis and nutrient metabolism. The pancreas is located in the abdomen cavity, between duodenum (pancreatic head) and spleen (tail) [1-3].

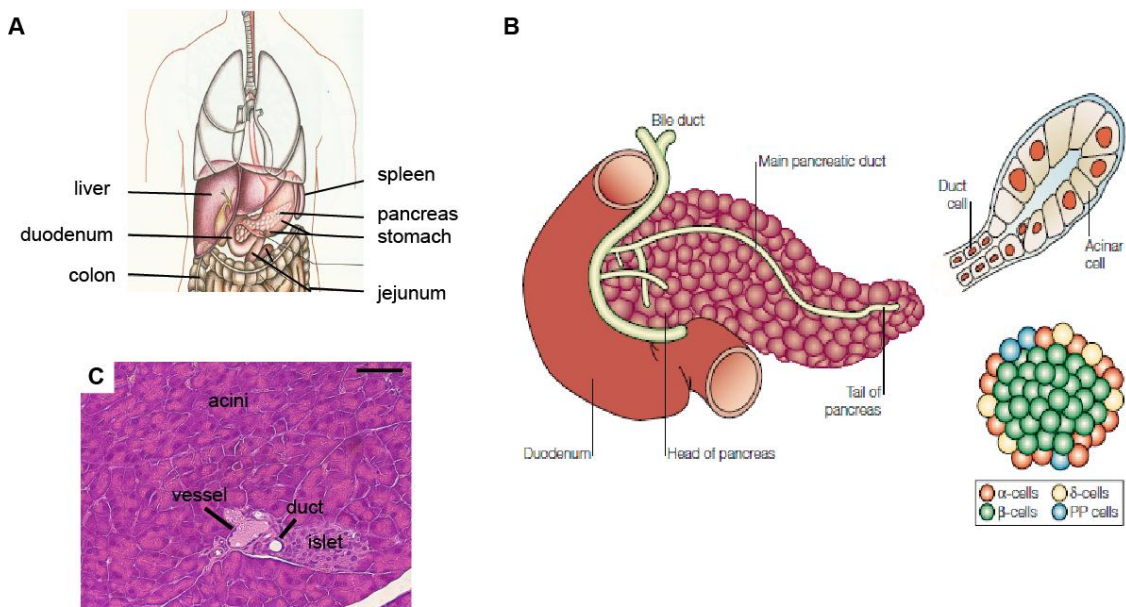


**Figure 1-1**

**Macroscopy of the pancreas.** (A) The pancreas is located in the abdomen cavity between duodenum and spleen behind stomach and liver. Adapted from Rohen and Lütjen-Drecoll [3].

(B) Gross anatomy and morphological elements of the pancreas [2] (C) Histological morphology of the mouse wild type pancreas. Scale bar equals 50  $\mu\text{m}$ .

### 1.1.2 Development of the pancreas

All cells of the pancreas, endocrine and exocrine, arise from a common field of cells in the primitive gut tube of the embryo. The pancreatic anlage forms and proliferates between embryonic day (E) 8.5 and E 11.5 in mice and the majority of cells at this stage express the transcription factors Pdx1, Sox9, Ptf1a, Hnf1b, Hes1 and Nkx6. At around E 10.5, a subset of these progenitors also starts to express carboxypeptidase A1 and Ngn3, two markers that are later associated with pre-acinar and pre-endocrine domains, respectively. Starting at around E 12.5, the pancreatic epithelium is progressively compartmentalized into “tip” and “trunk” domains, a process that, upon completion, results in the lineage restriction of tip progenitors to an acinar fate and trunk progenitors to an endocrine/ductal fate. Between E 14.5 and E 18.5 the embryonic pancreas produces hormones and forms acinar cells, the islets emerge after birth [1, 2, 4].

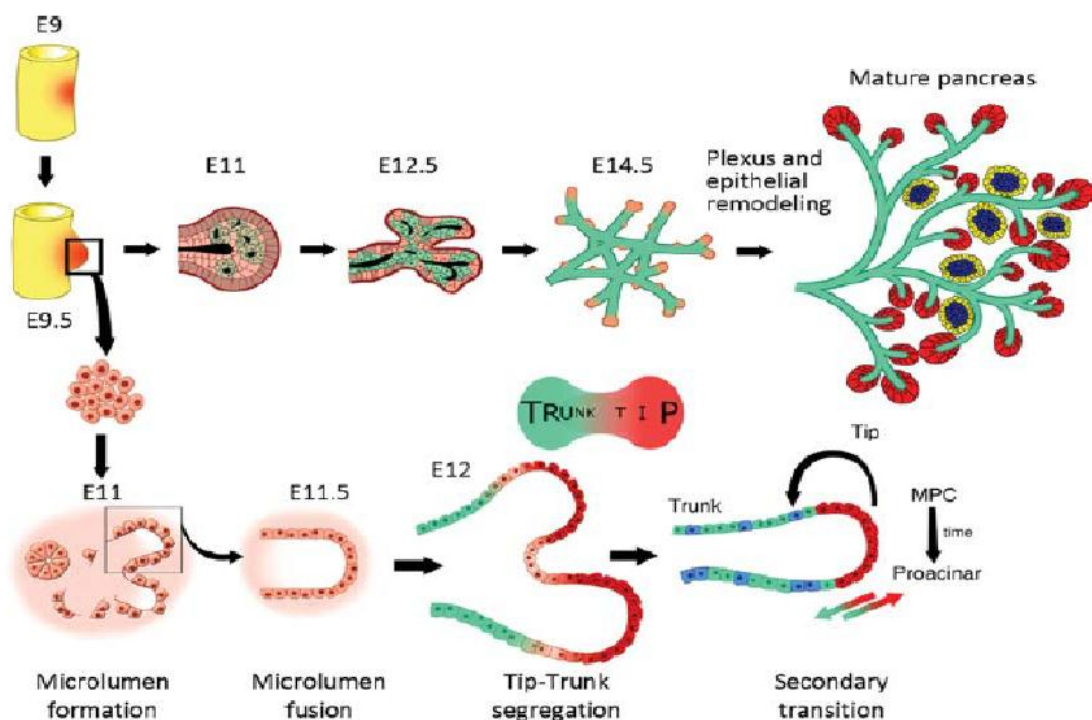


**Figure 1-2**  
**Overview of pancreatic development in the mouse.** Adapted from Pan and Wright 2011 [1].

As already mentioned several transcription factors and signaling molecules regulate and determine pancreatic development and differentiation. Among them are family members of the Hedgehog pathway, the bone morphogenetic proteins and transforming growth factor  $\beta$ , the Wnt and Notch pathways, the nuclear factor  $\kappa$ B and the G-protein coupled and tyrosines kinase domain receptors and ligands. Especially important of the transcription factors are Pdx1 and Ptf1a /p48, both expressed in the pancreatic progenitor cells that give rise to all mature pancreatic cell types [1, 2, 4].

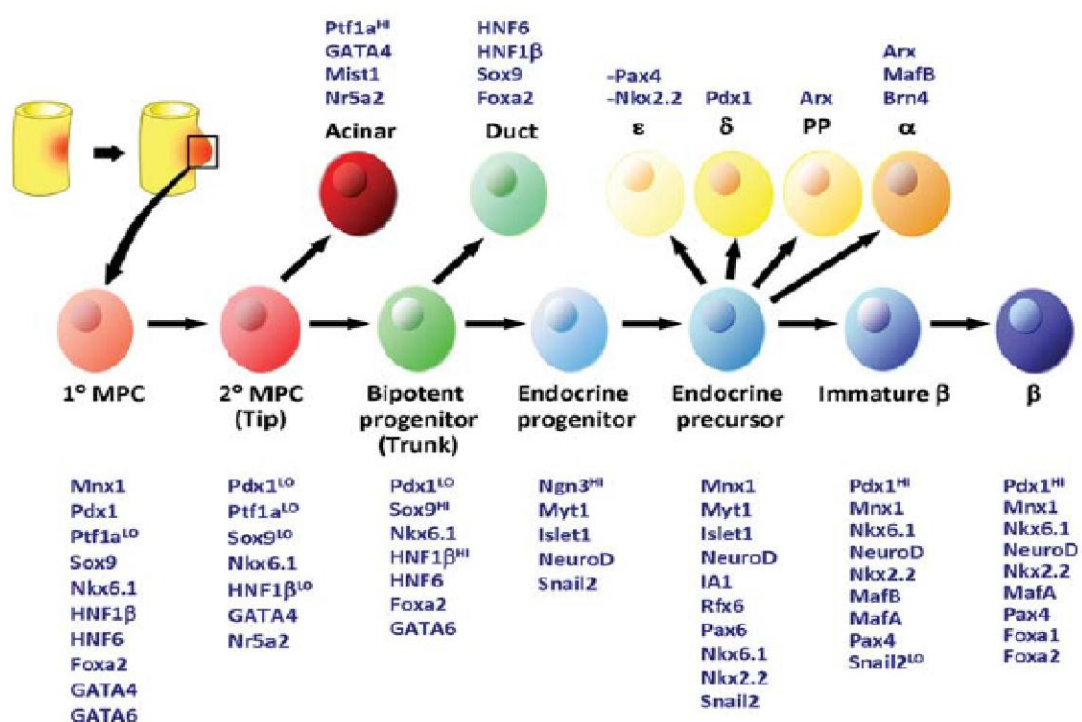


**Figure 1-3**

**Overview of transcription factors involved in pancreatic development.** – indicates absence of the factor being important. Adapted from Pan and Wright 2011 [1].

## 1.2 Pancreatitis and pancreatic cancer

The pancreas can suffer from multiple diseases of the exocrine and endocrine compartments. In the endocrine pancreas diabetes mellitus type I and type II are certainly among the most common widespread diseases. Cancer can originate from both endocrine and exocrine cells and acute and chronic pancreatitis are affecting mostly the exocrine part.

### **1.2.1 Acute Pancreatitis**

There are many potential causes of acute pancreatitis, the two major ones being gallstones and alcohol. Symptoms include severe pain in the upper abdomen, nausea and vomiting, obstipation and fever. To study the disease in detail the cerulein-hyperstimulation model is commonly used. In this model acute pancreatitis is induced upon repeated injections of the cholecystokinin analog cerulein that induces secretion of pancreatic enzymes and depending on the dose and schedule used, can cause either acute or mild forms of pancreatitis [5, 6]. The molecular mechanisms underlying the disease include disruption of the acinar cell plasma membrane, elevated cAMP levels that enhance the secretion of active digestive enzymes, inflammation and endoplasmic reticulum stress-CHOP (CCAAT/enhancer binding protein homologous protein) pathway activation that accelerates pancreatitis through induction of inflammation-linked caspases [7]. The pancreas possesses a great ability to restore its function after severe acute pancreatitis, but the recovery mechanisms are poorly understood. Siveke and colleagues for example could show that cellular regeneration was impaired in Notch compromised animals [8].

### **1.2.2 Chronic pancreatitis**

Chronic pancreatitis is characterized by chronic inflammation, progressive fibrosis, pain and loss of exocrine and endocrine function. Pancreatic stellate cells play a key role in pancreatic fibrosis because they produce reactive oxygen species that modulate their activation and the subsequent deposition of extracellular matrix, leading to pancreatic fibrosis [9]. Also increased infiltration of mononuclear cells may be a cause for inflammation and fibrosis. Alcohol abuse, genetic, host or environmental factors are thought to be responsible for development of chronic pancreatitis. Currently two experimental mouse models of chronic pancreatitis exist, being combinations of alcohol feeding, cerulein and cyclosporine or bacterial endotoxin LPS administration, but it is not clear if they can resemble the features of chronic pancreatitis sufficiently. For a review on chronic pancreatitis refer to Thrower and colleagues [7].

Both acute [10] and chronic [11] pancreatitis can contribute to and enhance the development of pancreatic cancer .

### **1.2.3 Pancreatic cancer**

Pancreatic neoplasias can probably arise from virtually all cell compartments of the pancreas and are classified upon cellular lineage and the histology they recapitulate. These include besides the most common pancreatic ductal adenocarcinoma (PDAC), endocrine neoplasms, acinar cell carcinoma, cystic serous and mucinous neoplasms, solid pseudopapillary tumors, squamous cell carcinoma, pancreatic lymphoma and metastatic lesions of the pancreas [12]. The most common pancreatic cancers are presented in the following.

#### **1.2.3.1 Acinar Cancers**

Acinar cell carcinomas (ACC) account for less than 1 % of pancreatic cancers and show a pure acinar phenotype. They are cell-rich, have an abundant cytoplasm and only rarely show desmoplasia. ACC stain positive for pancreatic enzymes such as trypsin, chymotrypsin, amylase or lipase. Unlike typical pancreatic adenocarcinoma the genetic mutations in *Kras*, *p53* and *Smad* are only rarely detected but alterations in the adenomatous polyposis coli- $\beta$ -catenin pathway were found [12].

#### **1.2.3.2 Endocrine neoplasms**

Pancreatic endocrine tumors constitute 1 to 2 % of pancreatic tumors. They are usually classified according to the hormones they produce, for example insulinomas, gastrinomas, VIPomas or glucagonomas. Morphologically they are solid and recapitulate in shape pancreatic islets. The tumors are associated with several inherited syndromes, including multiple endocrine neoplasia type I (MEN-1) and von Hippel Lindau disease (vHL) [12].

#### **1.2.3.3 Pancreatic ductal adenocarcinoma**

Pancreatic ductal adenocarcinoma (PDAC) is the fourth leading cause of cancer deaths in the western world although it is only the 10<sup>th</sup> cancer cause [13]. This high lethality with a median survival of less than 6 months and a 5-year survival

rate of < 4 % is due to its late detection, early metastasis and its high intrinsic resistance to chemotherapy. This fatal diagnosis has basically not changed during the last 20 years [13] despite great efforts in research and drug development and increasing knowledge of the cancer's underlying mechanisms. To date, the only opportunity for improved survival is complete surgical resection for those with localized disease. However, this is only achievable for < 15 % of patients [14]. Differential diagnosis of PDAC is challenging and chronic pancreatitis often bears ductal lesions that resemble PDAC precursors. The striking feature of PDAC is an extensive desmoplastic reaction with ubiquitous fibrosis and inflammation. The majority of PDAC is well-differentiated with a glandular pattern that resembles duct-like structures and a strong fibrotic reaction, called desmoplasia. But also undifferentiated PDACs with a more uniform cell mass are common and have an even worse prognosis due to increased aggressiveness. PDAC can develop via different types of preneoplastic lesions although the cell of origin is unknown. Recent and growing evidence using mouse genetic *in vivo* experiments suggest that epithelial cells of the pancreatic ducts and acinar cells that undergo acinar-to ductal metaplasia (ADM) are most likely to be the origin of these lesions and PDAC [15-17]. Figure 1-4 depicts a schematic for the different cells of origin and their route to PDAC.

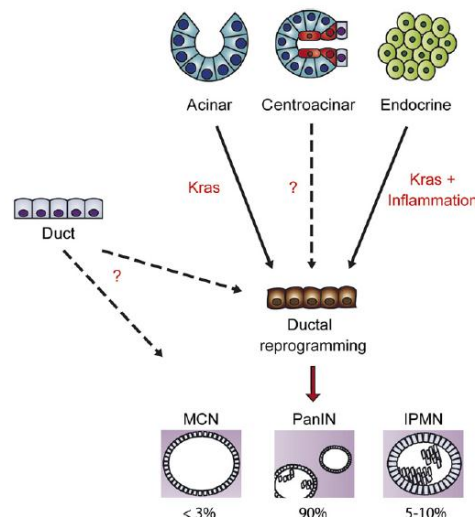


**Figure 1-4**  
**Cells of origin of PDAC.** Adapted from Mazur and Siveke 2011 [16].



#### 1.2.3.4 Preneoplastic pancreatic lesions

There are three major types of pancreatic precursor lesions to PDAC: Pancreatic intraepithelial neoplasias (PanIN), intraductal mucinous cystic neoplasms (IPMN) and mucinous cystic neoplasms (MCN).

PanINs are the most common precursor lesion type and are subclassified into PanIN1A, PanIN1B, PanIN2 and PanIN3 with increasing nuclear and architectural abnormalities, abnormal mitoses and so called “bridging” of cells into the lumen during their progression to high grade PanIN3. Whereas PanIN1 are frequently found in histological specimens from pancreatic surgeries, PanIN3 can be detected in only less than 5 % of preneoplastic pancreata implicating that high grade PanINs are indeed precursor lesions of PDAC. Also PanIN stages correlated with increasing mutation frequency and variety. 15-40 % of PanIN1 possess mutated KRAS but have only very rarely mutations in p53 or SMAD4, whereas PanIN3 most likely have both oncogenic KRAS and mutations in p53, SMAD4 and BRCA2. PanINs can be clearly detected upon staining for the marker mucin5.

IPMNs and MCNs are both cystic lesions, less frequent and therefore less well characterized than PanINs, although IPMNs are increasingly detected in the clinic due to improvements in diagnostic imaging modalities. IPMNs have mucin producing papillary epithelial cells filling the lumen and are classified into gastric, intestinal, pancreatobiliary and oncocytic types according to morphology and mucin subtype (MUC1, MUC2, MUC5AC) expression. MCNs consist of multilocular mucin filled cysts encircled by columnar epithelial cells, which are surrounded by an ovarian-like stroma, which expresses progesterone and estrogen receptors. Figure 1-5 depicts the different preneoplastic lesions and PDAC. The molecular mechanisms underlying PDAC development and several models to study PDAC are discussed in the following chapters.

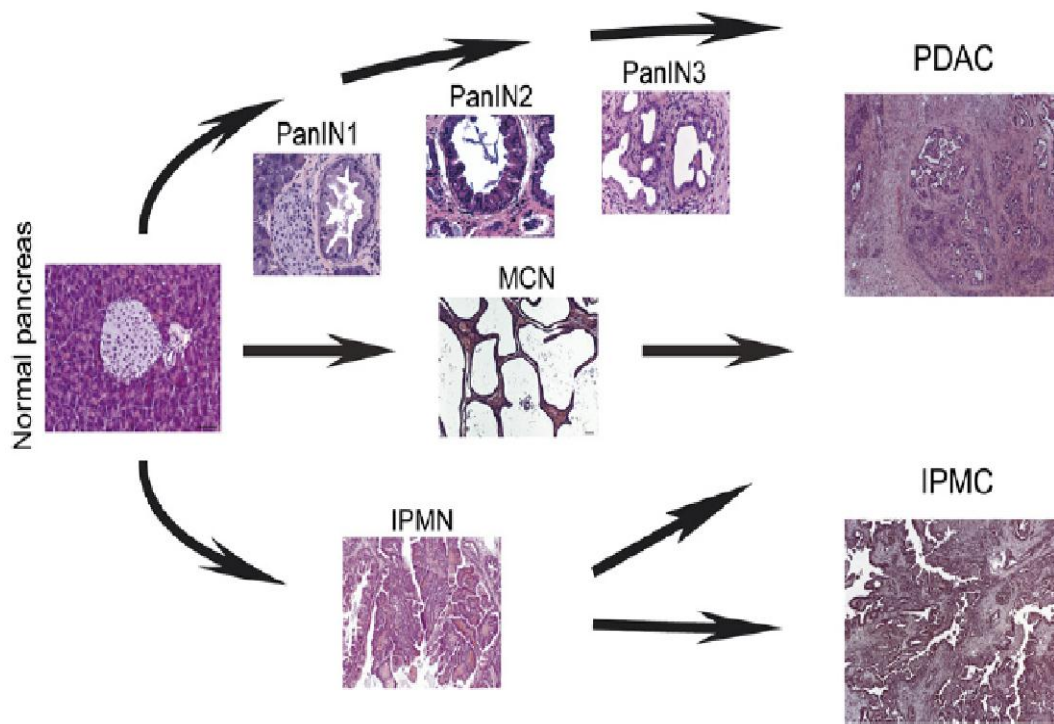


**Figure 1-5**  
**Pancreatic preneoplastic lesions.** Adapted from Mazur and Siveke 2011 [16].

#### 1.2.4 Therapy of pancreatic cancer

PDAC is a very fatal disease not least because of the barely successful therapy options available for patients. In only less than 15 % of patients complete resection is possible, and only those have an increased opportunity for survival. The median survival for those patients is 17 months. In the majority of patients, however, the tumor is too far progressed or has already metastasized upon diagnosis so that adjuvant therapy with gemcitabine remains the only option. Gemcitabine is an analog of the pyrimidine cytosine and has a cytostatic effect because it can replace the nucleoside cytosine in the DNA upon replication and therefore cause cell deaths. But gemcitabine therapy has a response rate of only 24 % and the median survival under gemcitabine treatment is 5.9 months. Due to the improved understandings of the molecular mechanisms underlying PDAC development numerous targeted chemotherapies are currently in clinical trials, among them inhibitors of Hedgehog and Notch signaling, VEGF-inhibitors and last but not least several inhibitors of tyrosine kinase receptor signaling

family members including Ras, Raf, Mek, PI3K and Egfr. Erlotinib, a small molecule tyrosine kinase domain inhibitor specifically blocking the epidermal growth factor receptor (EGFR) is to date the only approved targeted therapy for PDAC. It increases the overall median survival slightly but significantly to 6.3 months, although a subgroup of patients that develop rash grade 2 as a side effect have a median survival rate of 10.8 months [18]. For a review on targeted therapeutic approaches in pancreatic cancer please refer to Yeh and Der 2007 [19], for the molecular mechanisms underlying these approaches please also refer to the chapters 1.2.6 and 1.3.

### **1.2.5 Models of pancreatic cancer**

Because of the need for developing and evaluating new therapies for PDAC and to study the molecular mechanisms leading to pancreatic cancer several model systems are developed and in use. Pancreatic cancer cell lines, xenograft and genetically engineered mouse models are employed depending on the specific requirements of the studies. Especially genetically engineered mice (GEM) have tremendously contributed to our understanding of PDAC development and provide promising, predictive study platforms for the evaluation and development of new PDAC therapies.

#### **1.2.5.1 Pancreatic cancer cell lines**

Cell lines in culture offer an excellent alternative to *in vivo* models since they are easily accessible and easy to cultivate. They allow short-term *in vitro* studies of therapy responses and evaluation of genetic backgrounds of the tumor. Also for mechanistic and functional studies established pancreatic cancer cell lines are suited. Several cell lines are established and well characterized regarding histology, genetic mutations and source. Examples are listed in Table 1-1. On the other hand, pancreatic cancer cell lines as a model system to study PDAC have several disadvantages. They are isolated cells, sometimes in culture over years and decades and therefore resembling only a clonal subpopulation of the original tumor, not reflecting the full spectrum of genetic alterations and signaling mechanisms. Also, not only tumor cells themselves determine the

reactions and mechanisms taking place in a solid tumors but also the microenvironment consisting of stromal, inflammatory and vascular cells. This, however, cannot be addressed in cell line studies [20, 21].

**Table 1-1**  
**Examples of established pancreatic cancer cell lines, their source, genetic and histological background.** Adapted from Melstrom and Grippo 2008 [20].

Cell line	Source	Genetic mutations	Histology and grade
AsPC-1	Ascites	<i>Kras, p53, p16</i>	PDAC, G2/G3
BxPC-3	Primary tumor	<i>p53, p16, Smad4</i>	PDAC, G2/G3
CaPan-1	Liver metastasis	<i>Kras, p53, p16, Smad4</i>	PDAC, G1
CaPan-2	Primary tumor	<i>Kras, p16, Smad4</i>	PDAC, G1
MiaPaCa-2	Primary tumor	<i>Kras, p53, p16</i>	PDAC, G3
Panc-1	Primary tumor	<i>Kras, p53, p16</i>	PDAC, G3
Panc89	Lymph node met.	<i>p53, p16</i>	PDAC, G2
PancTu-1	Primary tumor	<i>Kras, p53, p16</i>	PDAC, G3
Pt45P1	Primary tumor	<i>Kras, p53, p16</i>	PDAC, G3

#### 1.2.5.2 Xenograft models

Xenogeneic cell transplantation, generally under the skin (subcutaneous) or to the pancreas (orthotopic) of immunodeficient mice is a very popular model to study pancreatic cancer in a semi-natural environment that resemble at least in part some aspects of cancer microenvironment including invasion or angiogenesis and tissue context of tumor growth. For a detailed review on xenograft models see Grippo and Sandgren 2005 [22].

#### 1.2.5.3 Genetically engineered mouse models

In the past years identification of the molecular and morphological basics of pancreatic cancer and essential findings in the field of genetic engineering techniques have allowed to develop sophisticated endogenous mouse models for pancreatic cancer. Genetically engineered mouse models do not only mimic end-stage PDAC but resemble the development of preneoplastic lesions including changes of the microenvironment, the desmoplastic reaction and the change in vascularization. Most conditional GEM are based on the *Cre/loxP* system, where the bacteriophage P1 derived *Cre* recombinase is expressed cell lineage restricted under the control of a specific promotor. The CRE enzyme can specifically excise DNA sequences that are flanked and therefore

recognized by *loxP* sites, short (34 bp) DNA repeats. The two most commonly used Cre GEM in pancreatic cancer research are the transgenic *Pdx1-Cre* mouse or a gene targeting endogenous construct, the *Ptf1a*<sup>+Cre</sup> model. In the first model *Cre* is expressed under the control of the *Pdx1* promoter and therefore in all pancreatic progenitor lineages. Since the model is transgenic it does not affect the endogenous *Pdx1* gene expression or function. *Cre* expression is mosaic, not affecting all pancreatic cells, and recent research has shown that *Pdx1* is also expressed in the suprabasal layers of the skin [23]. In the *Ptf1a*<sup>+Cre</sup> model *Cre* is expressed in all cells of the developing pancreas. On allele of the endogenous *Ptf1a* gene is replaced by the *Cre* gene sequence that is expressed under the control of the endogenous *Ptf1a* promoter. Therefore these mice are per se haploinsufficient for *Ptf1a*. In this model CRE is active in almost all cells of the developing pancreas, but *Ptf1a* is also expressed in the nervous system including brain, spine and retina [24].

The first attempt in the development for PDAC GEM was achieved with the *Ela-Tgfa* model by Sandgren and colleagues [25]. This transgenic mouse expresses the epidermal growth factor receptor (EGFR) ligand TGFA under the control of an artificial *Elastase* promoter, which is active in pancreatic acinar cells. The mice develop epithelial hyperplasia and pancreatic metaplasia but do not show preneoplastic pancreatic lesions. A major breakthrough in the development of GEM for PDAC was achieved with the *Kras*<sup>+LSL-G12D</sup> model developed by Hingorani and colleagues [26]. In this model one endogenous *Kras* allele is replaced with a mutated knock-in construct silenced by a *STOP* cassette flanked by *loxP* sites. The mutated constitutively active KRAS<sup>G12D</sup> is therefore only expressed in cells when CRE recombinase has excised the *Lox-Stop-Lox* (*LSL*) sequence. These mice show PanIN lesions, desmoplasia and invasive and metastatic PDAC resembling all stages of human PDAC development, although due to CRE activation mutant KRAS<sup>G12D</sup> is activated in the developing pancreas not reflecting sporadic mutations as in human cells. Still, in the mouse pancreatic carcinogenesis requires 12 to 15 months although first PanIN lesions can be detected at 4 to 6 weeks of age, implying that additional genetic mutations need to be acquired in the cells on their route to PDAC. In the

following years further GEM were developed by introducing additional genetic mutations to the basic *Pdx1-Cre;Kras<sup>+/LSL-G12D</sup>* or the *Ptf1a<sup>+/CRE</sup>;Kras<sup>+/LSL-G12D</sup>* models. For example combination of the *Ela-Tgfa* mouse with the model lead to the *Ptf1a<sup>+/CRE</sup>; Ela-Tgfa;Kras<sup>+/LSL-G12D</sup>* model which do not o *Ptf1a<sup>+/CRE</sup>;Kras<sup>+/LSL-G12D</sup>* only develop PanIN but also IPMN lesions and show an accelerated carcinogenesis [27]. For reviews on mouse models of pancreatic cancer refer to Mazur and Siveke 2011, and Grippo and Sandgren 2005 [16, 22]. The following Table 1-2 provides examples of the most common GEM of PDAC.

**Table 1-2**

**Examples of GEM for PDAC.** Adapted after Mazur and Siveke 2011 [16]. Listed are the genotype of the mouse, the type of preneoplastic lesions that develop, the onset and the median survival in months and the reference for first publication.

genotype	preneoplastic lesion type	onset of PDAC in months	median survival in months	reference
<i>Pdx1-Cre;Kras<sup>G12D</sup></i>	PanIN	> 12	> 12	[26]
<i>Ptf1a<sup>+/CRE</sup>;Kras<sup>G12D</sup></i>	PanIN	> 12	> 12	[26]
<i>Ela-Tgfa</i>	-	rarely cancer	> 12	[25, 28]
<i>Ptf1a<sup>+/CRE</sup>; Ela-Tgfa;Kras<sup>G12D</sup></i>	PanIN/IPMN	5	7	[27]
<i>Pdx1-Cre;Kras<sup>G12D</sup>;Ink4a/Arf<sup>LOX/LOX</sup></i>	PanIN	2	2	[29]
<i>Pdx1-Cre;Kras<sup>G12D</sup>;Ink4a/Arf<sup>+/-</sup></i>	PanIN	8	10	[30]
<i>Pdx1-Cre;Kras<sup>G12D</sup>;Ink4a<sup>-/-</sup></i>	PanIN		5	[30]
<i>Pdx1-Cre;Kras<sup>G12D</sup>;Ink4a<sup>-/-</sup>;p53<sup>LOX/LOX</sup></i>	PanIN	1.5	2	[30]
<i>Pdx1-Cre;Kras<sup>G12D</sup>;p53<sup>LOX/LOX</sup></i>	PanIN	1.5	3	[30]
<i>Pdx1-Cre;Kras<sup>G12D</sup>;p53<sup>R172H/+</sup></i>	PanIN	2.5	5	[31]
<i>Ptf1a<sup>+/CRE</sup>;Kras<sup>G12D</sup>;Notch1<sup>LOX/LOX</sup></i>	PanIN	> 6	12	[32, 33]
<i>Ptf1a<sup>+/CRE</sup>;Kras<sup>G12D</sup>;Notch2<sup>LOX/LOX</sup></i>	MCN	> 9	> 15	[32]
<i>Pdx1-Cre;Kras<sup>G12D</sup>;Smad4<sup>LOX/LOX</sup></i>	IPMN	4	9	[34, 35]
<i>Ptf1a<sup>+/CRE</sup>;Kras<sup>G12D</sup>;Smad4<sup>LOX/LOX</sup></i>	MCN	3.5	8	[36]
<i>El-tTA/teO-Cre;Kras<sup>G12D</sup></i>	PanIN	6 months, only with induced pancreatitis		[11]

## 1.2.6 Signaling pathways in pancreatic cancer

Not only in PDAC but in all types of cancer aberrant activation or mutation of signaling pathways that are usually involved in embryonic development and tissue homeostasis can be frequently found. These pathways for example contribute to uncontrolled proliferation, resistance to apoptosis and cell repair mechanisms and changes in the plasticity of the cells. Several key mutations are involved in pancreatic carcinogenesis that regulate differentiation, cell cycle and survival. Especially KRAS, P16, P53 and TGF $\beta$ /SMAD4 mutations in PDAC are well characterized and in recent years also developmental signaling pathways like WNT, Hedgehog or Notch pathways came more into focus. Certain genetic alterations have been associated with specific steps in pancreatic tumorigenesis and support the progression model of PDAC, in which multistep accumulation of these mutations is critical for cancer development (see Figure 1-6). Several reviews focusing on mechanisms of pancreatic carcinogenesis are available [15-17, 37, 38] and cited in the following chapter that describes some of the changes in signaling pathways and molecular mechanisms underlying PDAC development.

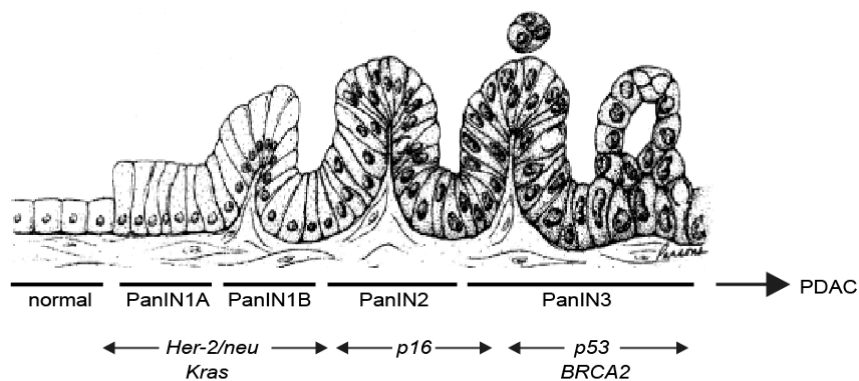


**Figure 1-6**  
**Progression model of PDAC.** Adapted from Schneider et al. 2005 [15].

### 1.2.6.1 Tumor suppressor genes

Between 80 to 95 % of PDAC have a mutation, deletion or promotor methylation in the *p16 (Ink/Cdkn2a)* tumor suppressor gene [39] and germline mutations of *p16* increase the risk for pancreatic cancer up to 13 times [40]. Since *p16 (INK4)* and *p19 (ARF)* overlay in their genome position they are also often lost

together (in up to 40 %). Because of this, two major tumor suppressor pathways are affected, the P53 and the RB (retinoblastoma) pathways. P16 normally blocks CDK4 (Cyclin dependent kinase 4) and therefore phosphorylation and deactivation of the RB cell cycle checkpoint which in turn inhibits progression to S phase. P19 inhibits MDM2 mediated degradation of P53 and therefore progression in cell cycle. Also *p53* itself is found to be mutated in up to 50 % of PDAC cases, typically late in the carcinogenic process. P53 is sensitive to DNA damage, hypoxia and cytotoxic stress and stops progression of the cell cycle upon any of these events. Upon loss or dominant negative mutation (as in the *Trp53<sup>+/-R172H</sup>* model, see 1.2.5.3) cell growth, survival and genetic instability are promoted. Figure 1-7 provides an overview of this signaling network.

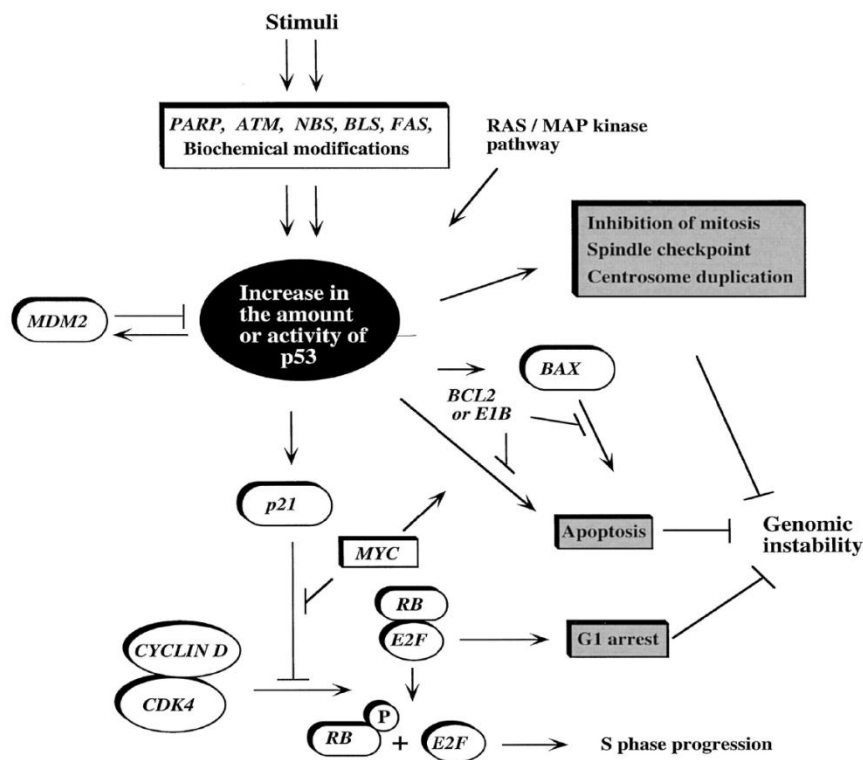


**Figure 1-7**  
**Overview of the P53 and RB signaling pathways.** Adapted from Agarwal et al. 1998 [41]

Also the TGF $\beta$ -SMAD4 signaling pathway is often affected in pancreatic cancer. Up to 50 % of all cases harbor mutations in *Smad4* [39]. Upon activation through TGF $\beta$ -mediated signaling SMAD4 translocates to the nucleus and controls cell proliferation, differentiation and death. Loss of SMAD4 results in aberrant TGF $\beta$  signaling because stimulation of P21 (CIP1) and P15 (INK4B)



and repression of MYC are disturbed. For a review on the SMAD family and their role in pancreatic cancer refer to Singh et al. 2011 [42].

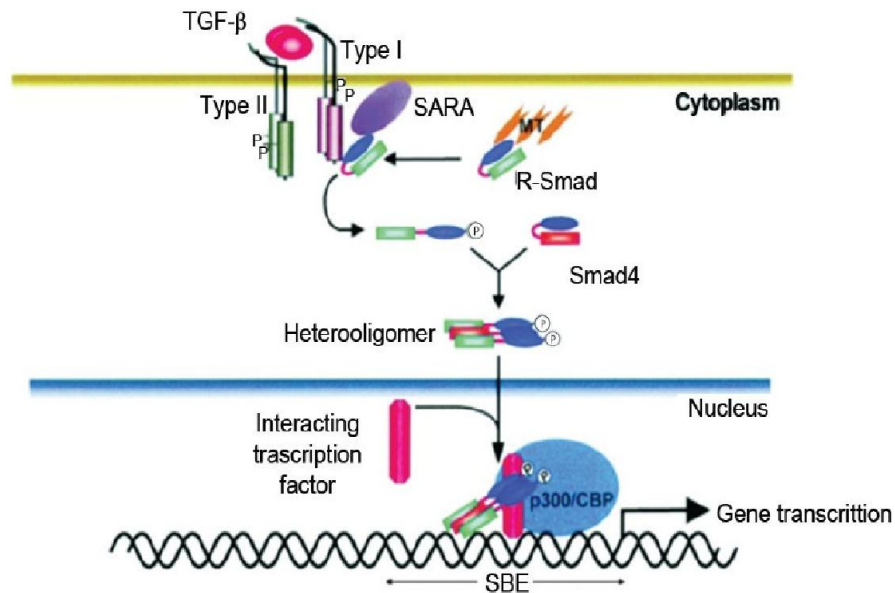


**Figure 1-8**  
**Schematic illustration of the TGFβ/SMAD4 signaling pathway.** Adapted from Singh et al. 2011 [42].

#### 1.2.6.2 Developmental pathways – Notch, Wnt and Hedgehog

The Notch pathway plays a major role during pancreatic development. Deletion of the Notch downstream target *Rbpj* blocks exocrine cell expansion and leads to premature differentiation of progenitor into endocrine cells [43]. Recent studies have shown that Notch2 has a pro-tumorigenic role in PDAC development whereas Notch1 may be a tumor suppressor. Deletion of Notch2 leads to prolonged survival and late appearing cancer. Reason for this is inhibition of Notch2 activated MYC signaling that seems to be important for KRAS driven PADC development [32].

Also the WNT pathway is involved in pancreatic cancer development and progression. In PanIN lesions and PDAC both nuclear and cytoplasmic accumulation of  $\beta$ -Catenin are found and increasing levels correlate with PanIN grade and invasive PDAC. Also, inhibition of  $\beta$ -Catenin inhibits proliferation of PDAC and enhances apoptosis, although the exact mechanisms for  $\beta$ -Catenin accumulation in PADC development remain unclear [17].

PDAC belongs to the Hedgehog-driven tumors which are resistant to ligand inhibition. On the contrary, paracrine ligand secretion from tumor cells promotes stroma remodeling and reduction and Hedgehog inhibitors are in clinical trials [44]. GLI activation is uncoupled from upstream signaling and instead regulated through TGF $\beta$  and KRAS [17].

#### 1.2.6.3 The KRAS pathway

Constitutively activating mutation of the *Kras* gene is the absolute key event in pancreatic cancer development. Up to 95 % of all PDAC cases harbour a *Kras* mutation and they are already found in still normal appearing pancreata on their route to cancer development. The percentage of *Kras* mutations increases with progression in preneoplastic precursor lesions and PDAC development. In fact, a point mutation in either exon 12 or 13 or to a lower frequency in exons 59, 61 or 63 is responsible to transform the proto-oncogene *Kras* into an oncogene. Usually glycine is transformed into aspartic acid, glutamic acid or valine on amino acid level, blocking the GTP hydrolytic capacity of the protein and therefore keeping KRAS in a constitutively active, GTP-bound state upon activation through receptor tyrosine kinase signaling, such as the epidermal growth factor receptor (EGFR). The mouse models described above show that *Kras* mutation alone is sufficient to initiate pancreatic carcinogenesis, however, in normal human pancreata sometimes *Kras* mutations are found and these pancreata do not progress to neoplasia. This implies that additional factors might be important for KRAS induced pancreatic carcinogenesis. KRAS activates several downstream effector pathways which contribute essentially to proliferation, differentiation and cell survival of tumorigenic cells. KRAS as an oncogene is described in several reviews, highlighting its exceptional role in PDAC development [15-17, 37-39], the KRAS downstream effects as part of the EGFR signaling pathway will be described in detail in the following chapter 1.3.4.

### 1.3 The epidermal growth factor receptor (EGFR)

In development and tissue homeostasis, communication between cells is essential. Cell surface receptors transfer signals from the surface to the inner cell and start signaling cascades that can process and react to them. One important group of these receptors is the big family of receptor tyrosine kinases (RTK), among which the epidermal growth factor receptor (EGFR) is the prototype not least because it was the first receptor described to possess tyrosine kinase activity and the first RTK to be sequenced [45, 46]. The gene symbol of EGFR is *ErbB*, derived from a viral oncogene the family members are homologous to: erythroblastic leukemia viral oncogene [47].

The ERBB family consists of four members and several ligands can activate signal transduction. Table 1-3 provides an overview of the receptors and their specific ligands. In this chapter structure of EGFR and its homologous, the ERBB ligands, EGFR activation and degradation, the signaling pathways activated through EGFR and its biological function, its role in cancer and how it can be chemotherapeutically targeted are discussed.

**Table 1-3**  
**Overview of ERBB receptors and their cognate ligands.** Adapted from Normanno et al. 2006 [48].

ERBB receptors	ERB1	ERBB2	ERBB3	ERB4
cognate ligands	EGF	none	NRG1	NRG1
	TGF $\alpha$		NRG2	NRG2
	AREG			NRG3
	EREg			NRG4
	BTC			Tomoregulin
	HB-EGF			HB-EGF
	EPGN			BTC
				EREg

#### 1.3.1 ERBB family members

The human *Egfr* gene is located on chromosome 7, the murine on chromosome 11. It consists of 28 exons coding for a 170 kDa transmembrane protein. The

ERBB family consists of four members, ERBB1, also called EGFR or HER1 (Human Epidermal growth factor receptor 1), ERBB2/HER2neu, ERBB3/HER3, and ERBB4/HER4. These four homologous can form heterodimers and differ in their C-terminal domains therefore increasing the possible combinations for specific ligand binding domains and in that way increasing the number of specific signaling pathway activations [49, 50]. All family members have an extracellular ligand-binding domain, a single hydrophobic transmembrane domain and a cytoplasmic tyrosine kinase-containing domain followed by a C-terminal regulatory domain [50]. Especially the intracellular tyrosine kinase domain is highly conserved among the members. A notable exception represents ERBB3, in which some amino acids are substituted so that it lacks kinase activity and is therefore only biologically active in heterodimers with one of the other ERBB members [51].

The extracellular domain is subdivided into four further domains, two large EGF-binding domains and two cysteine-rich domains, arranged in an alternate manner. An N-lobe and a C-lobe build the tyrosine kinase domain and ATP-binding is performed in the cleft formed by the lobes. Upon ligand binding several tyrosine residues are phosphorylated specifically in the C-terminal domain by the intrinsic tyrosine kinase activity that becomes activated through homo- or heterodimerization of the receptors. This asymmetric tail-to-head dimerization is mediated by the rotation of the domains I and II, leading to promotion from a tethered to an extended configuration [52]. Figure 1-9 depicts the structure of EGFR and its conformational changes upon ligand binding.

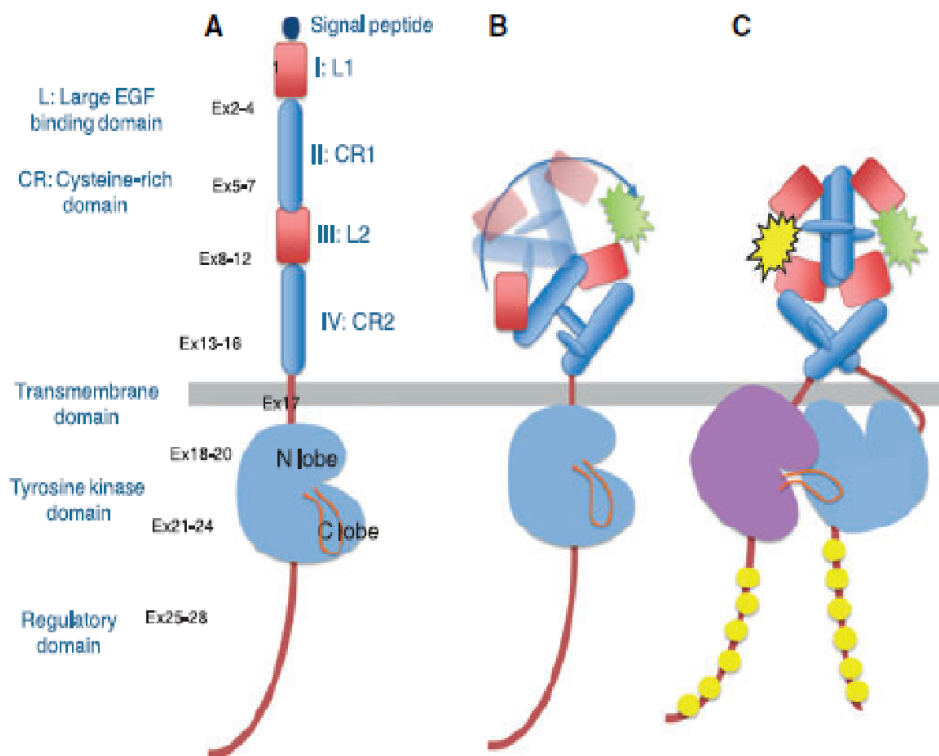


**Figure 1-9**  
**Schematic of the EGFR.** Structure of the EGFR (A), its conformational change upon activation (B) and dimerization (C). Adapted from Mitsudomi et al. 2009 [52].

### 1.3.2 EGFR ligands

In the 1960s a protein from the mouse salivary gland was isolated that induced eye-lid opening and tooth eruption in newborn mice [53]. Three years later the same research group published that this protein stimulates the proliferation of epithelial cells, therefore it was named epidermal growth factor (EGF) [54]. Years later specific binding receptors for EGF on the surface of target cells were identified [55]. Since then, seven ligands that can activate EGFR have been characterized: EGF, transforming growth factor  $\alpha$  (TGF $\alpha$ ), heparin-binding EGF-like growth factor (HB-EGF), amphiregulin (AREG), betacellulin (BTC), epiregulin (EREG) and epigen (EPGN). HB-EGF, BTC and AREG can also bind ERBB4 and EGFR/ERBB4 heterodimers. ERBB2 has no known ligands, but it forms heterodimers with the other ERBB monomers and enhances their downstream effects. The mature proteins are characterized by an N-terminal extension including a consensus sequence known as the EGF motif. Six

conserved cysteine residues form three intramolecular disulfide bonds, defining the A, B and C loop, respectively [56]. Additionally they have a short juxtamembrane stalk, a hydrophobic transmembrane domain and a cytoplasmic tail at the C-terminus. EGF is the only ligand having nine EGF motifs, although only the one closest to the membrane can bind EGFR. All ligands exist in a transmembrane bound proform that needs cleavage by metalloproteases for activation to a soluble ligand. No consensus sequence for the predicted cleavage sites is defined but for example ADAM (a disintegrin and metalloprotease) 17, also known as TACE (TNF alpha converting enzyme) can cleave HB-EGF, AREG and TGF $\alpha$  [57-61]. Although cleavage of ligands is discussed to be a regulatory step in EGFR activation, membrane bound forms of TGF $\alpha$ , BTC and AREG for example have also been found to be active implicating a juxtacrine function of these molecules (reviewed by Singh et al. 2005 and Schneider and Wolf 2009 [56, 62]). Figure 1-10 depicts the schematic illustration of the EGFR ligands and the EGF motif.

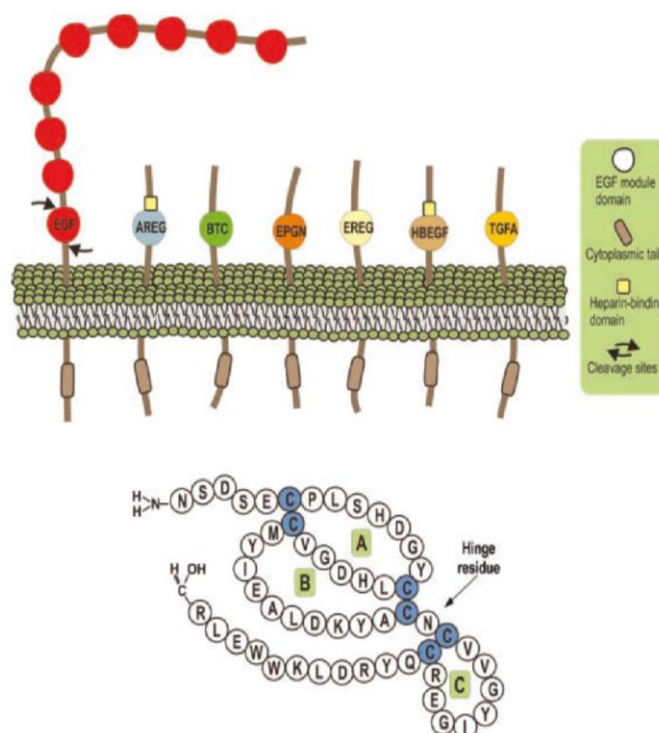


**Figure 1-10**  
**Schematic view of EGFR ligands.** Depicted are the structures of the EGFR ligands in the upper panel and the EGF motif in the lower panel. Adapted from Schneider and Wolf 2009 [62].

### 1.3.3 EGFR activation and degradation

EGFR can be detected on all epithelial and stromal cells and also on some glial and smooth muscle cells. Upon transcription from a TATA-less promoter two predominant large mRNAs (6 kb and 9 kb in humans) that differ in their 3'untranslated region can be found. Although regulation on transcriptional level is not well studied, mRNA levels seem to decrease with increasing cell age. On the contrary, post-translational processing and trafficking of EGFR is very well characterized. In polarized epithelial cells EGFR is localized to the basolateral site to facilitate communication between epithelial cells and stroma, which expresses TGF $\alpha$  and other EGFR ligands. Next to this paracrine signaling, also juxtacrine (on neighbor cells without ligand cleavage), autocrine (on the own cell membrane) and endocrine (on distant cells) activation of EGFR is known. Figure 1-11 illustrates the different ways of EGFR activation through ligand binding.

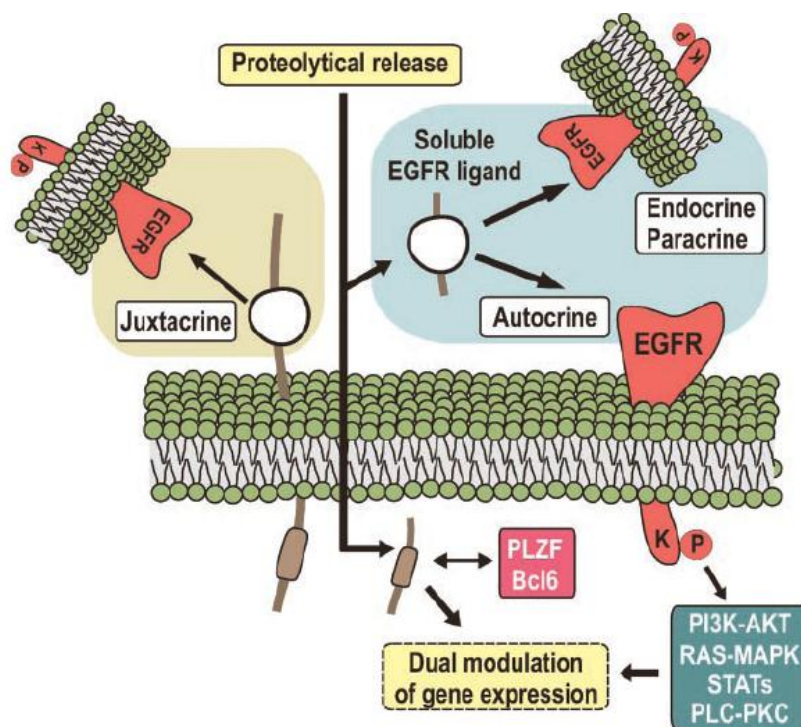


**Figure 1-11**

**Different possibilities of EGFR activation.** EGFR can be activated through its ligands in a juxtacrine, autocrine, paracrine or endocrine manner. Adapted from Schneider and Wolf 2009 [62].

As mentioned in 1.3.1, ligand binding to extracellular domain of EGFR induces conformational changes, dimerization and subsequent activation of the intracellular intrinsic tyrosine kinase domain. This in turn phosphorylates specific tyrosine residues in the cytoplasmic tail that are docking sites for adaptor proteins containing SH2 and SH3 (Src homology) and PBT (phosphotyrosine binding) domains, which serve as signaling branchers and induce activation of downstream signaling cascades (see 1.3.4), for example GRB2 (growth factor receptor-bound protein).

As soon as EGFR is activated it is also endocytotically internalized. This can happen in a clathrin-coated or clathrin-independent manner. Sigismund and colleagues [63] found that clathrin-mediated endocytosis is essential to sustain EGFR signaling but high EGFR ligand levels induce clathrin-independent endocytosis and terminate EGFR signaling. The endocytotic sorting mechanism at the membrane involves for example GRB2, which recruits an ubiquitin E3 ligase CBL and tags it for endosome transport [64, 65]. On the other hand AIP2 (activation induced phosphatase 4), another ubiquitin ligase, ubiquitinylates clathrin-binders such as HRS (hepatocyte growth factor regulated tyrosine kinase substrate), which in turn is recruited to EGFR by its ubiquitin tags. In that way EGFR is directed to lysosomal degradation [66]. However, EGFR can also be recycled back to the plasma membrane. This process is mediated by deubiquitylating enzymes (DUBs). If EGFR undergoes degradation or recycling is also dependent on the ligand that induced activation. EGF, which remains bound to the receptor in the late acidic endosome, directs EGFR to degradation, whereas TGF $\alpha$  that dissociates from EGFR dependent on the pH, tags it for recycling to the membrane [45, 67]. Avraham and Yarden provide an excellent review on EGFR recycling mechanisms and regulation [68].



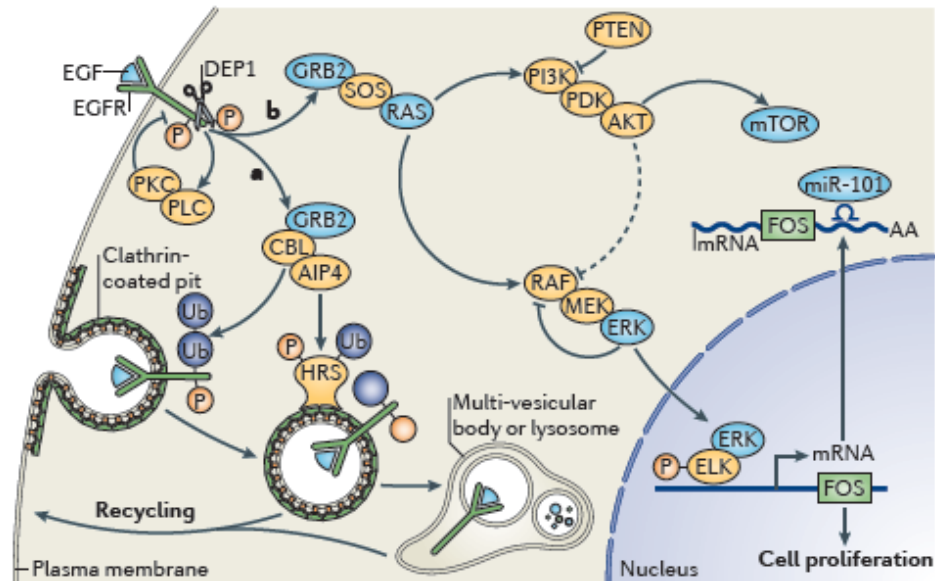


**Figure 1-12**  
**Schematic illustration of EGFR endocytotic mechanisms.** Adapted from Avraham and Yarden 2011 [68].

### 1.3.4 EGFR signaling pathways and its biological function

As described in 1.3.3, upon ligand binding and activation intracellular tyrosine residues of EGFR become autophosphorylated and therefore can be recognized and bound by specific adaptor proteins containing SH and PBT domains. Among them for example GRB2 and SHC can then in turn bind SOS and therefore promote SOS activation of RAS/MEK/ERK signaling cascade. Also the P85 regulatory subunit of PI3K (Phosphatidylinositol 3-Kinase) can bind to the phosphorylated tyrosines and then activate PI3K downstream signaling. The same applies for phospholipase C ( $PLC_{\gamma}$ ), which activates calcium release and protein kinase C (PKC) through the second messengers  $IP_3$  (inositol-1,4,5-trisphosphate) and DAG (diacylglycerol), respectively. STAT (Signal transducer and activator) 1, 3 and 5 associate already with the inactive EGFR and STAT1 becomes phosphorylated by it upon ligand induced activation. Phosphorylated STAT can enter the nucleus and start transcription of target genes. Also VAV1, a member of the Rho family of guanine nucleotide exchange factors, becomes activated by EGFR-mediated phosphorylation. It is an activator of the RAC small GTPases and facilitates the exchange of GDP-bound RAC to GTP-bound active RAC, which in turn can for example activate

PAK serine/threonine kinase, NF-κB and CyclinD1 [19]. Figure 1-13 shows the signaling pathways activated by EGFR and the most important steps will be described in this chapter. For detailed reviews please refer to Yeh and Der 2007, Normanno et al 2006, Singh and Harris 2005, and Wheeler et al. 2010 [19, 48, 56, 69].

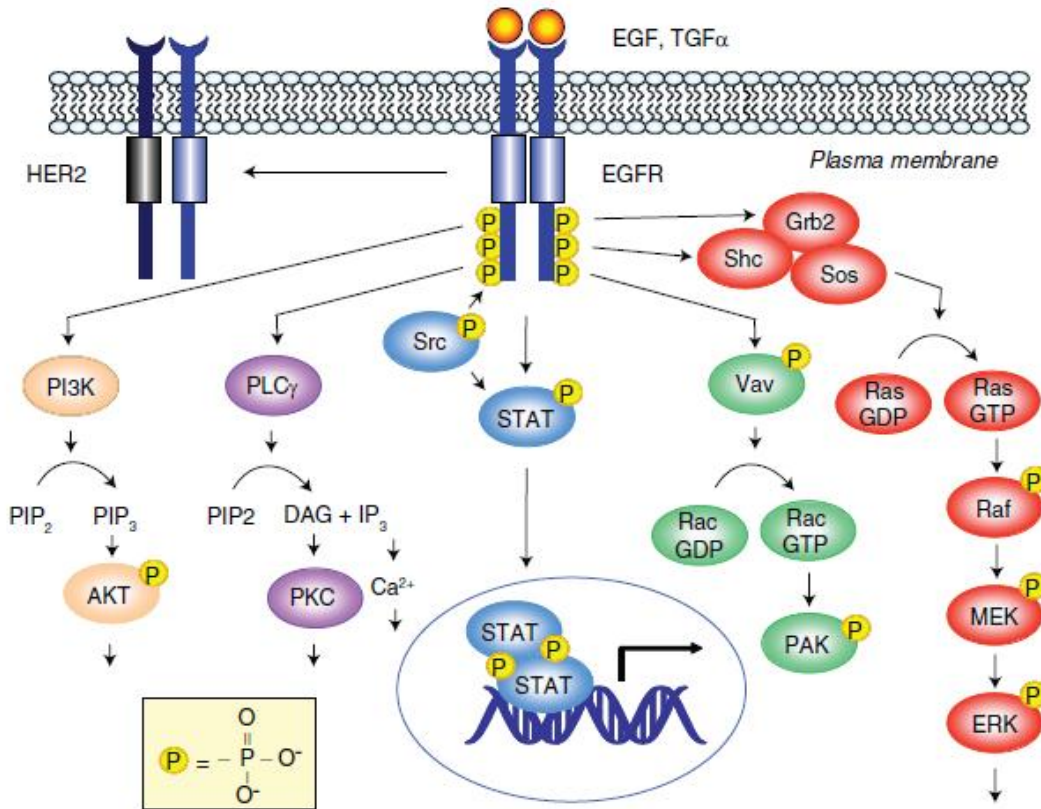


**Figure 1-13**  
**Overview of signaling pathways activated through EGFR.** Adapted from Yeh and Der 2007 [19].

One of the certainly best characterized EGFR downstream pathways is the RAS pathway. The family of RAS-GTPases consists of H-RAS, K-RAS and N-RAS. They function as GDP/GTP binary switches, existing in either the active GTP-bound or the inactive GDP-bound form. GDP to GTP exchange is mediated by GEFs (guanine exchange factors), the hydrolysis of GTP back to GDP is promoted by GAPs (guanine nucleotide activating proteins). GTP-bound RAS can stimulate or bind to several important signaling mediators, which are depicted in Figure 1-14. RAS can for example directly activate PLCγ, RAC and RAL.

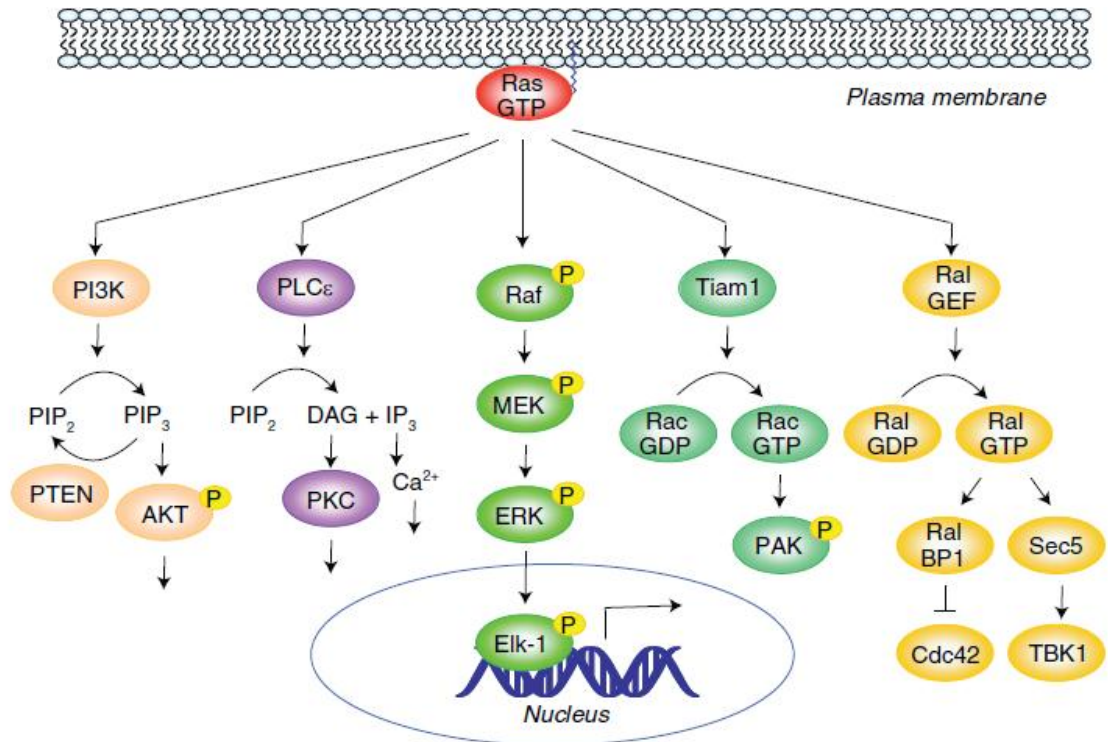


**Figure 1-14**  
**Schematic illustration of RAS downstream effectors.** Adapted after Yeh and Der 2007 [19].

Among the RAS effectors are the catalytic subunits of the PI3K, for example p110 $\alpha$ . Upon PI3K activation, phosphatidylinositol(4,5)-disphosphate (PIP<sub>2</sub>) is phosphorylated to phosphatidylinositol(3,4,5)-trisphosphate (PIP<sub>3</sub>) by PI3K, which then in turn can be bound by AKT (v-akt murine thymoma viral oncogene homolog). Bound to PIP<sub>3</sub>, AKT becomes activated by PDK (protein dependent kinase) 1 and 2. PTEN (phosphatase and tensin homolog) terminates the activation by dephosphorylating PIP<sub>3</sub> back to PIP<sub>2</sub>. AKT signaling is especially important for cell survival and proliferation, phosphorylated AKT at its threonine residue 308 is usually detected to assess pathway activation.

The most well described RAS effectors are the RAF serine/threonine kinases. Active RAS phosphorylates RAF, which then phosphorylates MEK1/MEK2 (mitogen activated protein kinase kinase). These in turn phosphorylate ERK1 and ERK2 (extracellular signal-related protein kinase), also known as MAPK (mitogen activated protein kinase). ERK1 and ERK 2 have multiple downstream effects, for example ELK1 that activates transcription of target genes. Around

160 substrates of ERK have been described already which are involved in translation, mitosis and apoptosis (reviewed by Yoon et al. 2006 [70]).

Knockout mouse studies have provided insight into the different biological functions of ERBB family members. ERBB2, ERBB3 or ERBB4 depleted mice are all embryonically lethal and show a variety of developmental defects of the heart and the nervous system [71]. In 1995, Miettinen and colleagues described EGFR knockout in mice. EGFR<sup>-/-</sup> mice survive up to 8 days after birth, although a high percentage dies already at around embryonic day 10 or later. Reason for this were proportionally smaller placentas, explained by the role of EGFR in fetoplacental interactions. Parallel studies from Sibilian and colleagues and from Threadgill et al. reported the same phenotype, although newborn mice lived up to 20 days, depending on the mouse strain background of EGFR<sup>-/-</sup> mice [72, 73]. Born EGFR knockout mice suffered from impaired epithelial development in several organs like skin, lung, gastrointestinal tract, brain, kidney, liver and eye. They showed growth retardation and epithelial immaturity and dysfunction, resembling a phenotype associated with premature birth in humans [72, 74]. The observed phenotype correlated with the expression pattern of EGFR in the developing embryo as it was monitored by  $\beta$ -galactosidase reporter staining [72]. EGFR as well as its ligands EGF and TGF $\alpha$  are expressed throughout the developing pancreas [75]. TGF $\alpha$  overexpressing mice under control of the elastase promoter show metaplastic ducts and islets neogenesis, indicating involvement of EGFR signaling in proliferation and differentiation of ductal cells [25]. In 2000 Miettinen et al. characterized in more detail the pancreatic phenotype of EGFR<sup>-/-</sup> mice. Macroscopically, the pancreata appeared normal, comparable to wild type mice. Closer examination revealed that the islets, instead of forming circular clusters, showed a more streak-like structure directly associated with pancreatic ducts. The proliferation rates of neonatal  $\beta$ -cells were significantly reduced in EGFR<sup>-/-</sup> mice and islets differentiation was delayed. These results indicated that EGFR is involved proliferation of pancreatic cells [76].

Taken together, the biological function of EGFR lies mainly in induction of proliferation and differentiation of epithelial cells in multiple organs.

### 1.3.5 EGFR signaling in pancreatic cancer and targeted chemotherapy

EGFR overexpression or aberrant activation has been described in several cancers. Almost 100 % of head and neck cancers display EGFR overexpression, and also colorectal, breast, prostate, bladder, ovarian and non-small-cell lung cancers and glioblastomas have aberrant EGFR signaling. In approximately 50 % of PDACs [77] EGFR overexpression could be detected and its expression correlates with poor prognosis [78].

Different mutations of EGFR in cancer have been described. One of the most important is the deletion mutation EGFRvIII, in which the amino acids 30 to 297 of the extracellular domain are deleted. This leads to constitutive EGFR activation without ligand binding and is often accompanied with gene amplification. But although this mutation is often found in glioblastomas and lung cancer, it could not be detected in PDAC [79]. 90 % of EGFR mutations can be found in the first four exons of the *Egfr* gene and therefore affect the tyrosine kinase domain. This leads to constitutive active tyrosine kinase activity. For an overview of the different mutations found in *Egfr* please refer to Mitsudomi and Yatabe 2009 [52]. Still, EGFR mutations or overexpression are anyway discussed to be redundant in pancreatic cancer since 90 % of PDACs show activating KRAS mutations.

The overexpression of EGFR in cancer activates basically the same pathways as it does in its normal biological function. Mainly, the PI3K/AKT and the RAS/MEK/ERK pathways are aberrantly signaling. But also the STAT, PLC $\gamma$  and PKC pathways are activated in PDAC. Recent studies for example have shown that STAT3 activation promotes pancreatic cancer development [80]. The activated pathways promote tumor cell survival and proliferation, angiogenesis and invasion. Additionally, new functions of EGFR in cancer besides classical pathway activation have been identified in the last years. For example it was found, that membrane bound EGFR works as a chaperone for the sodium/glucose cotransporter SGLT1 and therefore prevents autophagic cell death by maintaining intracellular glucose levels. This implicates a kinase-independent role of EGFR in cancer cell homeostasis [81]. In cancer cells EGFR can also frequently be detected in the nucleus. Upon ligand binding EGFR

is internalized and degraded or recycled. Recent studies have shown that cell exposure to oxidative stress or radiation induces phosphorylation of the threonine residue at position 654 [82] which facilitates receptor internalization in caveolae, consisting of proteins of the caveolin family associated with sphingolipids and cholesterol at the plasma membrane. This leads to nuclear accumulation of EGFR and persistent kinase activity [83]. Nuclear EGFR correlates with poor prognosis and treatment resistance of patients [84]. Persistent kinase activity of EGFR in the nucleus phosphorylates proliferating cell nuclear antigen (PCNA) and therefore enhances proliferation of cancer cells [85]. EGFR can also directly interact with the transcription factors STAT5 and E2F1 and in that way enhance the transcription of for example B-MYB [86, 87]. Other target genes of nuclear EGFR include *Cdk1*, coding for Cyclin D1, and iNOS (inducible nitric oxide synthase), which both contribute to G1 to S phase cell cycle progression and proliferation of cancer cells [88, 89].

Mutations and overexpression of EGFR have made it a potential target for chemotherapy and recent developments have generated several EGFR inhibitors that are approved or in clinical trials (excellently reviewed by Wheeler et al. 2010). In general, these inhibitors can be divided into two groups: monoclonal antibodies (MAb) or small molecule tyrosine kinase domain inhibitors (TKI). Monoclonal antibodies, like cetuximab or panitumumab, target the extracellular domain of EGFR. They target the receptor for cell-mediated cytotoxicity, enhance receptor internalization and block endogenous ligand binding to EGFR. Cetuximab was approved by the FDA (Food and Drug Administration) in 2004 in the United States for the therapy of metastatic colorectal cancer (CRC) and head and neck squamous cell carcinoma (HNSCC). Panitumumab received approval from the FDA in 2006 for application in patients with EGFR-expressing metastatic colorectal cancer. TKIs, like erlotinib or gefitinib, are derived from quinazoline. The low molecular weight synthetic molecules block the magnesium-ATP-binding pocket of the tyrosine kinase domain. Gefitinib was approved in 2003 for the therapy of advanced non-small-cell lung cancer (NSCLC) and erlotinib received approval in 2005 for the therapy of metastatic PDAC in combination with gemcitabine (see 1.2.4).

Table 1-4 provides examples of EGFR targeting drugs currently approved or in clinical trials.

Although EGFR inhibition seems to be a powerful therapeutic approach in cancer, several resistance mechanisms have been reported and weaken the effects. Among them are the activations of pathways downstream of EGFR, making EGFR targeted therapy futile. KRAS mutations, which are found in up to 90 % of PDAC patients, for example are discussed to be the reason for only slight effects of erlotinib in pancreatic cancer therapy. Another mechanism of resistance are mutations in the ATP-binding domain of EGFR, decreasing its affinity for ATP and reducing the effects of erlotinib and gefitinib. This was for example reported to be the case in up to 50 % of NSCLC patients who acquired resistance to TKI therapy (reviewed by Faller and Burtness 2009 [90]).

**Table 1-4**  
**Examples of EGFR inhibitors.** Adapted from Wheeler et al. 2010 [69].

inhibitor	company	class	specificity	FDA indication, year of approval
Cetuximab	ImClone Systems	mouse-human chimeric MAb	EGFR	advanced HNSCC in combination with radiotherapy (2006); EGFR-expressing CRC (2004)
Panitumumab	Amgen	human antibody	EGFR	EGFR-expressing CRC (2006)
Matuzumab	EMD Pharmaceuticals	mouse-human chimeric MAb	EGFR	not yet approved
Erlotinib	Genentech	quinazoline based reversible inhibitor	EGFR	advanced PDAC in combination with gemcitabine (2005); NSCLS (2004)
Gefitinib	Astra Zeneca	quinazoline based reversible inhibitor	EGFR	locally advanced NSCLC (2003)
Lapatinib	GlaxoSmith Kline	quinazoline based reversible inhibitor	EGFR HER2	metastatic breast cancer (2006)

## 1.4 MALDI IMS

Matrix assisted laser desorption/ionization (MALDI) imaging mass spectrometry (IMS) is a powerful technique for simultaneous label free detection of multiple molecules in tissue sections while keeping morphological information. These molecules can be proteins, peptides, lipids or small molecules (drugs). In a single IMS experiment the mass spectra of multiple points of a two dimensional sample (usually a tissue slice) are taken simultaneously in a raster that defines the spatial resolution. For each single measuring spot, also called pixel, the mass spectrum is acquired, which results in a two-dimensional distribution map for every single measured  $m/z$  species.

The typical workflow of a MALDI IMS experiment is depicted in Figure 1-15 A. In brief, cryosections of unfixed, snap-frozen tissue are transferred to indium-tin-oxide coated microscopic glass slides that allow lead of an electric current. The matrix of choice, usually a light-absorbing organic acid with low molecular weight) is applied either manually or with and automatic image prep device. Which matrix is used depends on the analytes that shall be measured. Matrix choice has to be established individually, because small proteins and peptides for example crystallize well with sinapinic acid, whereas small molecules like erlotinib are better detectable in  $\alpha$ -cyano-4-hydroxycinnamic acid (CHCA) matrix. Please compare to Table 1-5 for an overview of the recommended matrices for the specific analyte type. Application with an automatic image prep device ensures comparability and reproducibility and is therefore preferable to manual methods of matrix application. The matrix is uniformly deposit on the surface of the tissue slice in a controlled manner ensuring maintenance of the spatial resolution. The analytes are absorbed to the above matrix and co-crystallize with it. The very controlled application method ensures that the analytes crystallize according to their spatial and morphological distribution. On the other hand this is a resolution-limiting step, since morphology can only be kept in the size of the matrix-droplets that are sprayed on the tissue. The second resolution-limiting step is the size of the laser focus used for irradiation. Maximum spatial resolutions obtainable at the moment lay between 10 and 100



$\mu\text{m}$ . Upon laser irradiation, most of the energy is absorbed by the matrix and used for ionization of the analytes. Currently, there are three methods established for ionization used in IMS experiments. Desorption electrospray ionization (DESI), secondary ion mass spectrometry (SIMS) and matrix assisted laser desorption/ionization (MALDI). MALDI IMS was first described 1997 by Caprioli and colleagues [91]. A big advantage of MALDI is that it allows to measure both low and high molecular weight proteins. Upon laser irradiation, in positive ionization mode singly protonated molecular ions  $[M+H]^+$ , in negative ionization mode singly deprotonated molecules  $[M-H]^-$  are generated from the analytes in the matrix. The most commonly used method of detection for MALDI is time of flight (TOF) analysis. After acceleration at a fixed potential the ions are separated and recorded according to their molecular mass to charge ratio ( $m/z$ ). Since the charge in MALDI is normally one, the read-out is the protonated or deprotonated molecular mass of the analyte. The principle of MALDI TOF measurement is depicted in Figure 1-15 B. TOF analysis has been shown to be most sensitive for the detection of molecular masses going up to 30 kDa [92]. Since the measured section stays intact it can be stained for H&E after performing the experiment. This allows the correlation of the obtained relative mass distributions with the morphology of the sample. Each detected  $m/z$  species can be revisualized on the H&E staining in a relative intensity scale (usually in a heat map illustrations where either weak color or a color gradient starting with blue illustrate low relative intensity levels and strong or red color mark high relative mass intensity of the  $m/z$  species in question). Several data processing and statistical programs allow analysis of the obtained data, either to identify discriminating masses between different morphological areas, i.e. for example between normal and tumor areas, or to follow and investigate the relative intensity and distribution of certain masses of interest, i.e. for example the known masses of a chemotherapeutical drug and its metabolites, in specific morphological areas. These programs allow supervised or unsupervised analysis of the normally huge data sets obtained in even a single IMS experiment. For excellent reviews on MALDI IMS please refer to Balluff et al. 2011, Schwamborn and Caprioli 2010, or Walch et al. 2008 [93-95]. For a

review specially addressing drug imaging please refer to Castellino and colleagues 2011 [96].

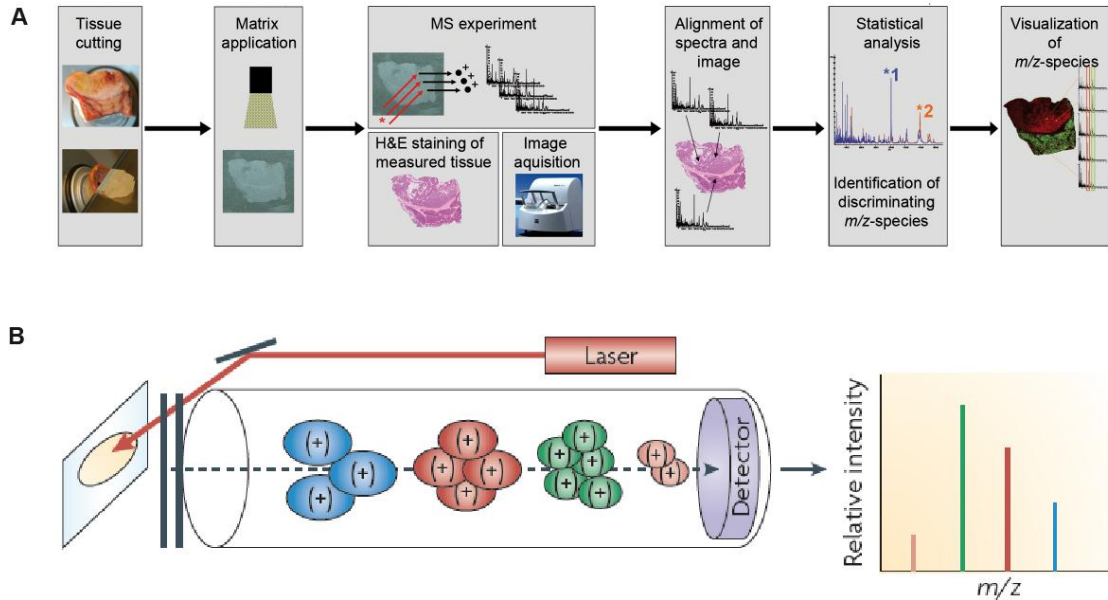


**Figure 1-15**

**Overview of MALDI-IMS workflow and schematic outline of MALDI TOF principle.** (A) Matrix is applied to tissue cryosections and MS experiment is performed. Every 70  $\mu\text{m}$  the mass spectrum of a specific morphological point is measured. Afterwards the measured section can be H&E stained and the obtained spectra can be aligned with the morphological image. Statistical analysis can be performed to identify discriminating  $m/z$  species or to detect relative mass intensities of  $m/z$  species of interest (i.e. a certain drug). The  $m/z$  species of interest can be directly visualized on the measured section. (B) Upon laser irradiation analytes become protonated in positive ionization mode and are linearly separated based on their mass to charge ratio ( $m/z$ , very simplified: bigger masses fly slower). Detection follows in a time of flight (TOF) detector. Adapted from Schwamborn and Caprioli 2010 [94].

**Table 1-5**

**Overview of analytes and their recommended matrices.** Adapted from Balluff et al. 2011 [93].

Analyte	Matrix
Peptides	2,5-Dihydroxybenzoic acid (DHB, gentisic acid)
	$\alpha$ -Cyano-4-hydroxycinnamic acid (CHCA)
	3-Hydroxypicolinic acid (3-HPA)
	2,4-Dinitrophenylhydrazine (2,4,-DNPH)

<b>Proteins</b>	2,5-Dihydroxybenzoic acid (DHB, gentisic acid) α-Cyano-4-hydroxycinnamic acid (CHCA)
	3,5-Dimethoxy-4-hydroxycinnamic acid (SA, sinapinic acid)
<b>Oligonucleotides</b>	4,6-Trihydroxyacetophenone (THAP)
	3-Hydroxypicolinic acid (3-HPA)
<b>Lipids</b>	2,5-Dihydroxybenzoic acid (DHB, gentisic acid)
	2,6-Dihydroxyacetophenone (DHA)

MALDI IMS has already been applied in several diagnostic and prognostic studies, in drug response and drug discovery studies and for lipid imaging studies, for example in neurological disorders like Parkinson's or Alzheimer's disease [97, 98], but mainly in the oncological field. In gastric and breast cancer two studies could show that HER2 status could be accurately predicted with a signature of seven proteins, independent of the tumor entity [99, 100]. In another study Schwamborn and colleagues could show that lymph nodes from patients with classical Hodgkin lymphoma can be distinguished from lymph nodes of inflammatory changes with an accuracy of > 86 % [101]. In a study with ovarian cancer PSME1 (proteasome activator subunit 1), a fragment of the 11S proteasome activator complex, was found to be overexpressed in cancer samples in comparison to benign ovarian tumors [102]. In 2005 a study investigating gliomas was able to identify a protein signature that correlated with patient survival [103]. Two years before a signature for non-small cell lung cancer survival prediction was found [104]. In a drug response study Reyzer et al. found 2004 that transgenic mice with mammary tumors that have either been treated with erlotinib or erlotinib in combination with trastuzumab could be distinguished by several expressed proteins. In addition, resistance to therapy and synergy of the two inhibitors could be predicted [105]. In 2007 Stoeckli and colleagues measured the distribution of beta-peptide in whole body sections of mice [106]. Recently, derivatives of isoniazid could be detected in lung sections of

rabbits [107]. All these examples and many more not named show the variety of successful applications for MALDI IMS in the field of cancer research.

## **1.5 Aim of this thesis**

In this thesis the broad field of pancreatic cancer research should be addressed from different sides and with different methods.

In a proteomic imaging approach MALDI IMS should be used to compare mass spectra from preneoplastic pancreatic lesions with pancreatic cancer and healthy pancreatic tissue to identify potential biomarkers and to get an overview of the proteomic/peptidomic profile of these different tissues. This study should help to improve diagnostic possibilities for pancreatic cancer.

The same method could be used to investigate the distribution of erlotinib, the only approved targeted therapy for pancreatic cancer patients, in healthy and tumor tissue. This might contribute to understand the biological reasons for drug accessibility and distribution in pancreatic cancer and may help to improve therapeutic applicability in PDAC patients.

Finally, the third and biggest part of this thesis aims to investigate the role of EGFR in pancreatic tumorigenesis. Understanding the molecular mechanisms that underlie pancreatic carcinogenesis might contribute to the development of new therapeutic or preventional strategies and to enhance existing therapies.

All three of these projects shall be addressed with the help of genetically engineered mouse models that develop endogenous pancreatic ductal adenocarcinoma. They provide the study platform that allows to address both early tumorigenesis on the genetic level and to investigate fully developed pancreatic cancer for proteomic and therapeutic studies.

Therefore the results of this thesis might contribute to improve our knowledge of PDAC and to enhance therapy and prognosis of pancreatic cancer patients.

## 2 Materials and Methods

### 2.1 Mice

*Kras*<sup>+/*LSL-G12D*</sup>, *Ptf1a*<sup>+/*Cre*</sup>, *Ela-Tgfa*, *Trp53*<sup>*fl/fl*</sup>, *Trp53*<sup>+/*LSL-R172H*</sup> and *Egfr*<sup>*fl/fl*</sup> strains have all been described previously [25, 26, 31, 108-110] and were backcrossed to C57BL/6J background for at least four generations. Mice were intercrossed to obtain the indicated genotypes. Littermates without *Cre* expression served as wild type controls (*WT*). For all MALDI Drug Imaging studies (see 2.7) C57BL/6J mice were used for wild type (*WT*).

The following genotypes and abbreviations were used:

<i>Ptf1a</i> <sup>+/<i>Cre</i></sup> ; <i>Kras</i> <sup>+/<i>LSL-G12D</i></sup>	<i>Kras</i> <sup><i>G12D</i></sup>
<i>Ptf1a</i> <sup>+/<i>Cre</i></sup> ; <i>Kras</i> <sup>+/<i>LSL-G12D</i></sup> ; <i>Ela-Tgfa</i>	<i>Kras</i> <sup><i>G12D</i></sup> ; <i>Tgfa</i>
<i>Ptf1a</i> <sup>+/<i>Cre</i></sup> ; <i>Kras</i> <sup>+/<i>LSL-G12D</i></sup> ; <i>Trp53</i> <sup><i>fl/fl</i></sup>	<i>Kras</i> <sup><i>G12D</i></sup> ; <i>p53</i> <sup><i>KO</i></sup>
<i>Ptf1a</i> <sup>+/<i>Cre</i></sup> ; <i>Kras</i> <sup>+/<i>LSL-G12D</i></sup> ; <i>Trp53</i> <sup>+/<i>LSL-R172H</i></sup>	<i>Kras</i> <sup><i>G12D</i></sup> ; <i>p53</i> <sup><i>R172H</i></sup>
<i>Ptf1a</i> <sup>+/<i>Cre</i></sup> ; <i>Kras</i> <sup>+/<i>LSL-G12D</i></sup> ; <i>Egfr</i> <sup><i>fl/fl</i></sup>	<i>Kras</i> <sup><i>G12D</i></sup> ; <i>Egfr</i> <sup><i>KO</i></sup>
<i>Ptf1a</i> <sup>+/<i>Cre</i></sup> ; <i>Kras</i> <sup>+/<i>LSL-G12D</i></sup> ; <i>Ela-Tgfa</i> ; <i>Egfr</i> <sup><i>fl/fl</i></sup>	<i>Kras</i> <sup><i>G12D</i></sup> ; <i>Tgfa</i> ; <i>Egfr</i> <sup><i>KO</i></sup>
<i>Ptf1a</i> <sup>+/<i>Cre</i></sup> ; <i>Kras</i> <sup>+/<i>LSL-G12D</i></sup> ; <i>Trp53</i> <sup><i>fl/fl</i></sup> ; <i>Egfr</i> <sup><i>fl/fl</i></sup>	<i>Kras</i> <sup><i>G12D</i></sup> ; <i>p53</i> <sup><i>KO</i></sup> ; <i>Egfr</i> <sup><i>KO</i></sup>

For genotyping, mice were tailed between three and four weeks of age and DNA isolation and PCR was performed as described in 2.3.1 and 2.3.2.

All animal experiments were conducted in accordance with German Federal Animal Protection Laws and approved by the Institutional Animal Care and Use Committee at the Technical University of Munich.

#### 2.1.1 Induction of acute pancreatitis in *Kras*<sup>*G12D*</sup> mice

Induction of acute pancreatitis in 6 week old *Kras*<sup>*G12D*</sup> mice was performed as established by Morris et al. [111] with 2 sets of 6 hourly i.p. (intraperitoneal) cerulein (a cholecystokinin analogue) injections (50 µg/kg; Sigma- Aldrich) on alternating days separated by 24 hours. Mice were sacrificed on day 21 after the first induction and histologically analyzed (n = 4 mice per group).

### **2.1.2 Treatment with BAY 86-9766**

To evaluate the effect of MEK inhibition in *Kras*<sup>G12D</sup> mice after induction of acute pancreatitis (see 2.1.1) mice were treated with the specific MEK inhibitor BAY 86-9766 (generously provided by Bayer Schering). Starting on the first day after the last cerulein injection, mice were daily administered orally a single dose (25mg/kg) BAY 86-9766 or vehicle on 6 days per week for three weeks in total. Mice were then sacrificed and histologically analyzed (n = 4 mice per group).

### **2.1.3 Treatment of *Kras*<sup>G12D</sup>;*p53*<sup>KO</sup> mice with cetuximab or erlotinib**

Starting at day 7 of age *Kras*<sup>G12D</sup>;*p53*<sup>KO</sup> mice were injected daily i.p. with either erlotinib, a small specific EGFR tyrosine kinase domain inhibitor (Tarceva, Roche, 25mg/kg in 0.5 % methylcellulose, 0.9 % NaCl), cetuximab, an antibody against the ligand binding domain of the EGFR (pharmacy of the Klinikum rechts der Isar, 2mg/kg, twice per week because of long serum presence of the antibody, the other days with vehicle) or vehicle for three weeks, sacrificed on day 28 of age and histologically analyzed (n = 3 mice per group).

### **2.1.4 Treatment of *WT* and *Kras*<sup>G12D</sup>;*p53*<sup>KO</sup> mice with erlotinib for MALDI Drug Imaging**

To image the distribution of erlotinib (Tarceva, Roche) in the pancreata of *WT* and *Kras*<sup>G12D</sup>;*p53*<sup>KO</sup> mice as described in 2.7, they were administered a single dose of 25 mg/kg erlotinib diluted in 0.5 % methylcellulose with oral gavage. After a specific time (1 h for *Kras*<sup>G12D</sup>;*p53*<sup>KO</sup> and between 0.5 and 24 h for *WT*) mice were sacrificed and the pancreas immediately resected and snap frozen in liquid nitrogen without any further fixation.

## **2.2 Histological analyses**

### **2.2.1 Production of FFPE-tissue samples**

Either upon indicated time points (7 days, 4 weeks, 3 months, and 6 months) or upon tumor development and notable symptoms of disease such as cachexia

and pain (erected fur and relieve posture) the body weight of the mouse was measured and the mouse was anesthetized using isoflurane and killed by cervical dislocation. The pancreas was resected and pancreatic weight was measured. Additionally parts of the lung, liver, the upper duodenum and the spleen were resected. All organs were fixed overnight in 4 % paraformaldehyde and then dehydrated with increasing concentrations of ethanol, xylol and paraffin in a Leica S300 tissue processing unit. Finally, all organs of the mouse were embedded in liquid paraffin and then cooled to harden. The formalin-fixed, paraffin-embedded (FFPE) blocks were stored at room temperature.

### **2.2.2 Paraffin sections**

For histological analyses FFPE-blocks were cut to 2-3  $\mu\text{m}$  on a microtome (Leica), transferred to a 50 °C waterbath for stretching and collected on microscopic glass slides (Thermo scientific). Sections were allowed to dry overnight. Sections of human pancreatic tissue were a generous gift of the department of pathology of the TU Munich.

### **2.2.3 H&E**

For hematoxylin and eosin (H&E) staining paraffin sections were rehydrated in xylol, followed by ethanol at decreasing concentrations (100 % to 70 %, 3 min each). After washing, slides were stained with hematoxylin for 2 min to visualize all acidic structures, i. e. nuclei, in dark violet and then counterstained with eosin for 5 min to label basophilic structures like cytoplasm, connective tissue and other extracellular substances in pink. Slides were washed and dehydrated in 96 % ethanol, isopropanol and xylol (2 min each) and covered with mounting medium (pertex, Medite GmbH) and coverslips. Microscopic pictures were taken on a Zeiss Axiovert Imager.

### **2.2.4 Immunohistochemistry**

For immunohistochemical stainings FFPE-slides were rehydrated as described in 2.2.3. For antigen retrieval they were sub-boiled for 15 min in citrate buffer pH

6. To quench endogenous peroxidase activity sections were then treated with 3 % H<sub>2</sub>O<sub>2</sub> for 10 min. After washing unspecific antibody binding was blocked for one hour at room temperature with a mixture of 1 % BSA, 10 % FCS and 5 % serum from the species of which the secondary antibody was derived. Then the slides were incubated over night at 4 °C with the respective primary antibody diluted in blocking solution (see Table 2-1)

After washing the specific biotinylated secondary antibody (all Vector Laboratories) diluted 1:500 in blocking solution was added for one hour at room temperature. Signal detection was performed with the ABC kit and the DAB kit (both Vector Laboratories) according to manufacturer's instructions. Slides were counterstained with hematoxylin for 30 sec and dehydrated and mounted as described in 2.2.3.

Immunohistochemical analyses of sections from mice analyzed with MALDI Drug Imaging were cut as described in 2.7 and transferred to microscopic glass slides. After drying, they were fixed 8 min with acetone for CD31 staining or 5 min with 4 % formalin for Ki67 staining. Staining was performed on a Ventana Discovery autostainer with the Ventana DAB MAP kit.

## 2.2.5 Immunofluorescence

For immunofluorescent stainings FFPE-slides were treated and incubated with primary antibody as described in 2.2.4 except H<sub>2</sub>O<sub>2</sub> treatment. Fluorochrome-labeled secondary antibodies (Alexa 488, emission 488 nm, or Alexa 568, emission 568 nm, all Invitrogen) were used and sections were mounted with DAPI hard cover mounting medium (Vector Laboratories) to counterstain nuclei. Microscopic pictures were taken on an Apotome fluorescent microscope (Zeiss). Confocal images were collected on a Leica SP2 microscope at consistent gain and offset settings with the help of Dr. Lubeseder-Martellato.

**Table 2-1**  
**Primary antibodies for immunohistochemistry and immunofluorescence**

Antigen	species	Dilution	Company
Actin	goat	1:200	Santa Cruz
Albumin	rabbit	1:200	Santa Cruz
Amylase	rabbit	1:500	Sigma



CK19 Troma III	rat	1:200	DSHB
CD31	rabbit	1:50	Abcam
Egfr	rabbit	1:100	Millipore
Egfr pTyr1068	rabbit	1:200	Chemicon
Erk pThr202/pTyr204	mouse	1:1000	Cell Signaling
HepPar1	mouse	1:500	Dako
Ki67	rabbit	1:5000	Abcam
K-Ras	mouse	1:100	Santa Cruz
MUC5AC	mouse	1:500	Neomarkers
Nestin	mouse	1:200	B&D
Stat3 pTyr705	rabbit	1:100	Cell Signaling
Thymosin beta 4	sheep	1:100	Immundiagnostiks

## 2.2.6 Histological quantification

For quantification of CK19-positive areas or MUC5AC-positive PanIN lesions two representative slides per mouse were chosen and at least 5 pictures were taken from each slide and calculated manually or using the AxioVision 4.8 software (n = 3 to 4 mice per group).

## 2.2.7 Statistical analyses of histological quantifications and pancreas to body weight ratios

All statistical analyses were performed using the Mann-Whitney-test for non-normally distributed, unpaired data. For P values the following scale was applied: \* p = 0.05, \*\* p = 0.01, \*\*\* p = 0.001. The Graph Pad Prism5 software was used.

## 2.3 RNA/DNA analyses

### 2.3.1 DNA Isolation from mouse tails for genotyping

DNA from mouse tails was isolated using the tail and tissue lysis buffer from Peqlab with adding 5% Proteinase K (Roche). Tails were incubated over night at 56°C and then the enzyme was inactivated for 45 min at 85°C. 1 µl was used as template for PCR.

### 2.3.2 Genotyping PCR

If not indicated otherwise, all genotyping and other PCR were performed using the RedTaq Ready Mix (Sigma) with 1  $\mu$ l DNA template (see 2.3.1) and all primers at a final concentration of 10 pM. The following conditions were applied for amplification: 95°C 30 sec, 58°C 30 sec, 72°C 1 min for 35 cycles. Genotyping results were visualized on 2 % agarose gels.

The following genotyping primers were used and gave the indicated band sizes:

<i>Ptf1a</i> <sup>+/<i>Cre</i></sup>	wt 324 bp	lox 199 bp
ACCAGCCAGCTATCAACTCG/TTACATTGGTCCAGCCACC/CTAGGCCACAGAATTGAAAGA TCT/GTAGGTGGAAATTCTAGCATCATCC		
<i>Kras</i> <sup>+/<i>LSL-G12D</i></sup>	wt 300 bp	lox 200 bp
CACCAGCTTCGGCTTCCTATT/AGCTAATGGCTCTCAAAGGAATGTA/CCATGGCTTGAGTA AGTCTGC		
<i>Ela-Tgfa</i>	tg 550 bp	
TGAGAGGTCATAGACGTTGC/GGCTTTTTGACAACGCTATG		
<i>Trp53</i> <sup><i>fl/fl</i></sup>	wt 250 bp	lox 350 bp
CACAAAAACAGGTTAAACCCA/AGCACATAGGAGGCAGAGAC		
<i>Trp53</i> <sup>+/<i>LSL-R172H</i></sup>	wt 565 bp	lox 270 bp
AGCCTTAGACATAACACACGA ACT/GCCACCATGGCTTGAGTAA/CTTGGAGACATAGCCAC ACTG		
<i>Egfr</i> <sup><i>fl/fl</i></sup>	wt 180 bp	lox 320 bp
AAGGTCGGAACCTCTGAGACG/CAGAGAGATCTCCACACTTCC		

### 2.3.3 RNA Isolation

For each mouse tissue from three different parts of the pancreas was resected, immediately homogenized in RLT-buffer including 1%  $\beta$ -Mercaptoethanol and snap frozen in liquid nitrogen. RNA extraction was performed utilizing the RNeasy kit (Qiagen) according to manufacturer's protocol. RNA concentration was measured on a Nano-Drop 2000 spectrophotometer (Thermo Scientific) and quality was checked on a 1% agarose gel.

### 2.3.4 cDNA Synthesis

For cDNA synthesis 1 µg of total RNA was used. For Reverse Transcription RNA was incubated with 0.1 mM DTT, Oligodeoxythymidin (OligoDT), 5x buffer and dNTPs (all Invitrogen) for 5 min at 65°C and then with Superscript II and RNaseOUT for 50 min at 42°C. The reaction was stopped at 70 °C for 15 min.

### 2.3.5 Quantitative RT-PCR

Real-Time PCR was performed on a Lightcycler480 system using the SYBR Green master mix (both Roche). Cyclophilin was used for normalization. Values were calculated with the following exponential equation:  $2^{\Delta\Delta CT(\text{Cyclophilin}) - \Delta\Delta CT(\text{target gene})}$ . *P* values were calculated with the Mann-Whitney-test for non-normally distributed, unpaired data using the GraphPad Prism5 statistical software.

RT-PCR Program:

95°C 10 sec, 58°C 20 sec, 72°C 10 sec for 40 cycles

The following primers (final concentration 10 pM) were used:

Cyclophilin-F/-R	ATGGTCAACCCACCGTGT / TTCTGCTGTCTTTGGAACCTTTGTC
Tmsb4x-F/-R	CCTCTGCCTTCAAAGAAACA / GGGCAGCACAGTCATTTAAAC
Alb1-F/-R	TTGGTCTCATCTGTCCGTCA / GGCAGCACTCCTTGTTGACT
Transferrin-F/-R	ATCAAGGCCATTTCTGCAAGT / GGTTCAGCTGGAAGTCTGTTCC
Alpha-Fetoprotein-F/-R	GGAGGCTATGCATCACCAGT / CATGGTCTGTAGGGCTTTGC
Apolipoprotein A4-F/-R	AGAGCCTGAGGGAGAAGGTC / AGGTGTCTGCTGCTGTGATG
ErbB1-F/-R	GTCTGCCAAGGCACAAGTAAC / CACCTCCTGGATGGTCTTTAA
Tgfa-F/-R	CAGCATGTGTCTGCCACTCT / CTGACAGCAGTGGATCAGCAC
Egf-F/-R	AGCCACGCTTACATTCATTCC / GGAGGTTAATCCTGACCGTGTC

### 2.3.6 Extraction of pancreatic DNA from FFPE-blocks

To isolate DNA from FFPE-blocks the DNA blood and tissue kit (Qiagen) was used according to manufacturer's protocol.

### 2.3.7 *Kras* and *Egfr* deleted PCR

To determine if the *stop* cassette of the mutated *Kras*<sup>G12D</sup> allele and the *Egfr* gene were specifically deleted in the pancreas upon Cre-mediated recombination DNA from pancreas was isolated (see 2.3.6) and PCR was performed. DNA from tail and liver served as controls. For PCR, primers uniquely amplifying the *Kras*<sup>G12D</sup> allele with the deleted *stop* cassette or the deleted *Egfr* were employed.

Conditions and primers for *Kras*-recombined PCR:

Due to the GC rich nature of the *Kras* gene for this PCR the Advantage GC cDNA PCR Kit (Clontech) was used.

Wild type *Kras* 285 bp, removed *stop* cassette 315 bp

98°C 30 sec, 58°C 30 sec, 72°C 30 sec for 35 cycles

<i>Kras</i> -fw	GGGTAGGTGTTGGGATAGCTG
<i>Kras</i> -Rv	TCCGAATTCAGTGACTACAGATGTACAGAG

Conditions and primers for *Egfr*-deleted PCR:

floxed allele 1100 bp, wild type allele 1000 bp, deleted allele 550 bp

94°C 30 sec, 54°C 40 sec, 65°C 2 min for 40 cycles

EGFR-fwd1	AAGTTTAAGAAACCCCGCTCTACT
R4	GCCTGTGTCCGGGTCTCGTCG
R6	CAACCAGTGCACCTAGCCTGGC

## 2.4 Proteinbiochemistry

### 2.4.1 Isolation of protein from cells or tissue

To isolate whole protein tissue lysates of the pancreas pieces from three different regions of the pancreas were freshly resected and immediately snap frozen in liquid nitrogen and stored at -80 °C. Upon use, pieces were thawed in non denaturing lysis buffer (NDLB, 20 mM Tris HCl pH 8, 137 mM NaCl, 10 % Glycerol, 1 % NP-40, 2 mM EDTA pH 8) provided with Protease- and Phosphatase inhibitors (ready-to-use tablets, Roche) and homogenized using

an electrical tissue homogenizer (DiAx 900, Heidolph). For cell lysates of mammalian cells, cells were plated on a 10 cm cell culture dish and grown to approx. 80 % confluency. Medium was removed, once washed with cold PBS and NDLB was added directly to the cells. Cell pellets were harvested with a cell scraper. For both type of lysates (tissue or cell) the next step was to sonicate (Sonopuls, Bandelin) for 10 sec, keep on ice for 10 min and then centrifuge at 4 °C for 10 min at 13200 rpm. Supernatants were transferred to new vials and stored at -20 °C for short term, -80 °C for long term storage.

#### **2.4.2 Protein concentration determination**

Protein concentrations were determined using the BCA kit from Thermo Scientific with included Albumin standard according to manufacturer's instructions. Linear absorbance was measured at 570 nm on an E-max precision microplate reader (Molecular Devices).

#### **2.4.3 SDS polyacrylamide gel electrophoresis (SDS PAGE) and Western Blot**

50 µg protein lysate were supplemented with 5x Laemmli buffer (SDS 10%, TRIS-Base 300 mM, bromphenolblue 0.05 %, Glycerol 50 % and β-mercaptoethanol 5 %) and denaturated at 95 °C for 5 min. Protein separation was performed on a suitable SDS polyacrylamid (depending on the size of the protein that should be detected between 7.5 and 15 %) in SDS running buffer at 120 Volt in BioRad Mini Protean Gel System chambers.

Separating gel (15.75 ml, 10 %)

4 ml 1.5 M Tris pH 8.8

5.1 ml 30% Acrylamide/Bis solution

150 µl 10% SDS

75 µl 10% APS

25 µl TEMED, add 15.75 ml H<sub>2</sub>O dd.

Assemble gel (5.1 ml)

1.3 ml 0.5 M Tris pH 6.8

0.75 ml 30% Acrylamide/Bis solution  
50 µl 10% SDS  
25 µl 10% APS  
10 µl TEMED, add 5.1 ml H<sub>2</sub>O dd.

10x running buffer  
10 g SDS, 30 g TRIS, 144 g Glycin, add 1000 ml H<sub>2</sub>O dd.

Western Blot protein transfer to methanol-activated PDVF membranes (Immobilon-PSQ, Millipore) was performed at 350 mA for 1 h to 2.5h, depending on the size of the proteins that should be detected. The membrane and the gel were clamped between a sponge and two filter papers on each side and the blotting chamber was cooled with an ice pack for the time of the transfer.

10x transfer buffer for wet transfer  
144 g Glycin  
30 g Tris-Base add 1 l H<sub>2</sub>O dd.

1x transfer buffer for wet transfer  
100 ml 10x transfer buffer  
200 ml Methanol  
700 ml H<sub>2</sub>O dd.

After transfer membranes were incubated for 30 min with 3 % skim milk powder in TBS-T to block unspecific antibody binding sites and then incubated over night at 4 °C with the respective primary antibody in 3 % BSA in TBS-T. After washing with TBS-T the membrane was then incubated with the appropriate HRP-coupled (horse radish peroxidase) secondary antibody in blocking solution for 1 h at room temperature. Following additional washings detection was performed using the ECL Western Blotting Detection Reagents and Amersham Hyperfilms (both GE Healthcare). Quantification was performed using densitometric analysis utilizing Adobe photoshop CS5.

10x TBS  
80 g NaCl, 31.5 g Tris-HCl add 1 l H<sub>2</sub>O dd., pH 7.6

TBS-T

1 l 1x TBS, 1 ml Tween20

Secondary antibodies used:

HRP-coupled  $\alpha$ -rabbit IgG or  $\alpha$ -mouse IgG both 1:10000 from GE Healthcare

HRP-coupled  $\alpha$ -goat 1:5000 from Santa Cruz

**Table 2-2**  
**Primary antibodies used for Western Blot**

Antigen	Species	Dilution	Company
Akt 1/2	goat	1:200	Santa Cruz
Akt pThr 308	rabbit	1:1000	Cell Signaling
Albumin	rabbit	1:1000	Santa Cruz
Egfr	rabbit	1:500	Millipore
Egfr pTyr1068	rabbit	1:500	Cell Signaling
Erk 1/2	rabbit	1:1000	Santa Cruz
Erk pThr202/pTyr204	mouse	1:1000	Cell Signaling
Ras	mouse	1:500	Millipore
K-Ras	mouse	1:100	Santa Cruz
H-Ras	mouse	1:500	Santa Cruz
Stat3	mouse	1:1000	B&D
Stat3 pTyr705	rabbit	1:500	Cell Signaling
Hsp90	rabbit	1:3000	Santa Cruz
CyclinD1	mouse	1:1000	B&D
Rac	mouse	1:500	Millipore

#### 2.4.4 Ras and Rac activity assays

To determine the amount of active, GTP-bound Ras or Rac, in a protein lysate GTP-Ras or GTP-Rac pulldown assay was performed. For that the kits from Millipore were used. 500  $\mu$ g protein lysate in MLB lysis buffer (contained in the kit) were incubated either with Raf-1 agarose, which contains a Ras binding domain that specifically binds the GTP-bound Ras in the lysate but not the GDP-bound, or with Pak1 agarose that specifically binds GTP-bound but not GDP-bound Rac1. After 45 min of incubation at 4 °C the beads were washed 3 times with MLB buffer to remove unbound protein. Lysates were denatured with Laemmli buffer and separated with SDS PAGE on a 15 % polyacrylamide gel and detected with standard Western Blot (see 2.4.3). For loading control of total amount of Ras or Rac, a second gel was run with 50  $\mu$ g total protein lysate.

#### **2.4.5 Immunoprecipitation**

Primary murine PDAC cell lines of *Kras*<sup>G12D</sup> mice (see 2.5.1) were lysed in NDLB (see 2.4.1). 500 µg of protein were incubated for 2 h at 4 °C under gentle rotation with 4 µg primary antibody (Egfr and Ras, both Millipore, see Table 2-2). Pull-down of immunoprecipitates was achieved using 60 µl A/G agarose (Thermo Scientific) for 1 h at 4 °C with gentle rotation. To remove unbound protein beads were washed three times with NDLB. Lysates were denatured with Laemmli buffer and separated with SDS PAGE on a polyacrylamide gel and co-immunoprecipitated proteins detected with standard Western Blot.

#### **2.4.6 ELISA - Enzyme linked immunosorbent assay - for TMSB4X**

In collaboration with the surgical department of the Technical University Munich serum samples were obtained from 57 subjects with a histologically proven diagnosis of pancreatic ductal adenocarcinoma (21 women, 26 men, median age 67.1 years). Whole blood was collected prior to surgery. Control serum samples were taken from 10 healthy subjects (2 women, 8 men, median age 66.2 years) and from 12 patients with chronic pancreatitis (3 women, 9 men, median age 55.8 years). The study was approved by the local Ethics committee. All human subjects gave informed consent prior to inclusion in the study.

For the analysis of mouse serum samples, blood was taken from the aorta of *Kras*<sup>G12D</sup> or *WT* mice at mixed age immediately after scarification. Serum was isolated using “Microvette” (Sarstedt) serum tubules.

The ELISA kit for quantitative determination of TMSB4X concentrations in serum was obtained from Immundiagnostiks (Bensheim). ELISA was performed according to the manufacturer’s protocol. For each reaction 50 µl of serum or standard were used. The principle of the test is based on a competitive reaction between the free antigen in the sample and the immobilized antigen on the microplate. Standards or samples are transferred directly to the pre-coated plate together with the primary antibody against TMSB4X. The antigen of the sample competes with the immobilized antigen of the plate for the free binding



side of the antibody. Detection and quantitation are effected by the means of a peroxidase-labeled secondary antibody and the respective substrate reaction. In parallel, a standard curve, consisting of the optical density at 450 nm versus the standard concentrations, is compiled to determine the concentration in the samples. P values were calculated using the Mann-Whitney test for non-normally distributed data.

## **2.5 Cell culture**

### **2.5.1 Isolation and culture of primary murine tumor cell lines from the pancreas**

To isolate and culture primary murine pancreatic tumor cell lines small pieces of pancreatic tumors of *Kras*<sup>G12D</sup>, *Kras*<sup>G12D</sup>;*p53*<sup>KO</sup> and *Kras*<sup>G12D</sup>;*p53*<sup>KO</sup>;*Egfr*<sup>KO</sup> mice were immediately resected after scarification if mice had developed an apparent tumor (see 2.1). The pieces were cut on a 10 cm cell culture plate into very small pieces under sterile conditions. Then cell culture medium was added (DMEM high glucose with 10 % FCS, 1 % Penicillin/Streptomycin, 1x non-essential amino acids, all Invitrogen) and cells incubated in a 37 °C incubator with 5 % CO<sub>2</sub>. After 2 days medium was changed. During that time tumor cells attached and grew on the plate. Cells were split at least three times with 0.25% Trypsin EDTA (Invitrogen) and reseeded to ensure no contamination with fibroblasts. Then cells were used for further experiments.

### **2.5.2 Treatment of *Kras*<sup>G12D</sup>;*p53*<sup>KO</sup> and *Kras*<sup>G12D</sup>;*p53*<sup>KO</sup>;*Egfr*<sup>KO</sup> cell lines with EGF**

To assess the effect of EGF on pancreatic tumor cell lines with and without EGFR, two *Kras*<sup>G12D</sup>;*p53*<sup>KO</sup> and two *Kras*<sup>G12D</sup>;*p53*<sup>KO</sup>;*Egfr*<sup>KO</sup> cell lines were seeded on 10 cm cell culture plates and grown to 80 % confluency. Then medium was removed and cells were starved for 8 h in medium without serum. For each cell line three plates were seeded. After starvation one was treated for 5 min with normal full medium, the second one with DMEM plus 50 ng/ml EGF

(B&D), and the third remained untreated. Then protein was isolated as described in 2.4.1.

### **2.5.3 Isolation and culture of acinar epithelial explants**

Before starting the isolation of acinar cells the following solutions were freshly prepared:

Solution 1:

McCoy's 5A medium with L-Glutamin (Sigma), 0.1 % BSA, 4 µg Soybean Trypsin Inhibitor (SBTI, Sigma)

Solution 2:

McCoy's 5A medium with L-Glutamin (Sigma), 0.1 % BSA, 4 µg Soybean Trypsin Inhibitor (SBTI, Sigma), 1.2 mg/ml Collagenase VIII (Sigma)

Solution 3 (culture medium):

Waymouth's medium with L-Glutamin (Genentex), 0.1 % BSA, 4 µg Soybean Trypsin Inhibitor (SBTI, Sigma), SELENIX 1:100 (Invitrogen), 50 µg/ml bovine pituitary extract (BPE, Invitrogen), 0.2 % Penicillin/Streptomycin, 0.1 % FCS (Invitrogen), 0.25 ng/ml Amphotericin B (Sigma)

To isolate acinar epithelial explants of mice the pancreas of 4 week old mice was resected as fast as possible and immediately placed on a petri dish containing cold sterile PBS. The pancreas was washed twice with PBS, then put to a cell culture dish containing solution 2 and cut to very small pieces with a sterile scalpel. The dish was incubated for 10 min at 37 °C and then the content transferred to a falcon. Potential residues on the plate were washed with solution 1 and also transferred to the falcon. After centrifugation for 5 min at 300 rpm at room temperature the pellet was resuspended in solution 2, transferred to a new cell culture plate and again incubated for 10 min at 37 °C. The whole content was then filtered through a 100 µm nylon mesh and the mesh then washed with solution 1 to collect any remaining cells. Following a second centrifugation step the pellet was washed once with solution 1 and then resuspended in solution 3 containing 30 % FCS. Cells were left 1 h at 37 °C in the incubator to recover. After another centrifugation step the pellet was

resuspended in a 1:1 mixture of solution 3 and rat tail collagen (B&D) and plated to appropriate cell culture dishes (usually 24-well plates) freshly precoated with rat tail collagen. After incubation for 30 min in the incubator, acinar explants were additionally covered with another layer of collagen and again incubated for 30 min. Then explants were covered with solution 3. For explants from mice without *Kras*<sup>G12D</sup> expression EGF was added (50 ng/ml B&D) to stimulate ductal transdifferentiation. To assess the effect of MEK-inhibitor BAY 86-9766, the inhibitor was added to the medium at the indicated final concentrations. Medium was changed every day. Acinar cell explant experiments were performed under guidance of Dr. Lubeseder-Martellato.

#### **2.5.4 Quantitation of ductal transdifferentiation of acinar epithelial explants**

To assess the percentage of acinar-to-ductal metaplasia (ADM) *in vitro* acinar explants were cultured on 24-well plates coated with collagen as described in 2.5.3. Two optical fields per well were randomly chosen and the number of duct-like and acinar structures was counted manually on day 3 and day 5 in culture for explants from mice without *Kras*<sup>G12D</sup> expression (day 1 being the day of isolation) or on day 3 and 4 for explants derived from mice expressing *Kras*<sup>G12D</sup>. All experiments were performed in duplicates and were repeated independently at least 3 times for each genotype and treatment, always with EGF-stimulated and unstimulated acinar explants from a *WT* mouse as control.

#### **2.5.5 Immunofluorescence of acinar epithelial explants**

For immunofluorescent staining of acinar epithelial explants isolated acini were seeded and cultured on collagen coated 8-well chamber slides. At the indicated time points medium was removed, cells were washed with cold PBS and fixed with ice cold methanol for 5 min. Then cells were washed again and immunofluorescent staining (sequential if for two different antigens) was performed with blocking solution consisting of PBS with 1 % BSA, 10 % FCS and 5 % serum of the species the secondary antibody was derived for one hour, followed by primary antibody incubation overnight and secondary antibody

incubation for two hours. Primary and secondary antibodies were used as described in 2.2.5 and in Table 2-1. Nuclear counterstaining was performed using Hoechst33342 for 5 min. Confocal images of immunofluorescent stainings were collected on a Leica SP2 microscope at consistent gain and offset settings by Dr. Lubeseder-Martellato.

## **2.6 Matrix-assisted laser desorption/ionization Imaging mass spectrometry (MALDI-IMS)**

### **2.6.1 MALDI-IMS on tissue sections from mouse pancreata**

For MALDI-IMS pancreata were resected and snap-frozen in liquid nitrogen without any pretreatment. 10 µm cryosections were cut and transferred to Indium-Tin-Oxide (ITO) coated glass slides pretreated with poly-lysine 1:1 in water with 0.1% NP-40. Sections were fixed in 70% ethanol and 100% ethanol for one min. Matrix (10 g/l sinapinic acid in 60% acetonitrile and 0.2% trifluoroacetic acid) was uniformly deposited on the slide using the ImagePrep device (Bruker Daltonics). Mass spectra were measured using the MALDI TOF/TOF Analyzer Ultraflex III (Bruker Daltonics) with a spatial resolution of 70 µm in linear mode. Ions were detected in a mass range of  $m/z$  2500 to 25000 with a sampling rate of 0.1 GS/s. A ready-made protein standard (Bruker Daltonics) was employed for calibration of spectra, which was done externally on the same target before each measurement. After measurement the slides were washed in 70% ethanol to remove the matrix and counterstained with hematoxylin/eosin (H&E). High-resolution images of stained sections were taken using the Mirax Scan system (Carl Zeiss) and co-registered with the MALDI-IMS data to correlate mass spectra with the histological features of the same section.

### **2.6.2 Statistical analysis of MALDI-IMS data**

MALDI-IMS data were obtained and analyzed using the FlexControl 3.0, FlexImaging 3.0 and the ClinProTools 2.2 software (Bruker). With the FlexImaging software regions of interest (ROI) were defined according to the

morphology (PanIN, IPMN, PDAC, WT, CP) and 40 randomly chosen single spectra per mouse per ROI-group were exported to ClinProTools for further analysis. The extracted mass spectra were recalibrated on common “background” peaks (spectral alignment) and normalized on their total ion count. In all analyses, the spectra of two groups of ROIs were compared and *p* values were calculated with the combined Wilcoxon rank-sum test for two non-parametric, ordinal, independent samples and Benjamini-Hochberg corrected. *P* values  $\leq 0.05$  were considered significant.

For validation of discriminating peaks the Significance Analysis of Microarrays (SAM) test was performed and features with a false discovery rate less than 0.001 were considered significant. The optimal discriminating threshold was determined using Receiver Operating Characteristics (ROC) analysis. Validation was performed with an independent set of samples (Fisher exact t-test, *p* < 0.001). For these analyses the free available statistic software R (the R Project for Statistical Computing) was utilized.

### **2.6.3 Peptide and protein identification by liquid chromatography and tandem mass spectrometry (LC-MS/MS)**

As initial step for peptide identification the accurate mass of discriminating peaks was determined using direct MALDI-MS/MS. Therefore, adjacent sections from mouse pancreata where the respective peaks were detectable in high relative levels were coated with matrix and submitted to MALDI analysis. It was searched for regions on the slide where the respective peaks could be detected in linear MS mode and then subsequent MS/MS in reflector mode was performed. Mass accuracy was determined to an accuracy of 2ppm. In the next step peptides and proteins were extracted directly from the sinapinic acid prepared tissue slices. For the extraction, 1  $\mu$ l of 30% acetonitrile in 0.1% trifluoroacetic acid was applied onto the slice, removed and diluted into 10  $\mu$ l of 0.1% formic acid. The complete extract was used for LC-MS/MS analysis on an LTQ Orbitrap mass spectrometer (Thermo Fisher Scientific) coupled to a nano-HPLC (nanoLC Ultra, Eksigent Technologies). Peptides were separated on a self-packed 0.0075x40 cm reversed-phase column (Reprosil, Dr. Maisch) using

a 25min linear gradient (2-35% acetonitrile in 0.1% formic acid, flow rate 300nl/min). Intact masses of eluting peptides were determined at 30,000 resolution and the three most intense peaks were selected for further fragmentation by collision-induced dissociation (CID) and acquisition of fragment spectra with low resolution (1,000). Singly charged ions as well as ions with unknown charge state were rejected. Dynamic exclusion was enabled and dynamic exclusion duration was set to 10 seconds. Peaklist files were generated using Mascot Distiller version 2.2.1.0 (Matrix Science) and database searches were performed using the Mascot search engine version 2.2.04 (Matrix Science) against the IPI mouse database (version 3.26). Search result files were imported into Scaffold (Proteome Software).

## **2.7 Drug Imaging with MALDI-IMS**

### **2.7.1 Measurement of erlotinib on pancreatic sections**

To image the distribution of erlotinib in pancreata of mice they were treated and the pancreas resected as described in 2.1.4. 10  $\mu\text{m}$  cryosections were cut and transferred to Indium-Tin-Oxide (ITO) coated glass slides. Without further fixation sections were dried and  $\alpha$ -cyano-4-hydroxycinnamic acid (CHCA) matrix was applied to the glass slide with the ImagePrep™ station (Bruker) using the standard preparation method with the maximum wetness setting. Mass spectra were measured using the MALDI TOF/TOF Analyzer Ultraflex III (Bruker Daltonics) with a spatial resolution of 70  $\mu\text{m}$  in reflector mode. Ions were detected in a mass range of  $m/z$  200 to 500 with a sampling rate of 0.1 GS/s. After measurement the slides were washed in 70% ethanol to remove the matrix and counterstained with hematoxylin/eosin (H&E). High-resolution images of stained sections were taken using the Mirax Scan system (Carl Zeiss) and co-registered with the MALDI-IMS data to correlate mass spectra with the histological features of the same section. MALDI-IMS data were obtained and analyzed using the FlexControl 3.0, FlexImaging 3.0 and the ClinProTools 2.2 software (Bruker). With the FlexImaging software regions of interest (ROI) were defined according to the morphology for acinar versus tumor

versus lymph node tissue and for the comparison of different regions of tumor on the same and also on different pancreatic sections. For the comparison the relative mass intensity of erlotinib ( $[M+H^+] = 394.18$  Da) and its main metabolite desmethyl erlotinib ( $[M+H^+] = 380.16$  Da) were extracted with 500 and 300 randomly chosen spectra per ROI, respectively. Additionally, the masses of the main fragments of the two molecules were detected and confirmed specific molecule detection. The extracted mass spectra were recalibrated on common “background” peaks (spectral alignment), normalized on their total ion count and the average mass intensity per ROI was calculated and extracted with ClinProTools.

### 2.7.2 Statistical analysis of drug imaging data

Average mass spectra for erlotinib and demethylated erlotinib were extracted and compared using the Mann-Whitney-test for non-normally distributed, unpaired data using the GraphPad Prism5 statistical software. For demethylated erlotinib ( $[M+H^+] = 380.16$  Da) the detectable peak overlays with the first isotope of the matrix dimer (CHCA:  $2MH^++1$ ) since the resolution obtainable with the applied measurement was not high enough to discriminate the two masses. Therefore a mathematical extraction of the matrix-peak from the metabolite peak was performed, taking that in the isotope distribution of the matrix the first isotope of CHCA comprises 22 % of the original mass. This was calculated from the relative mass intensity of the peak at 379 Da, the matrix dimer peak, and subtracted from the relative mass intensity of the peak at 380 Da. The in this way obtained relative intensities were used for further analysis of metabolite distribution and intensity. To verify the correct measurement of desmethyl erlotinib, i.e. that the mass at 380 Da is at least partially representing the metabolite, FAST-SRM (Fast, targeted single reaction monitoring) on two different pancreatic sections was performed in collaboration with Bruker Daltonics in Bremen. With this method it is possible to measure the parent mass, i.e.  $m/z$  380, and in a second measurement step the specific fragments in the MS/MS mode. With this measurement it could be verified that  $m/z$  380 represents the metabolite of erlotinib since only this parent mass can

specifically disintegrate to its known fragments. If the fragments are detectable as well this means also the parent mass is present.

To correlate average mass spectra with percentage of staining for the proliferation marker Ki67 and the endothelial marker CD31 sections adjacent to the ones measured with MALDI were immunohistochemically stained (see 2.2.4) and the same ROIs as for the drug imaging spectra were defined. For that all slides were scanned at 20x objective magnification by the Mirax Scan system (Carl Zeiss). For each of the resulting digital slide, ROIs were extracted and analyzed using a commercially available software (Definiens Enterprise Image Intelligence(tm) Suite, Definiens AG, Munich). A ruleset was developed in order to detect and quantify semantic classes. In a first step the algorithm segments pictures iteratively, recognizing groups of pixels as objects. Further the objects are classified based on staining intensity, morphology, neighborhood and special color features to distinguish the morphological classes “cluster, ductal, white space and diffuse” and their percentage of total area was calculated. With the same software, percentages of CD31-positive stained area per total area and Ki67-positive nuclei of total nuclei per area were calculated. These values were correlated with the average mass spectra per ROI using the GraphPad Prism5 software and Spearman correlation coefficient for non-normally distributed data and p-values for linear regression were calculated.



### 3 Results

#### 3.1 MALDI imaging mass spectrometry for *in situ* proteomic analysis of preneoplastic lesions in pancreatic cancer

##### 3.1.1 MALDI-IMS is a specific method to analyze sections from murine pancreata

To verify the applicability and accuracy of MALDI-IMS for detection of specific peptides and small proteins on pancreatic sections of mice, as first step the pancreata of 4 *WT* mice were resected and measured as described above (see 2.6). The detectable mass range of the applied method lays between 2500 Da and 25000 Da. The known molecular ion  $[M+H^+]$  of insulin, as a marker specifically expressed in pancreatic islets, is 5808 Da and therefore in the detectable range. Since all detectable masses can be re-visualized on the measured section in a heat map illustration utilizing the flex imaging software the insulin mass was chosen as a proof-of-principle marker.

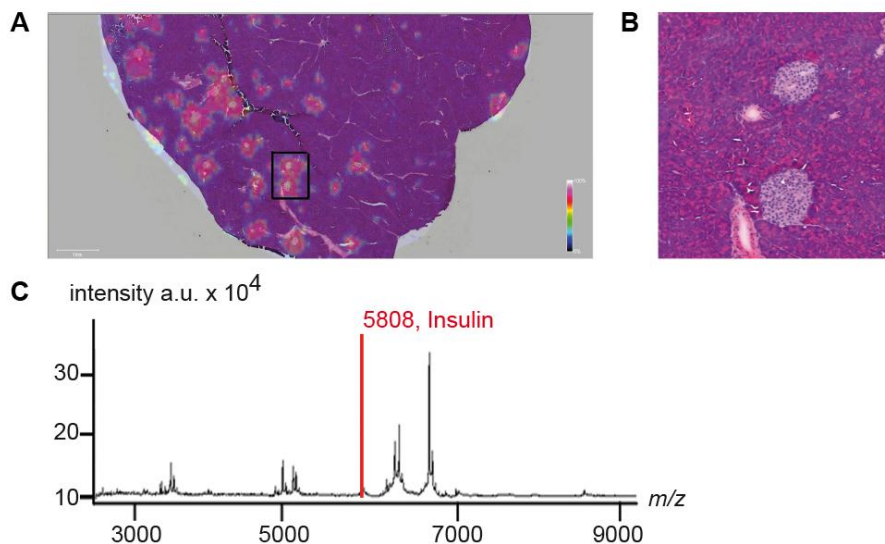


**Figure 3-1**

**Revisualization of the known molecular ion of insulin on a *WT* pancreatic section measured with MALDI-IMS.** (A) H&E staining of a *WT* pancreatic section overlaid with the heat-map illustration of the relative mass intensity, where blue means lowest and red highest intensity as indicated with the scale bar in the corner. (B) Magnification of the region indicated with the black box in (A) showing that the signal of the illustrated mass is detectable specifically on pancreatic islets. (C) Corresponding whole average mass spectra of the section illustrated in (A). The red bar depicts the mass which was chosen for visualization.

In Figure 3-1 the visualization of the insulin signal in a *WT* pancreas is illustrated. The mass can be chosen in the average mass spectrum of the whole section and is then displayed on every pixel of the section where it could be detected. This display is performed in a heat-map illustration to indicate the relative mass intensity. Therefore the morphological correspondence with the detected signal is possible. Using the mass of insulin as a marker, on all four measured pancreata the colocalization with the islets of Langerhans could be visualized (Figure 3-1 B), demonstrating the specific correlation of measured *m/z*-species to morphological features with MALDI-IMS.

### **3.1.2 Detection of specific discriminating *m/z*-species for pancreatic lesions and cancer**

To identify *m/z*-species that can specifically discriminate the most common preneoplastic pancreatic lesion, PanINs, from IPMNs as well as from PDAC and healthy *WT* tissue, pancreata from 13 *Kras*<sup>G12D</sup>, 8 *Kras*<sup>G12D</sup>;*Tgfa* and 5 *Kras*<sup>G12D</sup>;*Tgfa*;*p53*<sup>R172H</sup> mice of mixed age (3 to 18 month, depending on the genotype) were dissected. These mice had developed PanIN and IPMN lesions at different stages and/or PDAC of various differentiations. This mixture was chosen to obtain a very diverse group of lesions and PDAC stages for further analysis. Since chronic pancreatitis (CP) often bears ductal lesions that resemble PDAC precursors and is the most important differential diagnosis to PDAC, also pancreata from 7 mice with conditional inactivation of Thioredoxin2 were dissected, with typical features of chronic pancreatitis including inflammatory cell infiltration and fibrosis (mice will be described in detail elsewhere and were generously provided by Prof. R.M. Schmid). To compare the spectra of different morphological areas, regions of interest (ROI) for PanIN, IPMN, PDAC, CP and normal exocrine tissue were defined (in collaboration with PD Dr. Irene Esposito, Institute of Pathology of TUM, an expert in pancreatic pathology) on the pancreata using the FlexImaging software and were used for comparison of the spectra of respective regions from the same section as well as from other sections to each other.

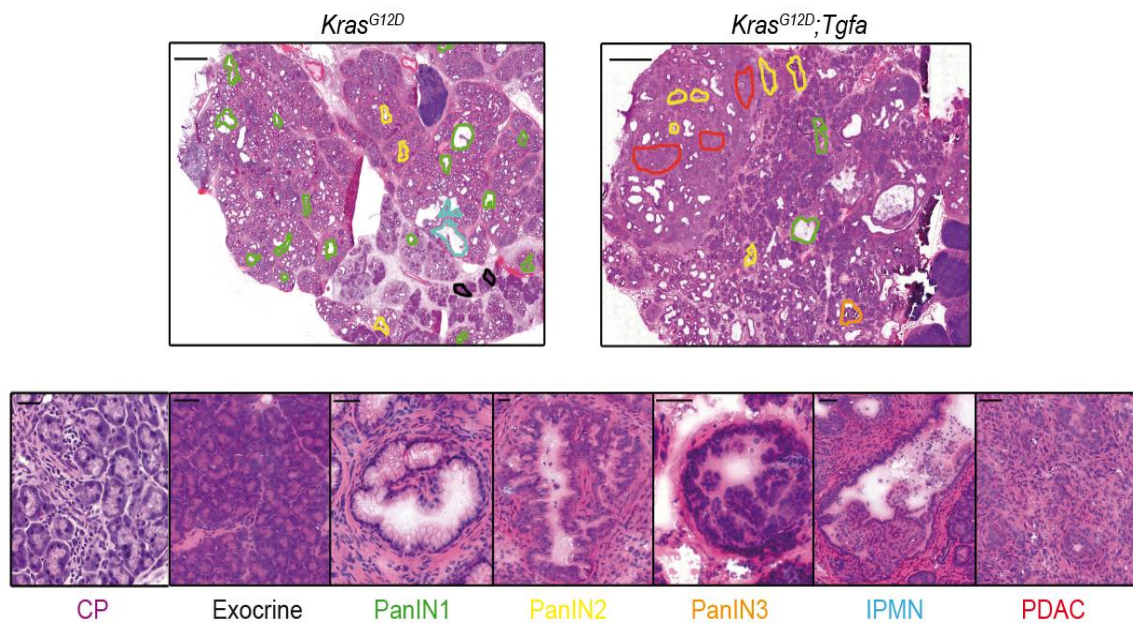


**Figure 3-2**

**Definition of ROIs on pancreatic sections.** Sections measured with MALDI-IMS were stained for H&E afterwards and regions of interest (ROIs) were defined according to morphology (upper panel, scale bars represent 100  $\mu$ m). For each ROI an example is illustrated in the lower panel; scale bars represent 10  $\mu$ m.

Figure 3-2 illustrates the definition of ROIs on the sections after measurement and the distinct morphological features. The single spectra of these ROIs were exported to ClinProTools analysis software. As a first control experiment the spectra of normal pancreatic tissue (acini and ducts) from *WT* mice with phenotypically normal appearing acinar and ductal tissue from *Kras*<sup>G12D</sup> mice. No differences in the spectra between these two groups were detectable, therefore ensuring that there are no detectable variances in the spectra of *WT* and GEM. For further analysis, phenotypically normal ROIs from both genotypes were classified as “normal”.

In a next step spectra from normal tissue of *WT* and *Kras*<sup>G12D</sup> mice ( $n = 11$ ) were analyzed against spectra from preneoplastic lesions of *Kras*<sup>G12D</sup> and *Kras*<sup>G12D</sup>;*Tgfa* mice (PanINs and IPMNs,  $n = 24$ ). These two groups could be distinguished by 76 statistically significant peaks (Wilcoxon rank-sum test,  $p$  values Benjamini-Hochberg corrected) of which 26 were lesion-specific (i.e. specific for IPMNs and PanINs) and 50 normal-specific with  $p$  values between

0.000001 and 0.05. For PanINs 25 ( $p = 0.000001$  to  $p = 0.05$ ) and for IPMNs 18 ( $p = 0.03$  to  $p = 0.05$ ) specific  $m/z$ -species could be found, respectively, which could discriminate them from normal tissue. Also, IPMNs and PanINs could be discriminated from each other by 6 PanIN-specific peaks ( $p = 0.02$  to  $p = 0.05$ ,  $n = 19$  vs. 13 mice). When comparing the preneoplastic lesions with PDAC ( $n = 24$  vs. 10 mice) 57 lesion-specific and 11 PDAC-specific masses were detected ( $p = 0.00169$  to  $p = 0.038$ ). To ensure that the PanIN-specific  $m/z$ -species are not detectable in tubular complexes and sites of inflammation as encountered in CP, additionally the spectra from PanINs were compared with those from CP ( $n = 19$  vs. 7 mice). Here 22 PanIN-specific and 37 CP-specific peaks were identified ( $p = 0.000045$  to  $p = 0.05$ ). Table 3-1 provides an overview of all compared groups, the number of discriminating  $m/z$ -species, the corresponding  $p$  values and the number of animals used. Supplementary Table 7-1 to Table 7-12 give detailed information of all significantly identified  $m/z$ -species of the most important comparisons.

**Table 3-1**

**Statistical analysis of the different ROI groups for discriminating  $m/z$  species using ClinProTools.** Listed are the compared groups, number of identified  $m/z$ -species specific for the indicated groups, the range of the corresponding  $p$ -values and the number of animals analyzed per group.

compared groups	number of discriminating $m/z$ -species	$p$ values	Total number of animals (different genotypes)
Acini GEM vs Acini WT	0	-	6 vs 4
PanIN + IPMN vs normal	26 PanIN + IPMN 50 normal	0.000001 – 0.05	24 vs 11
PanIN vs normal	25 PanIN 67 normal	0.00001 – 0.05	19 vs 11
IPMN vs normal	18 IPMN 28 normal	0.00005 – 0.05	13 vs 11
PDAC vs normal	17 PDAC 31 normal	0.0001 – 0.05	10 vs 11
PanIN vs IPMN	6 PanIN 0 IPMN	0.03 – 0.05	19 vs 13
PanIN + IPMN vs PDAC	5 PanIN + IPMN 11 PDAC	0.00169 – 0.037	24 vs 10

IPMN vs PDAC	7 IPMN 2 PDAC	0.01 – 0.05	13 vs 10
PanIN vs PDAC	15 PanIN 15 PDAC	0.00082 – 0.045	19 vs 10
PanIN vs CP	22 PanIN 37 CP	0.000045 – 0.05	19 vs 7
IPMN vs CP	18 IPMN 26 CP	0.00037 - 0.05	13 vs 7
PanIN + IPMN vs CP	17 PanIN + IPMN 25 CP	0.00001 – 0.05	24 vs 7
PDAC vs CP	20 PDAC 25 CP	0.003 – 0.05	10 vs 7

### 3.1.3 *m/z*-species 2790, 2812 and 2829 are specifically found in PanIN lesions

Closer examination of PanIN-specific peaks revealed that the *m/z*-species 2790, 2812 and 2829 were discriminating PanINs from normal tissue and from CP but stayed upregulated in PDAC (see Table 7-1 to Table 7-12). Since these peaks could not discriminate PanINs from PDAC they seemed to be suitable candidates for PanIN and early PDAC detection. The overlay of the average spectra from PanINs and normal pancreatic tissue revealed that in the latter the peaks were nearly not detectable (Figure 3-3 A). Further statistical examination of these peaks (Wilcoxon test, Bonferroni correction) revealed *p* values below 0.00001. The distribution Box Plot for the mass 2829 Da of PanINs and normal tissue depicted clear discrimination between the two groups (Figure 3-3 B).

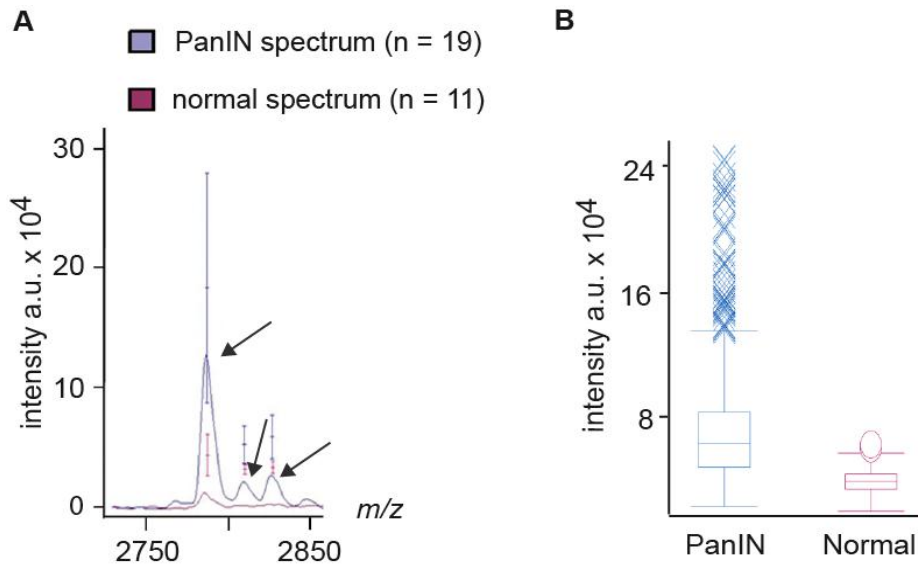


**Figure 3-3**

**Statistical evaluation of PanIN-specific  $m/z$ -species.** (A) Overlay of the average mass spectra from the ROIs PanIN vs. normal. The arrows indicate the masses 2790, 2812 and 2829 that are almost exclusively detectable in the PanIN spectrum. (B) Box Plot illustration of the distribution of the relative intensity of the mass 2829 Da in PanIN and normal ROIs.

We next visualized  $m/z$  2790 and  $m/z$  2829 on the tissue sections demonstrating specificity of these peaks for PanIN regions in the heat map illustration (Figure 3-4 upper two panels), whereas a peak at  $m/z$  6645, which was unique for normal tissue specifically re-visualized in regions with morphologically normal pancreatic tissue (Figure 3-4, third panel).



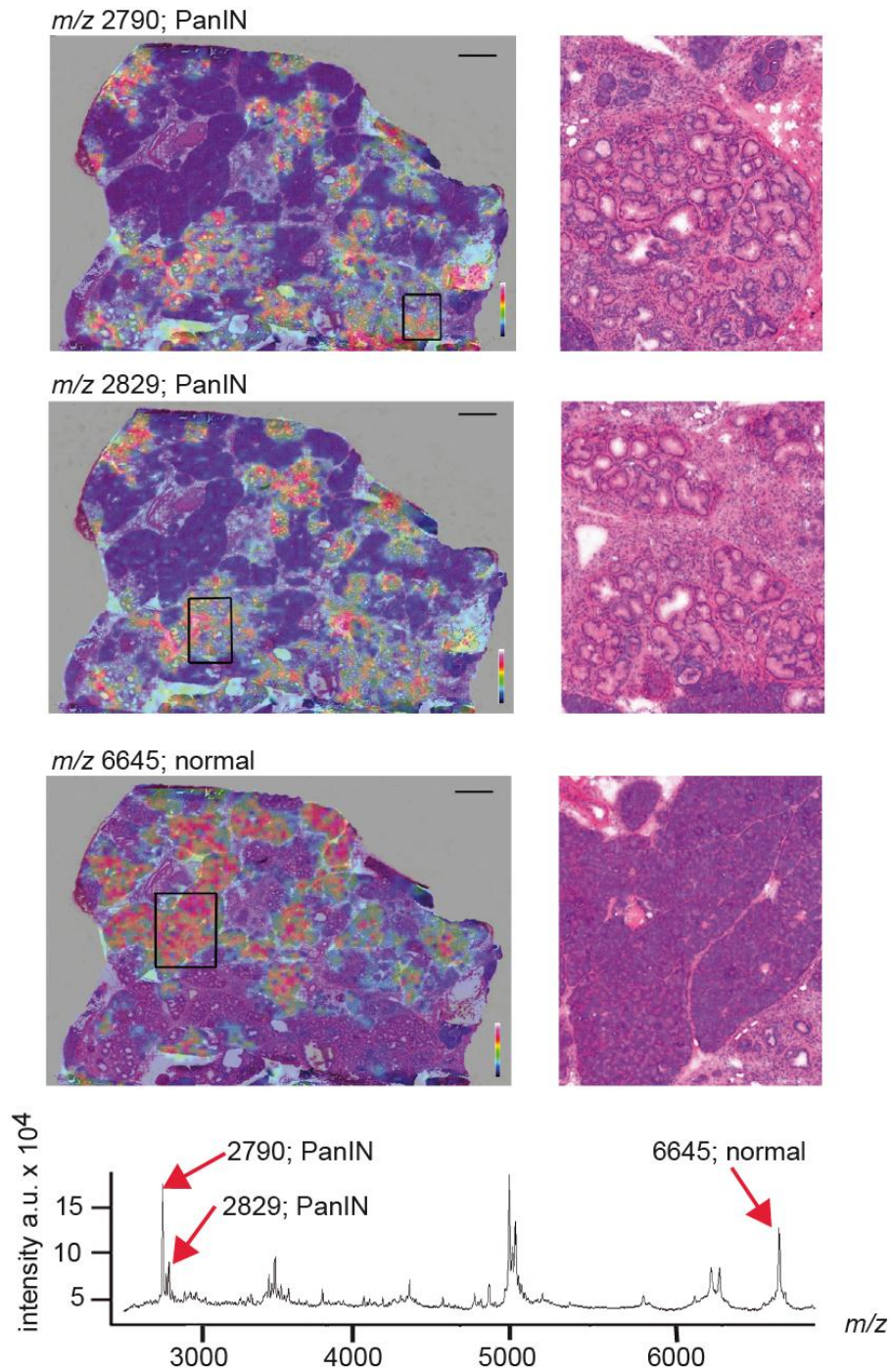


**Figure 3-4**

**Revisualization of discriminating *m/z*-species.** Depicted are the revisualizations of two PanIN-specific and one wild type specific peak on a section of a *Kras*<sup>G12D</sup> mouse, as well as magnifications of the excerpts indicated with black boxes to distinguish the corresponding morphology. Below the average mass spectrum of this section is shown with red arrows highlighting the visualized masses. All scale bars represent 100  $\mu$ m.

### 3.1.4 Validation of significant discriminating peaks in an independent sample set

To validate the significance of *m/z* species 2790 and 2829 in an independent sample set, Receiver Operating Characteristics (ROC) analysis was performed with these peaks to determine the optimal discriminating thresholds utilizing the R statistical software. With these thresholds it was possible to distinguish tissue from 10 independent mouse pancreata (4 *Kras*<sup>G12D</sup> and 6 *WT* littermates at an age of 6 months) with an accuracy of 100% (Fisher test,  $p < 0.001$ ).

### 3.1.5 Protein identification of the three most significant species by LC-MS/MS

For protein identification of discriminating PanIN-specific significant *m/z* species, peptides were directly extracted from MALDI-IMS slides and analyzed by Liquid chromatography and tandem mass spectrometry (LC-MS/MS). Sequence database search of the LC-MS/MS results using the Mascot search engine allowed the identification of three highly significant *m/z* species pointing to two different proteins. The *m/z* 2790 species was identified as a peptide representing the amino-terminus of the mature form of murine serum Albumin (ALB1), whereas both, the *m/z* 2812 and the *m/z* 2829 species represented two different peptides belonging to the carboxy-terminus of Thymosin beta-4 (TMSB4X). The identification of TMSB4X was further supported by identification of additional four different peptides of the protein's carboxy-terminal region that were not in the mass range of MALDI-IMS and therefore not detected as discriminating in the original measurement. The manually verified peptide identifications of ALB1 and TMSB4X, the corresponding MS/MS spectra and the sequence coverage of the identified peptides are listed in Table 3-2 and available in the Supplemental Material (see 7.1.2 and 7.1.3).

#### Table 3-2

**Overview of identified *m/z* species.** Depicted are the MALDI-IMS candidates, the identified peptide sequences and the proteins they belong to, as well as the corresponding Mascot ion scores of identification and the calculated and expected peptide masses with their deviation in ppm.



Significant MALDI-IMS species	Peptide sequence	Protein name	Mascot ion score	Observed m/z	Calculated peptide mass /Da	Expected peptide mass /Da	Deviation /ppm
2790	EAHKSEIAHRYNDLG EQHFKGLVL	ALB1	65.2	931.1487	2790.4226	2790.4204	0.80
2812	SKLKKTETQEKNPLP SKETIEQEK	TMSB4X	32.5	704.1362	2812.5137	2812.5187	-1.77
2829	KTETQEKNPLPSKETI EQEQQAGES	TMSB4X	38.4	708.1087	2828.4037	2828.4044	-0.24
	KETIEQEKQAGES	TMSB4X	47.0	738.8627	1475.7098	1475.7106	-0.53
	KNPLPSKETIEQEKQA GES	TMSB4X	33.7	705.0310	2112.0696	2112.0702	-0.27
	KTETQEKNPLPSKETI EQEQQ	TMSB4X	36.3	829.0988	2484.2729	2484.2712	0.69
	KTETQEKNPLPSKETI EQEQQAG	TMSB4X	41.1	654.0902	2612.3296	2612.3298	-0.07

### 3.1.6 Validation of identified candidates

To validate if the identified proteins ALB1 and TMSB4X were transcriptionally upregulated in the pancreas, total pancreatic RNA from 7 *Kras*<sup>G12D</sup> and 5 wild type littermates at mixed age between 4.5 and 9 months was isolated and quantitative RT-PCR analysis for the two candidates was performed. The expression of both transcripts was significantly upregulated in *Kras*<sup>G12D</sup> in comparison to *WT* mice ( $p \leq 0.05$ , Figure 3-5).

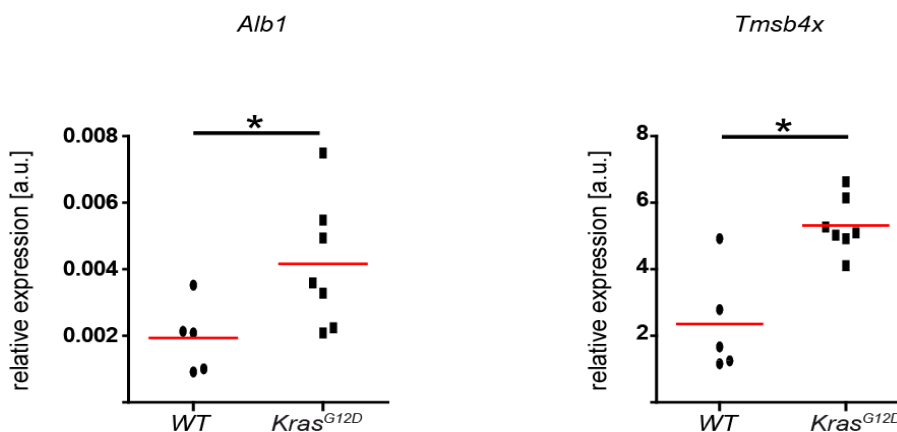


**Figure 3-5**  
**Quantitative RT-PCR analysis of *Alb1* and *Tmsb4x* in whole pancreatic lysates.** *Alb1* and *Tmsb4x* mRNA are significantly increased in *Kras*<sup>G12D</sup> mice compared to wild type control ( $p = 0.042$  for *Alb1*,  $p = 0.0117$  for *Tmsb4x*,  $n = 7$  vs. 5 mice).

### 3.1.7 ALB1 expression is associated with hepatic transdifferentiation of the pancreas during carcinogenesis

Upregulated ALB1 expression in the carcinogenic pancreas lead to the hypothesis that it is associated with hepatic transdifferentiation. It was previously reported that pancreatic exocrine cells can transdifferentiate to hepatocytes and that hepatic foci can be found in adult pancreas and in PDAC [112-115]. First, robust validation of the specific upregulation of ALB1 was performed. Immunohistochemical staining for ALB1 on sections from *Kras*<sup>G12D</sup> mice was observed in PanIN lesions but not in normal pancreatic ducts and acinar cells (n = 10). Immunofluorescence analysis for ALB1 and the ductal marker CK19 on sections from *Kras*<sup>G12D</sup> and *Kras*<sup>G12D</sup>;*Tgfa* mice demonstrated co-localization of the two proteins in PanIN lesions (Figure 3-6 A). Also Western Blot analysis of whole pancreatic lysates revealed increased ALB1 protein expression in *Kras*<sup>G12D</sup> mice in comparison to *WT* controls (Figure 3-6 B). Importantly, the *m/z* species 2790 did not re-visualize on small and large vessels of MALDI-IMS measured sections (Figure 3-6 C).

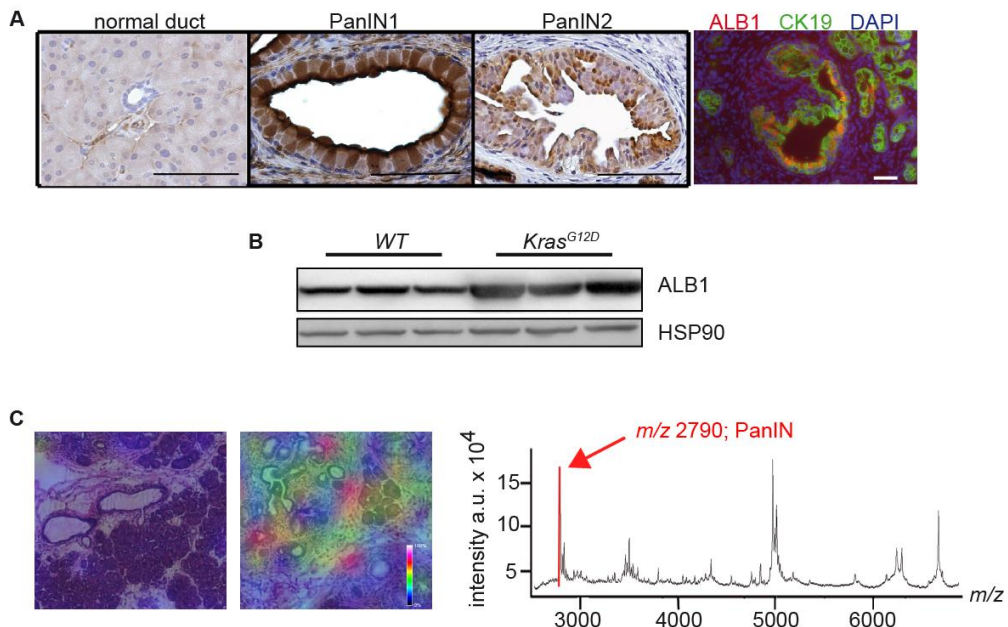


**Figure 3-6**

**ALB1 expression is specifically upregulated in the pancreas during carcinogenesis.** (A) Immunohistochemical analysis of ALB1 shows specific staining of PanIN lesions of *Kras*<sup>G12D</sup> mice but not ductal cells (n = 10 mice). Immunofluorescence staining for ALB1 and the ductal

marker CK19 demonstrates co-localization of the two proteins. All scale bars represent 50  $\mu\text{m}$ . (B) Western Blot for ALB1 on whole pancreatic lysates from *WT* and *Kras<sup>G12D</sup>* mice ( $n = 3$ ). ALB1 expression in preneoplastic tissue is robustly increased comparing to normal pancreas. (C) As indicated in the average spectrum, the mass 2790 was re-visualized on a section of a *Kras<sup>G12D</sup>* mouse pancreas. It is clearly detectable on PanIN lesions (depicted on the right side), but not on blood vessels (depicted on the left side). All revisualizations were performed with the same intensity settings. All scale bars represent 50  $\mu\text{m}$ .

Secondly, it was evaluated if this increase in ALB1 in the carcinogenic pancreas is accompanied with the upregulation of other liver-specific markers. Therefore RNA from whole pancreata of *Kras<sup>G12D</sup>* and *WT* mice between 4.5 and 9 months was isolated and quantitative RT-PCR for the liver specific markers *Transferrin (Tfn)*, *Alfa-fetoprotein (Afp)* and *Apolipoprotein A4 (ApoA4)* was performed. The expression levels of these markers were significantly increased in *Kras<sup>G12D</sup>* compared to *WT* mice indicating a possible transdifferentiation process occurring in PanINs (Figure 3-7 A). Additionally immunohistochemical analysis for the liver-specific marker HepPar1, an antibody specifically detecting hepatocytes in healthy and carcinogenic tissue [116], on 14 PanIN1, 4 PanIN2 and 4 PanIN3 lesions was performed. Two PanIN3 lesions were positively stained for HepPar1 (Figure 3-7 B), indicating hepatic cell features in high-grade PanINs.

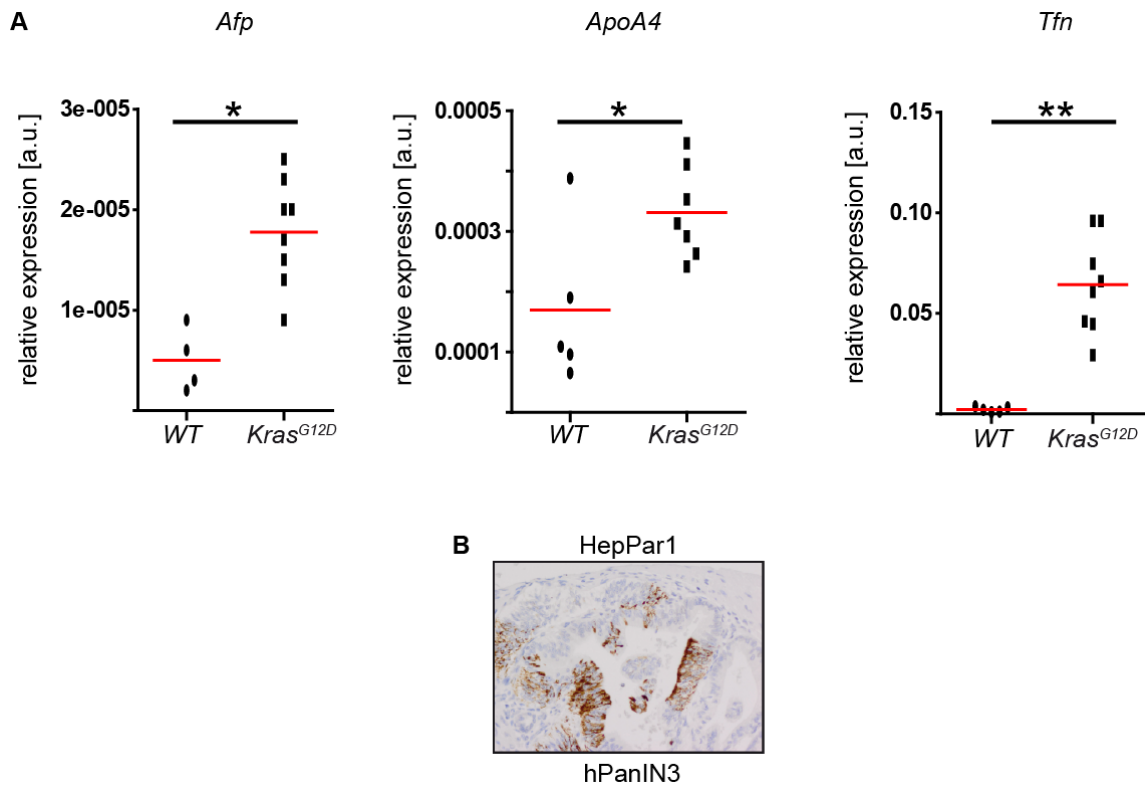


**Figure 3-7**

**ALB1 expression is associated with hepatic transdifferentiation during pancreatic carcinogenesis.** (A) The expression of the liver-specific genes *Afp*, *ApoA4* and *Tfn* is significantly increased in *Kras*<sup>G12D</sup> mice compared to WT ( $p = 0.0107$  for *Afp*,  $p = 0.048$  for *ApoA4*,  $p = 0.0016$  for *Tfn*). (B) The liver-specific marker HepPar1 could be detected on human PanIN3 lesions.

### 3.1.8 TMSB4X is specifically upregulated in the murine pancreas during PDAC development

To validate the specific expression of TMSB4X during pancreatic carcinogenesis immunohistochemical analysis of murine and human pancreatic sections was performed. TMSB4X expression was detected in murine and human PanIN lesions and PDAC but not in acinar, ductal and islet cells (Figure 3-8 A). For quantification sections from 10 *Kras*<sup>G12D</sup> mice with PanINs were stained and all of them were found to be positive for TMSB4X. Of note, expression was high already in low-grade PanINs and stayed in malignant lesions, supporting the results of the MALID-IMS-based approach for identification of preneoplastic lesion markers that are still present in PDAC.

Since TMSB4X is a small molecule and has been detected in body fluids earlier [117, 118], it was investigated whether it may be detectable by ELISA in serum

samples of mice with PanIN lesions. Interestingly, significantly upregulated blood levels were found in sera from *Kras*<sup>G12D</sup> compared to *WT* mice, supporting the principal value of the presented marker detection strategy (Figure 3-8 B). However, when an analysis using a set of human samples from donors and patients with chronic pancreatitis and PDAC was performed, no difference was notable between these groups (Figure 3-8 C) indicating that it is not a suitable marker for differential diagnosis.

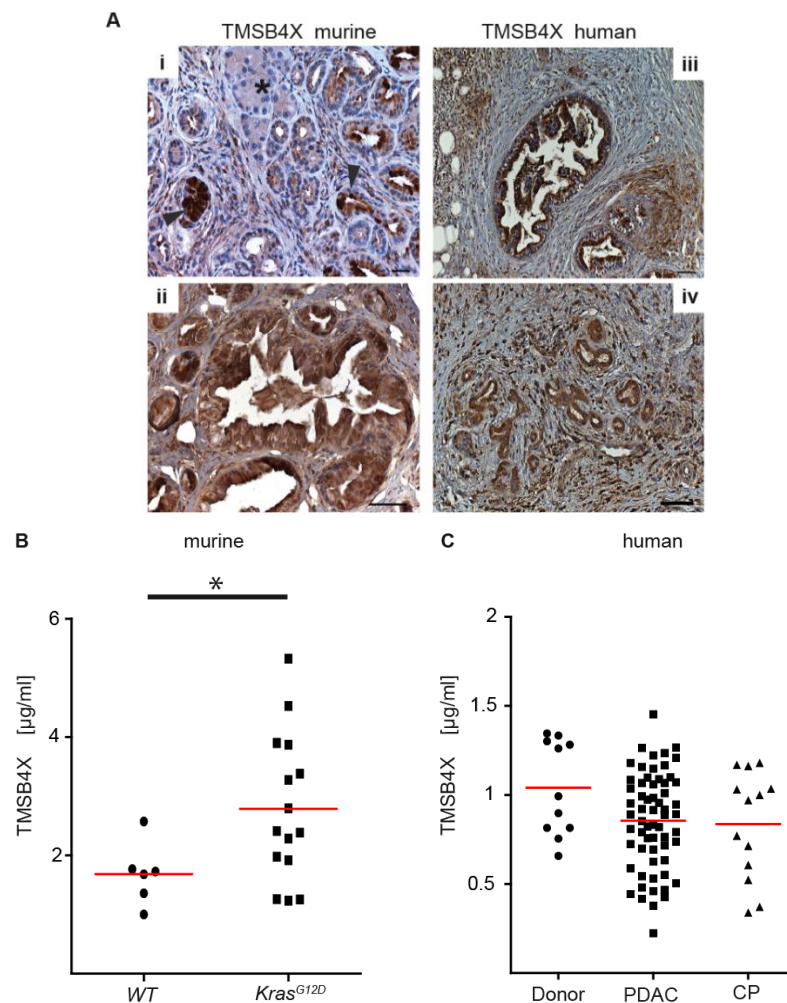


**Figure 3-8**

**TMSB4X is specifically upregulated in the murine pancreas during PDAC development.**

(A) Staining for TMSB4X on murine and human pancreatic sections illustrated the specific expression of the protein in murine PanINs (i, arrowhead) but not in acinar compartment (i, asterisk). Also on mPanIN3 it was highly expressed (ii). On human PanIN (iii) and PDAC (iv) sections its expression was specifically detectable as well. (B) ELISA for TMSB4X in sera from *Kras*<sup>G12D</sup> mice and *WT* mice revealed significantly ( $p = 0.0282$ ) higher levels of the protein in serum from *Kras*<sup>G12D</sup> mice. (C) ELISA for TMSB4X in sera from patients with PDAC or CP or from healthy donors did not show significant differences in the serum levels between the groups (donor vs. PDAC  $p = 0.0626$ ).

## 3.2 Analysis of erlotinib distribution in PDAC *in vivo*

### 3.2.1 Determination of time point for highest drug concentration

To analyze the distribution of erlotinib *in vivo* in the pancreas and to determine the time point for highest concentration after single dose application, *WT* mice were administered orally 25 mg/kg erlotinib diluted in methyl cellulose. After various time points between 0.5 and 24 hours mice were sacrificed and pancreata dissected and analyzed with MALDI-IMS. For the time point 0 h mice not treated with erlotinib were used. Additionally, for each time point mice only treated with the vehicle methyl cellulose alone were measured to ensure specificity of the measured peaks.

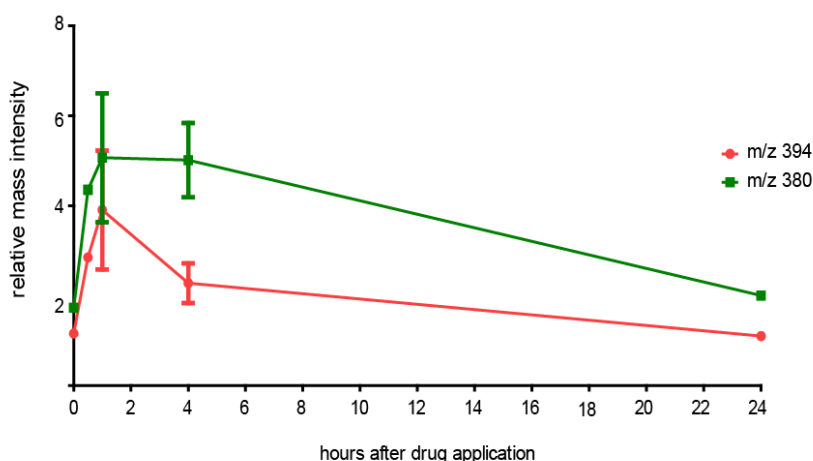


**Figure 3-9**

**Time course of relative erlotinib concentration in *WT* mice after single drug application.** Depicted is in red the relative mass intensity of erlotinib, in green the relative intensity of demethylated erlotinib at the indicated time points. For both masses 1 hour after application the highest relative intensity was detectable ( $n = 4$  mice at time point 1h and 4h, otherwise  $n = 1$ ).

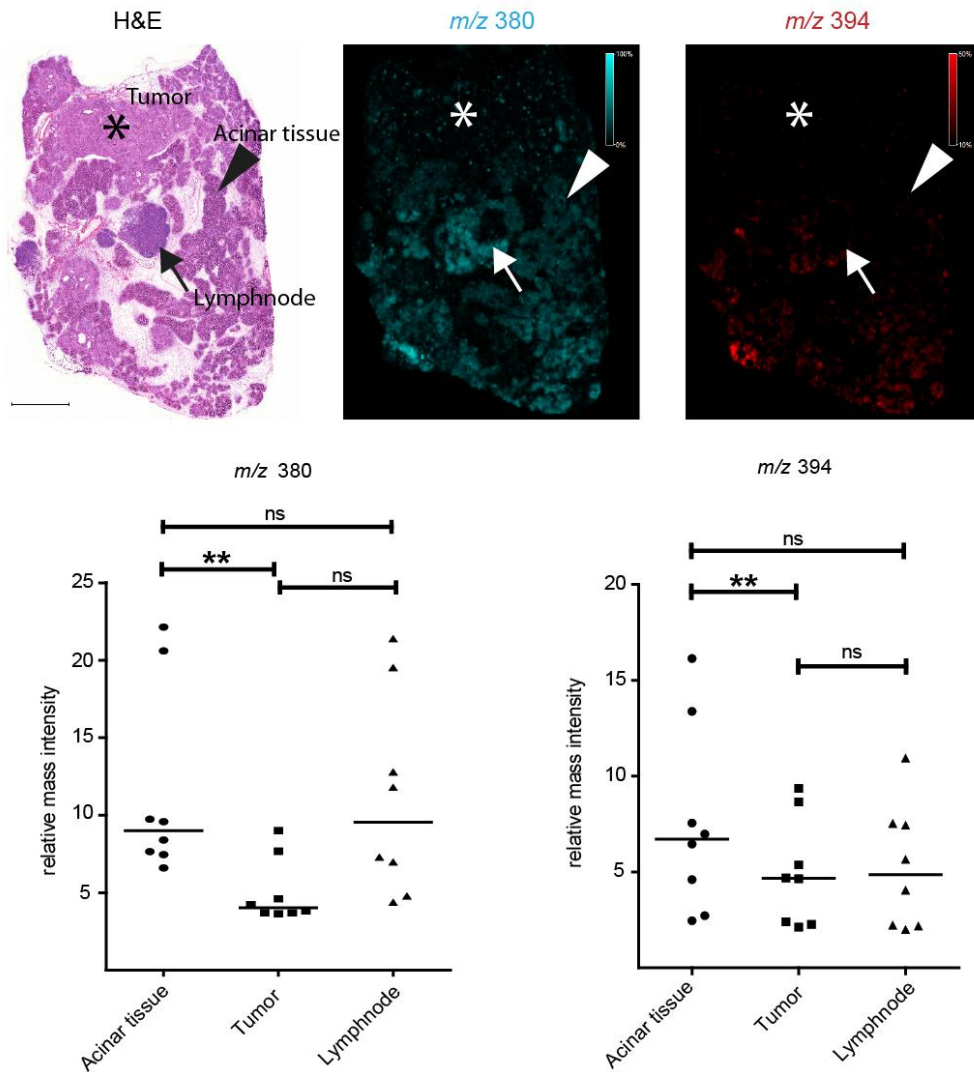
600 spectra per mouse were extracted and imported into ClinProTools to determine relative mass intensities for erlotinib ( $m/z = 394$  Da) and its active metabolite desmethyl-erlotinib ( $m/z = 380$  Da). One hour after drug application the relative intensities were highest in the pancreas for both masses (see Figure 3-9), therefore this time point was chosen for further analyses in PDAC bearing mice. Interestingly, the relative intensity of the metabolite was higher than that of erlotinib itself at any time point, indicating that drug metabolism is crucially

important to keep high levels of the drug in the tissue. Especially 4 hours after drug application, metabolite levels ( $m/z$  380) were still as high as at one hour time point although levels of erlotinib itself ( $m/z$  394) already decreased again.

### **3.2.2 Erlotinib levels are higher in healthy than in tumor bearing pancreatic compartments**

To determine if there are differences in the distribution and relative levels of erlotinib and its active metabolite in morphologically different pancreatic compartments, 8  $Kras^{G12D};p53^{KO}$  mice between 4 and 6 weeks of age were treated with a single dose of erlotinib and sacrificed after one hour. At this age mice of this phenotype have already developed PDAC but also have regions with still healthy acinar tissue. Additionally, 3  $Kras^{G12D};p53^{KO}$  mice were treated only with vehicle to ensure specificity of MALDI measurement. Sections of all mice were measured with MALDI-IMS to determine relative drug distribution. Re-visualization of relative drug intensities already depicted differences in the distribution of the drug in the pancreas. ROIs were defined for healthy acinar tissue, lymph nodes and PDAC on the sections and 500 randomly chosen spectra per region extracted and processed with ClinProTools to obtain not only visual but statistical data about distribution of erlotinib and its metabolite in the tumorigenic pancreas. Statistical analysis revealed significantly less erlotinib ( $p = 0.0078$ ) and metabolite ( $p = 0.008$ ) in tumorigenic tissue than in acinar tissue, indicating that the drug does not reach pancreatic tumors as efficiently as normal pancreatic tissue. Interestingly, the relative mass intensity in lymph nodes did not differ from that in tumors. This might be due to the distribution of the drug. Revisualization depicted high levels of drug and metabolite at the outer borders of the lymph nodes and nearly no signal in the middle of the nodes, indicating that drug and metabolite follow the fluid flow in the lymph nodes from cortex to medulla and that 1 hour was not enough to distribute in the whole lymph node (Figure 3-10).







### 3.2.3 Correlation of relative mass intensity with percentage of CD31-positive vessels in the tumor

To investigate whether the distribution of erlotinib in PDAC is correlated with the blood perfusion of the tumor, sections directly adjacent to the ones measured with MALDI were cut and stained for CD31 as marker for blood vessels. In parallel, ROIs in the tumors were defined, both on the MALDI-measured section and exactly the same on the CD31-adjacent section. For the definition of ROIs on the IHC-stained sections and the calculation of CD31-positive area percentage the Definiens software was used. This commercially available software detects and quantifies semantic classes (see 2.7.2). Average mass spectra for each ROI (12 ROIs per mouse section, 7 mice in total) for  $m/z$  394 and  $m/z$  380 were extracted and correlated with the percentage of CD31-positive area per total ROI area. Spearman correlation coefficient and linear regression coefficient for both masses were calculated. For  $m/z$  394 Spearman  $r_s = -0.009815$  and  $r^2 = 0.000002306$  and for  $m/z$  380  $r_s = -0.06650$  and  $r^2 = 0.004139$  were calculated.

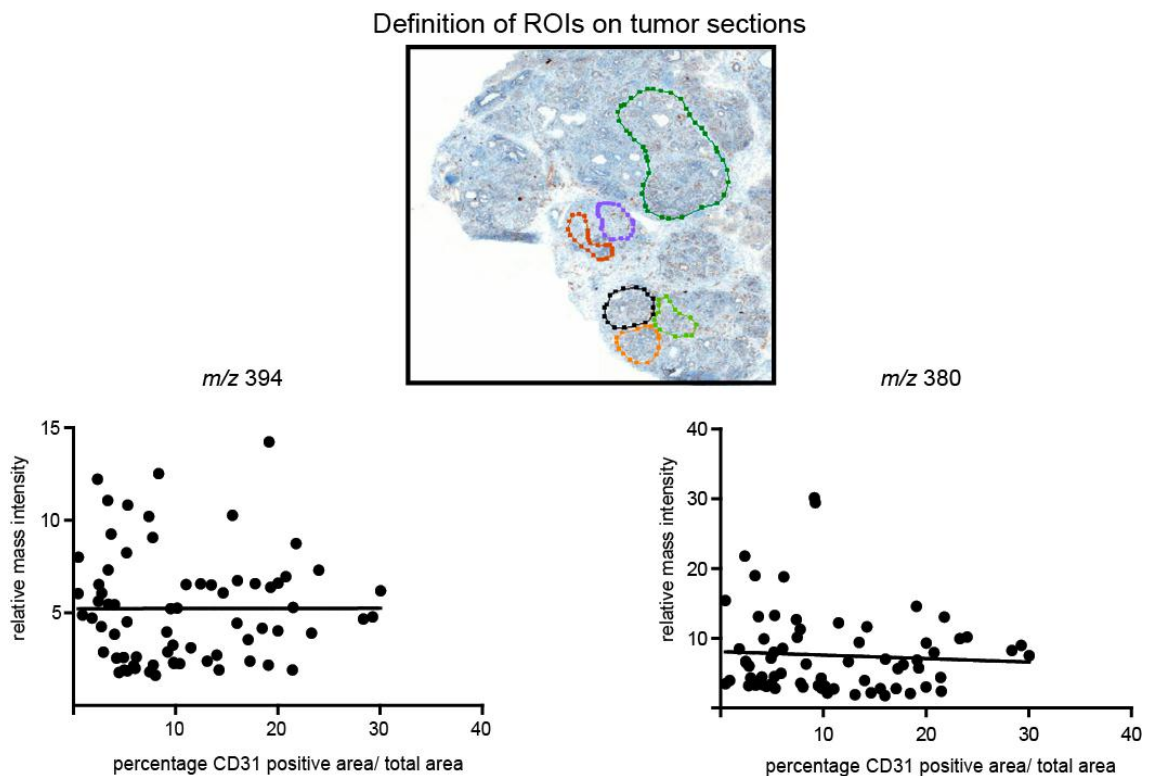


**Figure 3-11**

**Correlation of mass intensities of erlotinib and its metabolite with CD31-percentage.** In the upper panel ROI definition on a tumor section is depicted. For each mouse section 12 ROIs were defined. Below correlation of relative mass intensities of erlotinib (left site,  $m/z$  394) and its active metabolite (right site,  $m/z$  380) are depicted. As already obvious in the graphical illustration, CD31-percentage does not correlate with relative mass intensities of erlotinib and metabolite.

### 3.2.4 Correlation of mass intensity, proliferation rate and tumor differentiation

Since the relative mass intensities for erlotinib and its metabolite did not correlate with the perfusion in the tumor, it was investigated if there might be any correlation with other tumor characteristics. Therefore proliferation and differentiation of the tumors were analyzed. To determine the proliferation rate the sections adjacent to the ones measured with MALDI-IMS were stained for Ki67 (MKi67 gene encodes the Ki67 protein, a robust marker of cell proliferation [119]) and positive nuclei per total nuclei were calculated using the Definiens software. For differentiation an algorithm detecting ductal and diffuse stromal regions as well as unstained empty spaces was developed using the Definiens software. This was based on the distance between dark stained nuclei (see Figure 3-12).

Definition of ROIs on tumor sections

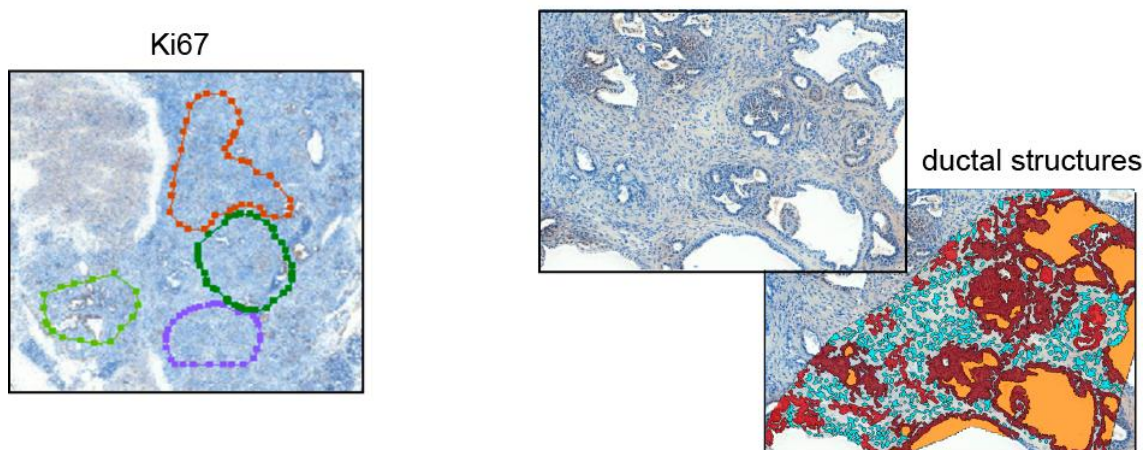


**Figure 3-12**

**Definition of ROIs for Ki67 and ductal structure analysis.** Depicted on the left is the definition of ROIs for Ki67-positive analysis, analog to definition of ROIs for CD31 (see above). On the right side an example for the algorithm detecting ductal structures is illustrated. As visible in the upper picture the algorithm can distinguish between white space (yellow), diffuse connective tissue (blue) and epithelial/ductal cells (light and dark red).

The percentage of ductal structures from whole ROI area but without white space was calculated. These values as well as the values for Ki67 were correlated with the relative mass intensities as described in 3.2.3. For the mass of erlotinib itself ( $m/z$  394) no correlation could be detected, neither with Ki67 ( $r_s = -0.1989$ ,  $r^2 = 0.003900$ ) nor with the percentage of ductal structures per ROI ( $r_s = -0.02199$ ,  $r^2 = 0.005594$ ). Figure 3-13 depicts the graphical illustrations of these correlations.

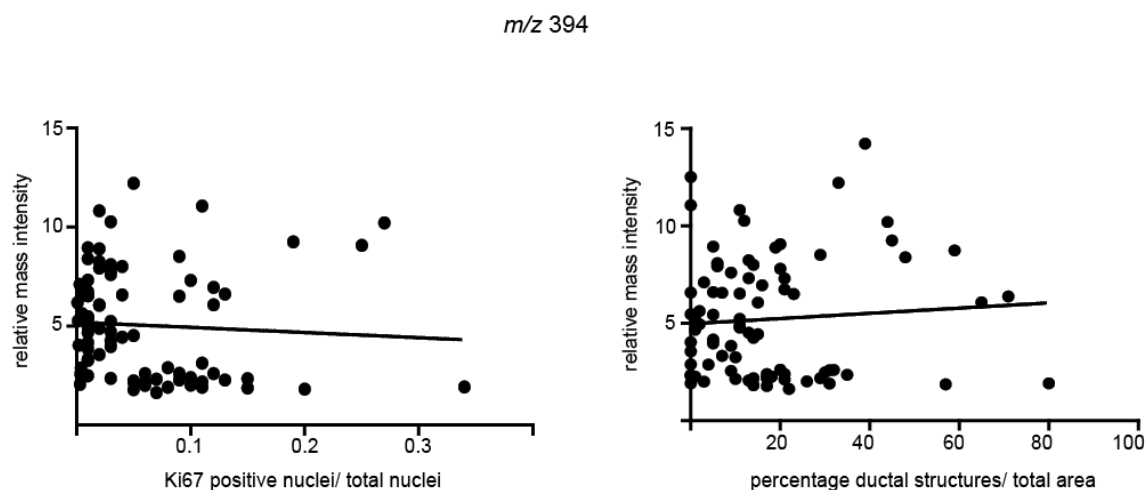


**Figure 3-13**

**Correlation of the relative mass intensity of  $m/z$  394 with proliferation and differentiation.** Depicted on the left side is the plot for Ki67 and mass intensity and on the right side for ductal structures and mass intensity. Both features do not correlate with erlotinib levels in the tumors.

For the active metabolite  $m/z$  380 however, there was a significant correlation both with the proliferation rate and the differentiation grade of the tumor. The more Ki67-positive nuclei per ROI were detectable the higher the relative mass intensity of the metabolite peak ( $r_s = 0.3819$ ,  $r^2 = 0.1510$ ). Also, the more ductal structures in the ROI the higher the relative mass intensity for the metabolite ( $r_s = 0.3477$ ,  $r^2 = 0.1446$ ). Although the correlation was not strikingly obvious, the  $p$ -values for the significance of the correlations were very low ( $p = 0.0004$  for the Ki67 correlation,  $p = 0.0014$  for ductal structure correlation). This indicates that these tumor properties might not be exclusively responsible for drug distribution but are clearly involved in the processes determining drug distribution (see Figure 3-14).

*m/z* 380

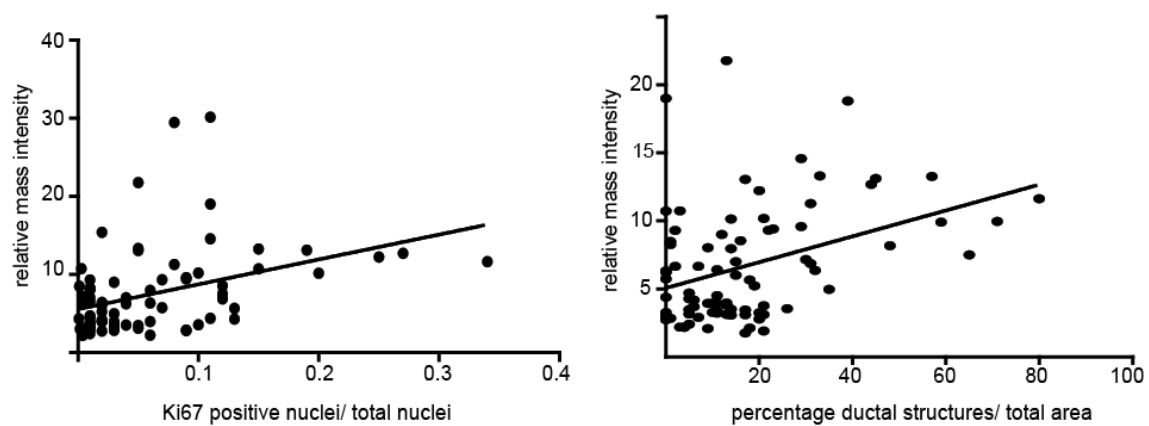


**Figure 3-14**

**Correlation of *m/z* 380 intensity with proliferation and differentiation.** The relative peak intensity of the active metabolite of erlotinib correlates with the number of Ki67-positive nuclei (left side) and also with the percentage of ductal structures per ROI (right side).

### 3.3 EGFR is essential for RAS-driven pancreatic carcinogenesis

#### 3.3.1 EGFR pathway upregulation precedes tumorigenesis in *Kras*<sup>G12D</sup> mice

EGFR is upregulated in PDAC [77, 120, 121] though its function has primarily been associated with enhanced proliferation and invasiveness [122-125]. To better dissect the role of EGFR in PDAC progression, it was tested if EGFR was activated in the *Kras*<sup>G12D</sup> mouse model, which reproducibly shows metaplasia and PanIN formation beginning at approximately 8 weeks of age, with progression to PDAC at around 1 year [26]. Immunohistochemistry for active EGFR (pY1068) was undetectable in the wild type pancreas, but easily detectable in acinar areas prior to tumor formation in 30 day old *Kras*<sup>G12D</sup> mice and in the lesions themselves in 3 months old *Kras*<sup>G12D</sup> mice (Figure 3-15).

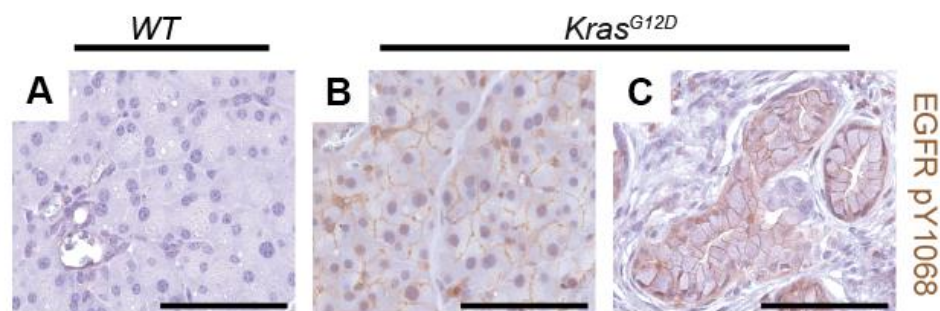


**Figure 3-15**  
**Activation of EGFR signaling during early PDAC development in *Kras*<sup>G12D</sup> mice.** (A-C) Staining for active EGFR (pY1068) in tissue sections of wild type and *Kras*<sup>G12D</sup> mice displays increased EGFR activation early during PDAC development. Scale bars = 50  $\mu$ m.

Also staining for total EGFR showed EGFR upregulation in discrete acinar cell clusters in *Kras*<sup>G12D</sup> pancreata, becoming very prominent in larger acinar clusters, especially near areas of metaplasia and PanIN and was particularly high in metaplasia and PanINs (Figure 3-16). These data suggest that upregulation of the EGFR pathway is a very early event in pancreatic tumorigenesis. Interestingly, the stochasticity of EGFR overexpression in acini

prior to tumor formation was reminiscent of the pattern of tumor formation in these mice, suggesting a possible role for EGFR signaling in transformation of the acinar cell compartment.

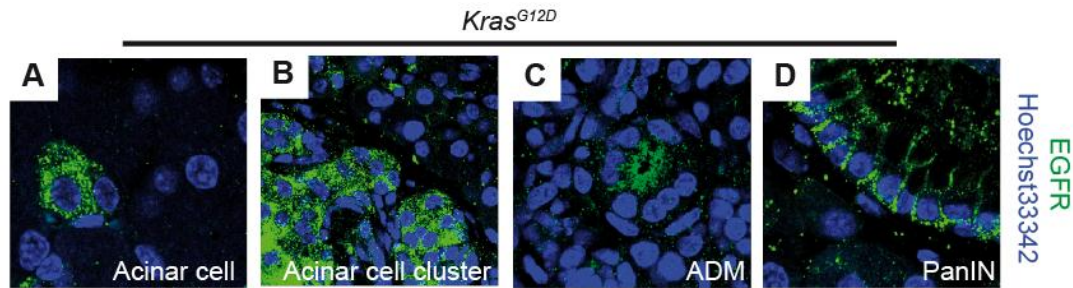


**Figure 3-16**  
**Upregulated EGFR expression during early PDAC development in *Kras*<sup>G12D</sup> mice.** (A-D) Confocal analysis shows EGFR expression already in distinct single acinar cells (A) and acinar cell clusters (B) of *Kras*<sup>G12D</sup> mice prior to formation of ADM (C) and PanINs (D).

To test if EGFR activation in acinar cells was coincident with transdifferentiation to a duct phenotype, primary acinar cell explants isolated from *Kras*<sup>G12D</sup> mice were examined, which spontaneously transdifferentiate into duct cells when embedded in fibrillar collagen. On the first day of culture, active pY1068 EGFR was undetectable, but was strongly positive by the third day, as transdifferentiation took place (Figure 3-17 A,B). As *in vivo*, this upregulation correlated with increased expression of EGFR, as determined by qRT-PCR (Figure 3-17 C). Thus, EGFR upregulation and activation is initiated by KRAS *in vitro* and *in vivo* in a manner consistent with its involvement in acinar cell transdifferentiation to preneoplastic ducts.

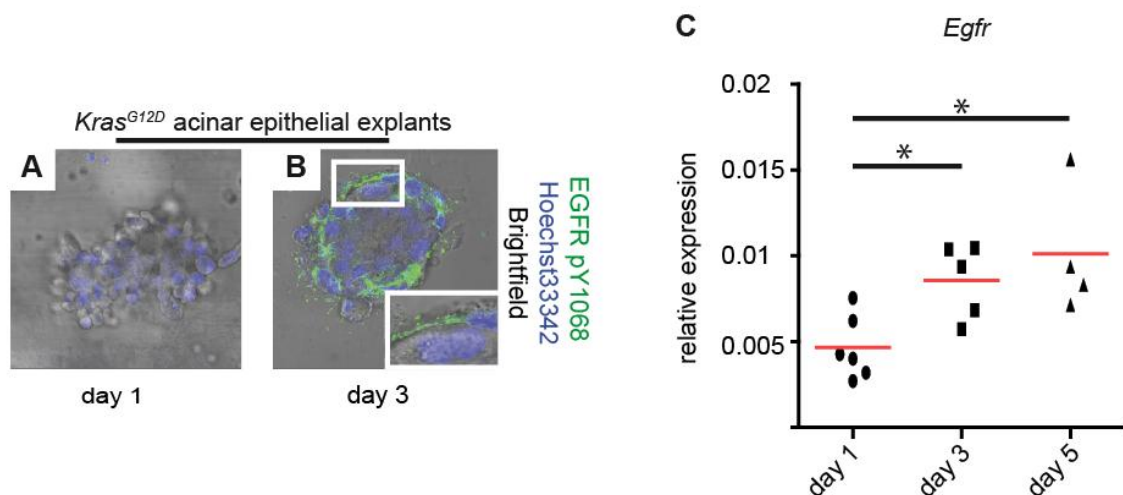




**Figure 3-17**

**Upregulated EGFR expression and activation during ADM of acinar explants from *Kras*<sup>G12D</sup> mice *in vitro*.** (A-C) Staining (A,B) and qRT-PCR analysis (C) of acinar epithelial explants from *Kras*<sup>G12D</sup> mice show upregulation of Egr expression (n = 4 to 6 per group, day 1 to day 3 p = 0.03, day 1 to day 5 p = 0.019) and EGFR activation during ADM *in vitro*.

### 3.3.2 EGFR activity is required for pancreatic tumorigenesis

To test the hypothesis that EGFR activity is required for pancreatic preneoplastic lesion formation, the effects of pharmacological EGFR inhibition in a highly aggressive model of PDAC were examined. *Kras*<sup>G12D</sup>;*p53*<sup>KO</sup> develop cancer at 4-6 weeks of age [30]. Starting at 1 week of age, *Kras*<sup>G12D</sup>;*p53*<sup>KO</sup> mice were treated daily with either erlotinib, a small molecule EGFR tyrosine kinase inhibitor; cetuximab, a monoclonal antibody that blocks ligand interaction with the receptor (due to high half-life of antibodies cetuximab treatment was only on two days per week in this group, the other days vehicle was applied to ensure comparable handling); or vehicle for 3 weeks. Histological examination of the pancreata showed substantial areas of normal, non-transformed tissue with either treatment and a significantly reduced number of CK19<sup>+</sup> ductal lesions compared to vehicle control (Figure 3-18).

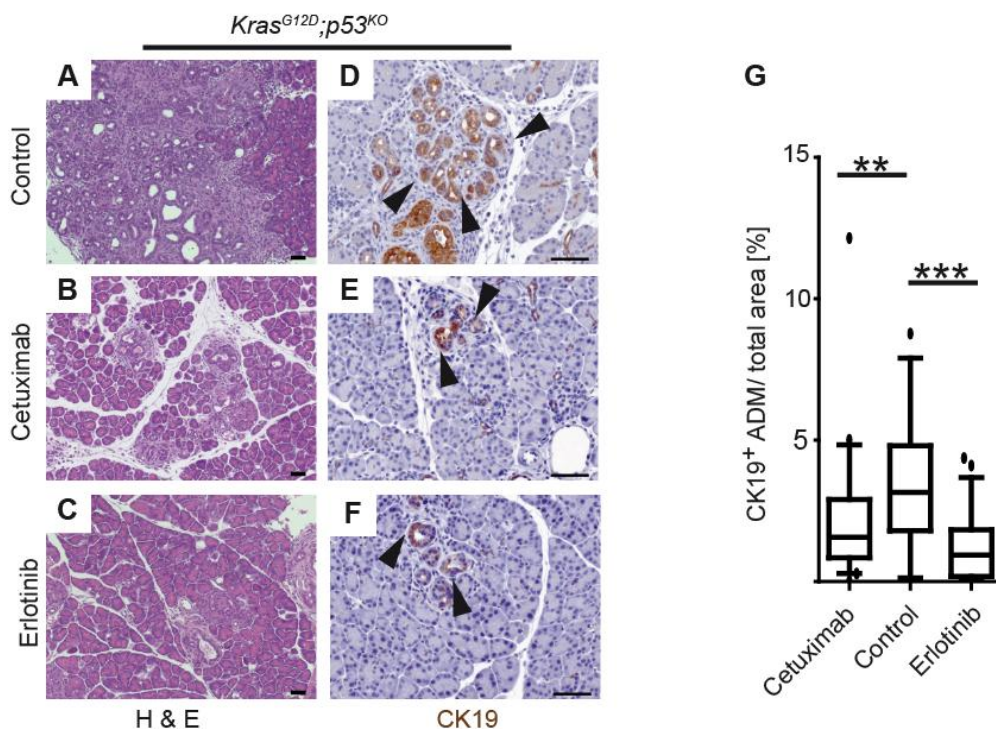


### Figure 3-18

**Pharmacological inhibition of EGFR signaling blocks KRAS-driven tumorigenesis.** (A-F) Histological analysis of 4 week old  $Kras^{G12D};p53^{KO}$  mice treated for 3 weeks with cetuximab, erlotinib or vehicle displays reduced tumor burden (A-C) and development of CK19<sup>+</sup> ADM and ductal lesions (D-F) in cetuximab and erlotinib treated animals in comparison to controls. (G) Quantitation of CK19<sup>+</sup> ADM revealed significantly reduced levels in cetuximab and erlotinib treated mice (n = 3, \*\* p < 0.01, \*\*\* p < 0.001). Scale bars represent 50  $\mu$ m.

The retention of substantial areas of normal tissue with EGFR inhibition supported a role for EGFR signaling in tumorigenesis, distinct from any contribution to cancer progression. To test this possibility definitively, mice with conditional *Egfr* knockout [110] were crossed to the established  $Kras^{G12D}$  model. In this construct part of the promoter and the first exon of the *Egfr* gene are flanked by *loxP* sites. *Egfr*<sup>KO</sup> mice with EGFR ablated from the pancreas were viable and developed a functional pancreas with no gross abnormalities (data not shown). Figure 3-19 A depicts the schematic illustration of the knockout construct. PCR specifically detecting the truncated allele in the pancreas was performed to test correct recombination (Figure 3-19 B), and Western Blot analysis of whole pancreatic lysates depicted loss of the protein in  $Kras^{G12D};Egfr^{KO}$  mice (Figure 3-19 C).

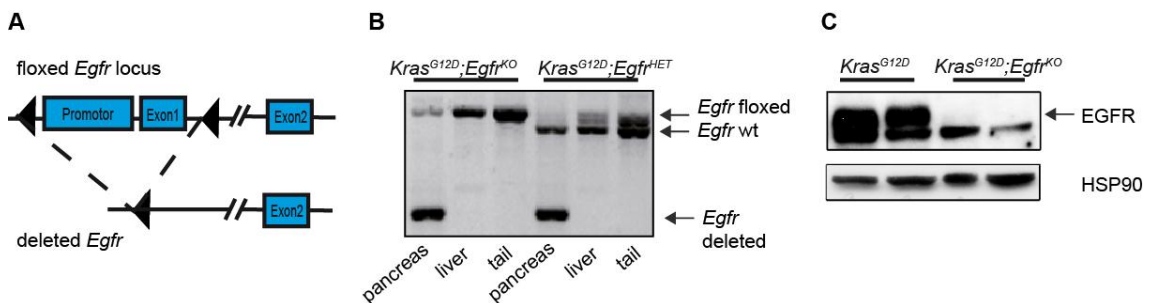


### Figure 3-19

**Conditional *Egfr*-knockout construct.** (A) For conditional knockout of *Egfr* part of the promoter and the first exon are flanked by *loxP* sites. Upon *Cre*-mediated recombination these parts of the *Egfr* gene are deleted resulting in a total knockout of the gene; black triangles represent the *loxP* sites. Adapted after [110]. (B) PCR for correct recombination of *loxP* sites depicts specific deletion of *Egfr* in the pancreas of  $Kras^{G12D};Egfr^{KO}$  and  $Kras^{G12D};Egfr^{HET}$  mice. (C) Western Blot analysis of whole pancreatic lysates from  $Kras^{G12D};Egfr^{KO}$  mice shows loss of the protein in the pancreas in comparison to  $Kras^{G12D}$  controls.

Tumor burden of  $Kras^{G12D}$  and  $Kras^{G12D};Egfr^{KO}$  mice was assessed at various ages by relative pancreatic mass, histological analysis and appearance of MUC5AC<sup>+</sup> ductal lesions. By all criteria, *Egfr* ablation resulted in an almost



complete blockade in KRAS-driven tumorigenesis (Figure 3-20 A-H). This blockade was not due to a failure to recombine the silenced *Kras*<sup>G12D</sup> allele in these mice (Figure 3-20 M). Consistent with the EGFR inhibitor experiments, genetic ablation of *Egfr* in the *Kras*<sup>G12D</sup>;*p53*<sup>KO</sup> mice also greatly inhibited, but did not entirely eliminate, PDAC formation in these mice (Figure 3-20 I-L).

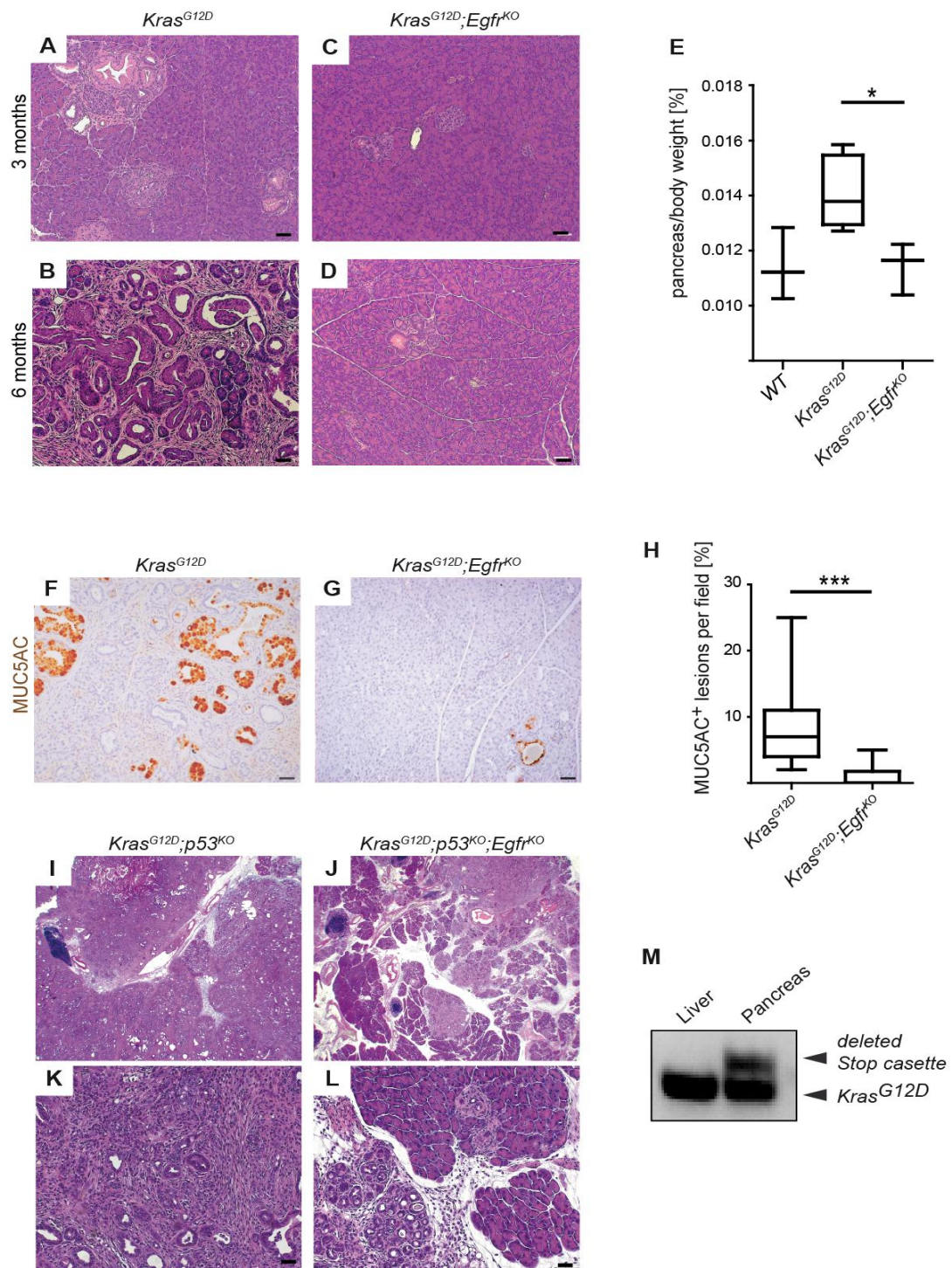


**Figure 3-20**

**Inhibition of EGFR signaling blocks KRAS-driven tumorigenesis.** (A-D) Histological analysis of 3 months (A,C) and 6 months (B,D) old  $Kras^{G12D}$  and  $Kras^{G12D};Egfr^{KO}$  mice depicted almost complete blockage of PanIN development in  $Kras^{G12D};Egfr^{KO}$  mice (C,D) in comparison to  $Kras^{G12D}$  mice (A,B). (E) Pancreas to body weight index measurement shows that in  $Kras^{G12D};Egfr^{KO}$  mice the index is reduced almost to wild type levels. (F-H) Staining (F,G) and quantification (H) of Muc5AC as marker for PanINs illustrates clear reduction in  $Kras^{G12D};Egfr^{KO}$  mice in comparison to  $Kras^{G12D}$  mice. (I-L) Even in the highly aggressive  $Kras^{G12D};p53^{KO}$  model  $Egfr$  depletion results in a clear reduction of tumor burden (J,L) in comparison to  $Kras^{G12D};p53^{KO}$  control mice. (M)  $Kras^{G12D}$  recombined PCR displays correct deletion of the *Stop cassette* preceding the mutated allele. All scale bars represent 50  $\mu$ m.

### 3.3.3 Pancreatitis-associated tumorigenesis requires EGFR

When oncogenic *Kras* expression is confined to the acinar cell compartment, pancreatitis is required for PDAC formation [11, 126]. The initiation of EGFR overexpression in acinar cells suggested that EGFR ablation was blocking transformation of this cellular compartment. To test if EGFR activity is required for pancreatitis-dependent, acinar cell-derived tumorigenesis, 4 week old  $Kras^{G12D}$  and  $Kras^{G12D};Egfr^{KO}$  mice were treated with 6 hourly injections of cerulein, a known inducer of pancreatic damage, on 2 consecutive days according to a protocol established by Morris and colleagues [111]. With cerulein treatment,  $Kras^{G12D}$  mice showed an almost complete replacement of normal pancreatic tissue with fibrotic, inflamed tissue and the majority of the epithelia replaced by metaplasia and PanIN 21 days after induction. Once again,  $Kras^{G12D};Egfr^{KO}$  mice were almost completely protected from this dramatic transition (Figure 3-21).

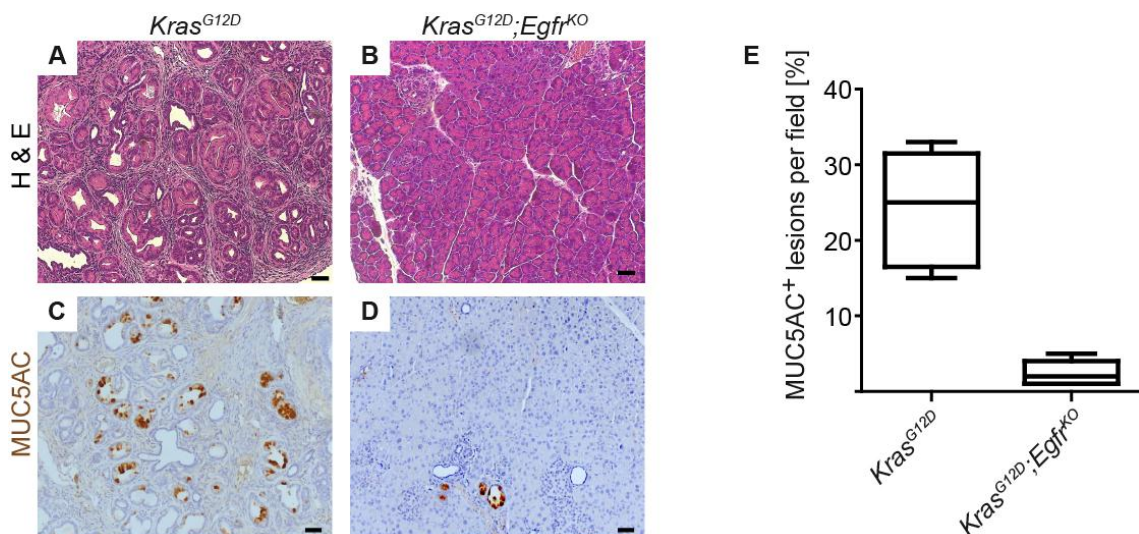




**Figure 3-21**

**EGFR depletion blocks Cerulein-induced PanIN formation in KRAS-driven tumorigenesis.** In  $Kras^{G12D}$  mice cerulein-induced acute pancreatitis promotes PanIN formation (A,C) whereas in  $Kras^{G12D};Egfr^{KO}$  mice (B,D) this process is almost completely blocked. (E) Quantification of Muc5AC positive PanINs in  $Kras^{G12D}$  and  $Kras^{G12D};Egfr^{KO}$  mice. All scale bars represent 50  $\mu$ m.

### 3.3.4 EGFR activity is required for the formation of metaplastic ducts

The dependency of acinar-cell derived pancreatic tumorigenesis on pancreatitis has been ascribed to the need for acinar-to-ductal metaplasia (ADM) prior to transformation [126]. Chronic activation of EGFR is known to be sufficient to induce ductal metaplasia *in vitro* [127] and *in vivo* [25]. To explore the possibility that EGFR signaling is necessary for this process, several *in vivo* and *in vitro* models of ADM were employed. Chronic transgenic overexpression of the EGFR ligand TGFA in the *Ela-Tgfa* transgenic model induces substantial ductal metaplasia and fibrosis after several weeks of transgene expression [25]. Ablation of *Egfr* effectively blocked TGFA-induced metaplasia *in vivo* even at one year of age, reinforcing the dependency on EGFR signaling of the ADM process (Figure 3-22 A&B). Also in the  $Kras^{G12D};Tgfa$  model at 7 days of age *Egfr* ablation blocked ADM of acinar cells but the stromal reaction typical for TGFA overexpression was still present. The 7 day time point was chosen to determine the effects of TGFA overexpression and EGFR ablation prior to total pancreatic morphological transformation (Figure 3-22 C&D).

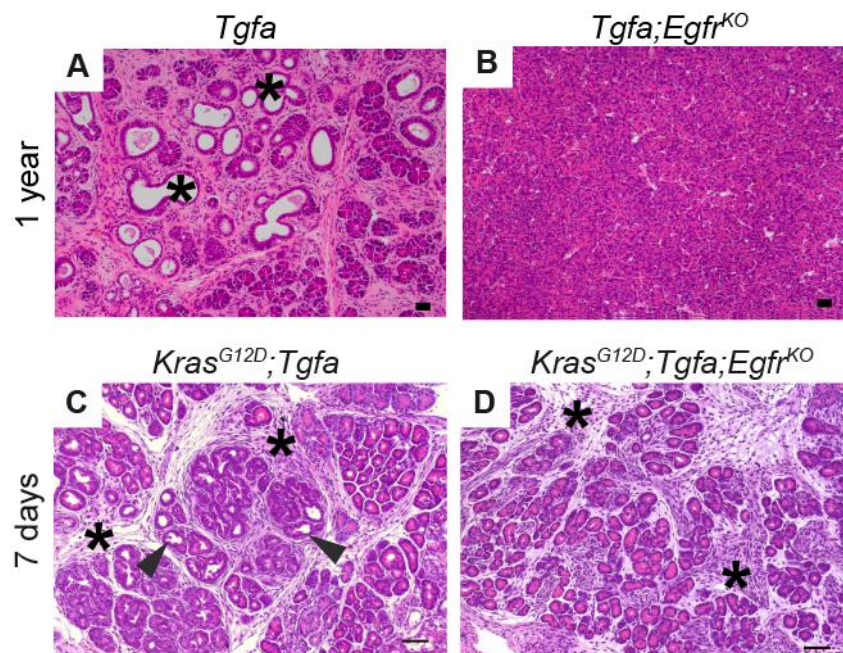


**Figure 3-22**

**EGFR activity is required for the formation of metaplastic ducts *in vivo*.** (A,B) 1-year old *Tgfa* mice show induction of extensive ADM (asterisks, A) and fibrosis, which is not detectable in *Tgfa;Egfr<sup>KO</sup>*. (C,D) In 7 day old *Kras<sup>G12D</sup>;Tgfa* ADM (arrowheads, C) and strong stromal reaction (asterisks, C) are depicted whereas in *Kras<sup>G12D</sup>;Tgfa;Egfr<sup>KO</sup>* mice (D) ADM is blocked but fibrosis (asterisks, D) is still detectable. Scale bars represent 50  $\mu$ m.

Next it was tested if *in vitro* ADM required EGFR activation. *In vitro* ADM in collagen-embedded acinar cell explants of *WT* mice is usually induced by the addition of ectopic EGFR ligand. To investigate whether ADM is inducible in acinar explants of *Egfr<sup>KO</sup>* mice they were stimulated with EGF for five days in culture. Unlike explants of *WT* mice transdifferentiation to a duct-like phenotype was blocked in *Egfr<sup>KO</sup>* explants, as additionally determined by coimmunofluorescence for the acinar and duct cell markers, amylase and Cytokeratin 19 (CK19), respectively (Figure 3-23 A&B). To bypass a direct stimulation of EGFR while investigating ADM *in vitro*, acinar explants from *Kras<sup>G12D</sup>* mice were taken into culture. Acinar explants from *Kras<sup>G12D</sup>* mice transdifferentiate spontaneously to duct-like structures in culture within 3 days. This transition was almost entirely absent in explants derived from *Kras<sup>G12D</sup>;Egfr<sup>KO</sup>* mice (Figure 3-23 C&D), with the transdifferentiation process arrested at a nestin-positive intermediate [128], a marker normally expressed in mesenchymal and not epithelial cells of the developing mouse pancreas [129] (Figure 3-23 E). This indicates that the transdifferentiation process starts but does not progress and EGFR plays an important role for this progression.

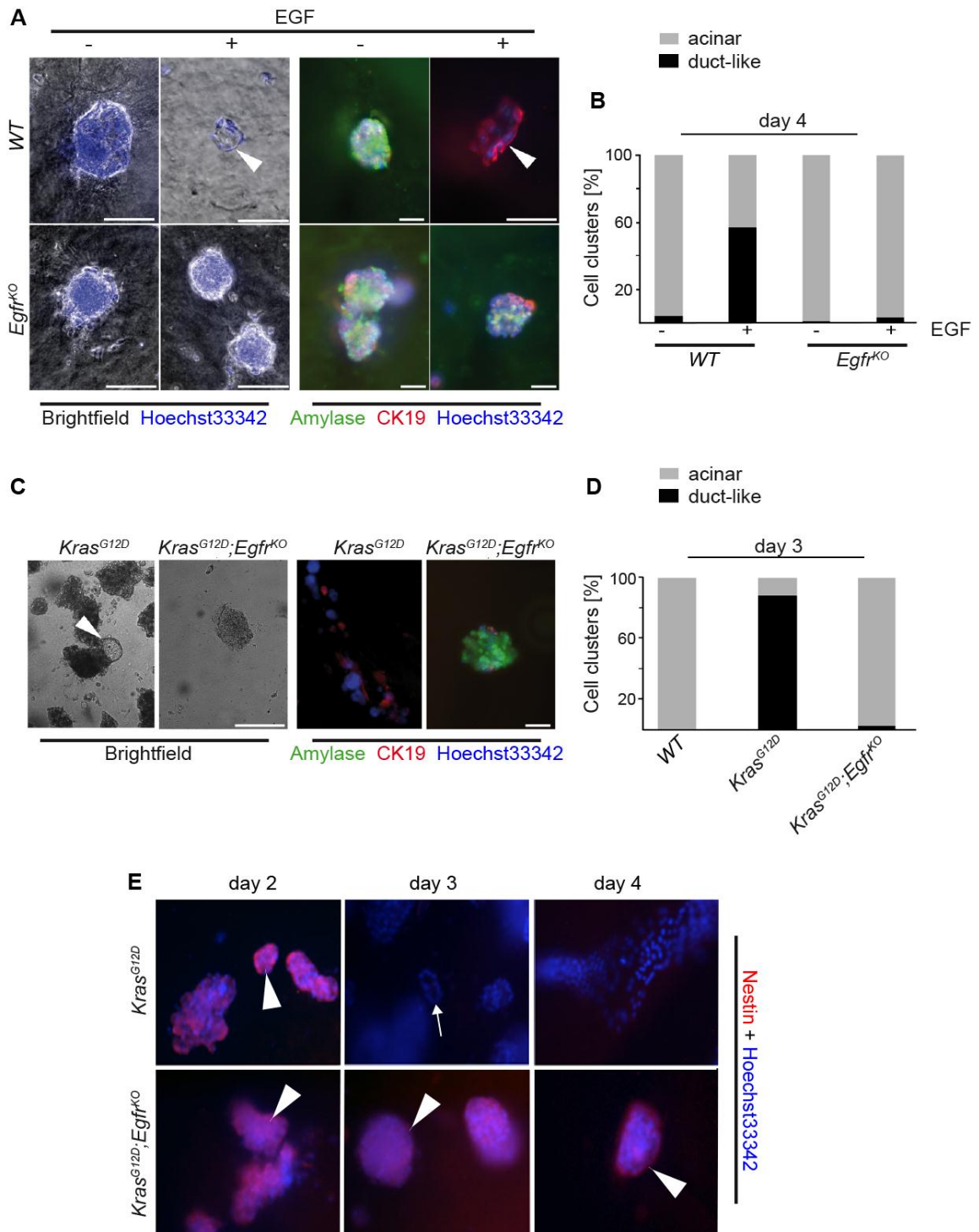


**Figure 3-23**

**EGFR signaling is required for KRAS-induced acinar cell transdifferentiation *in vitro*.**

(A,B) EGF-induced ADM in wild type acinar epithelial explants (upper panel) is blocked in *Egfr*<sup>KO</sup> (lower panel) acinar explants. Arrowheads point to duct-like structures or positive staining for CK19, respectively. (C,D) Acinar epithelial explants of *Kras*<sup>G12D</sup> mice undergo spontaneous ADM after three days in three-dimensional collagen culture and show a duct-like phenotype (white arrowhead) accompanied by CK19 expression and loss of Amylase expression. In *Kras*<sup>G12D</sup>;*Egfr*<sup>KO</sup> acinar cells this process is blocked, showing an acinar phenotype after three days in culture comparable to wild type controls. Scale bars represent 20  $\mu$ m. (B&D)

Quantitations show one representing out of at least 5 independent experiments per genotype. (E) Staining for the intermediate progenitor marker Nestin (white arrowheads) in acinar epithelial explants of *Kras*<sup>G12D</sup> mice is positive at day 2 in culture and lost again at day 3 upon ductal transdifferentiation (upper panel, white arrow). In acinar epithelial explants of *Kras*<sup>G12D</sup>; *Egfr*<sup>KO</sup> mice, Nestin expression is detectable at day 2 and remains expressed at day 3 and 4 in culture (lower panel). Scale bar = 20 μm.

### 3.3.5 RAS activity levels and localization are not altered in *Kras*<sup>G12D</sup>; *Egfr*<sup>KO</sup> pancreata

Pancreatic tumorigenesis is dependent on amplified activation of RAS GTPases. Sufficient RAS activity in pancreatic acinar cells induces several important pancreatic disease manifestations, including PDAC [130]. Therefore it was tested whether the levels of active GTP-bound KRAS differ between *Kras*<sup>G12D</sup> and *Kras*<sup>G12D</sup>; *Egfr*<sup>KO</sup> pancreata. However, while Raf-RGD peptide pulldown of GTP-bound KRAS and western blot of total KRAS confirmed the previously described upregulation of both active and total KRAS protein in *Kras*<sup>G12D</sup> mice [130], these levels were not detectably different in *Kras*<sup>G12D</sup>; *Egfr*<sup>KO</sup> lysates (Figure 3-24 A). Furthermore, active EGFR is known to relocalize wild type KRAS to the plasma membrane via Grb2/Sos where it is activated [131, 132]. Co-immunoprecipitation of KRAS and EGFR in primary murine PDAC cell lines (see 2.5.1) and co-immunofluorescence for KRAS and EGFR on pancreatic tissue sections from 3 months old *Kras*<sup>G12D</sup> mice showed a clear interaction (Figure 3-24 B) and colocalization (Figure 3-24 C) of KRAS and EGFR. Nevertheless, KRAS localization was not altered in acinar explants from *Kras*<sup>G12D</sup>; *Egfr*<sup>KO</sup> mice in comparison to explants *Kras*<sup>G12D</sup> controls (Figure 3-24 D). Therefore it was concluded that differences in KRAS activity and localization were not responsible for the dramatic effects in *Kras*<sup>G12D</sup>; *Egfr*<sup>KO</sup> mice. Interestingly, in 7 day old *Kras*<sup>G12D</sup>; *Egfr*<sup>KO</sup> pancreata relative expression levels of the main EGFR ligands *Tgfa* and *Egf* were not altered in comparison to *Kras*<sup>G12D</sup> pancreatic lysates. On the contrary – although not statistically significant - they were even slightly higher, indicating that oncogenic KRAS promotes expression of EGFR ligands (Figure 3-24 E,F).

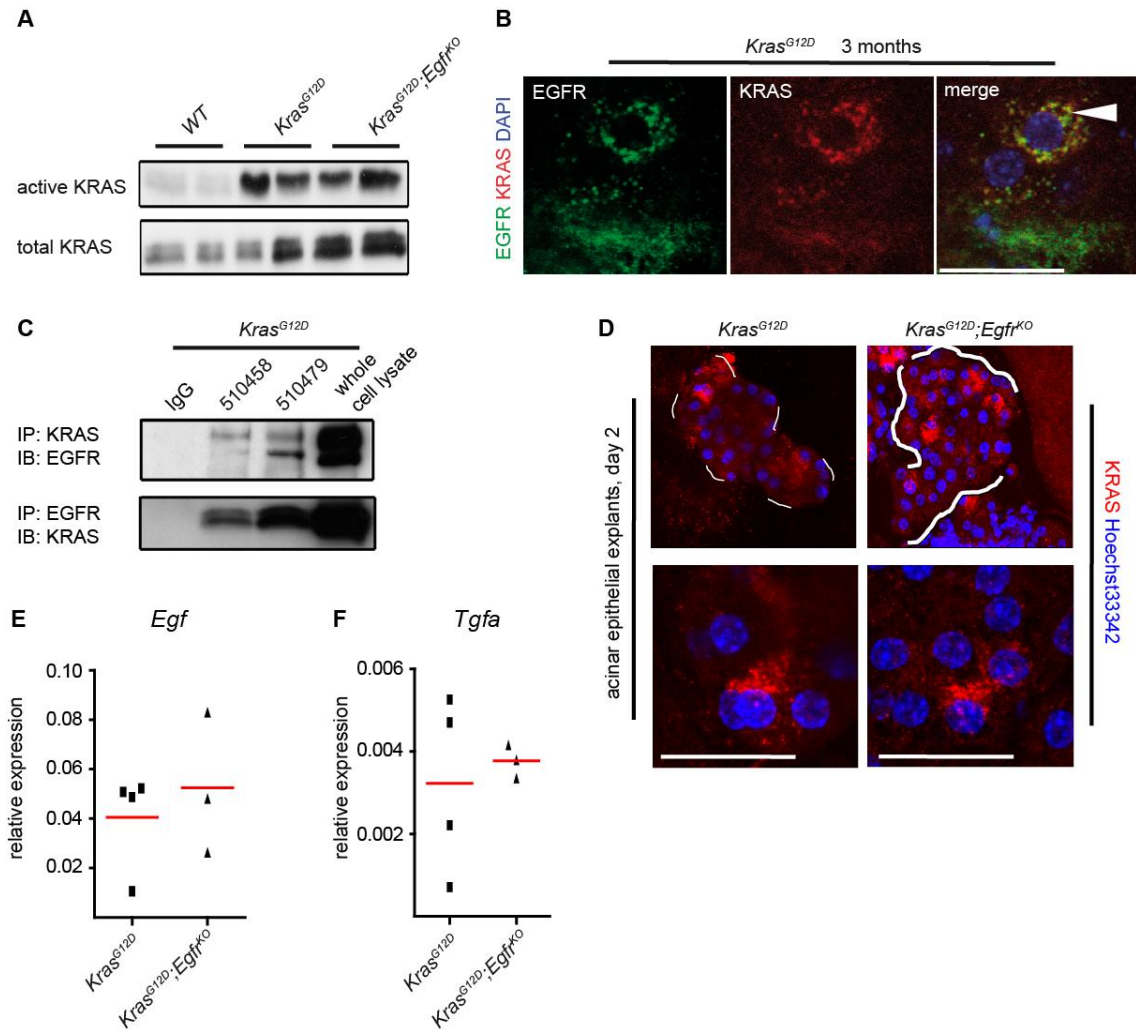


**Figure 3-24**

**RAS activity levels and localization are not altered in  $Kras^{G12D};Egfr^{KO}$  pancreata.** (A) RAS activity assay shows high levels of active GTP-bound KRAS in  $Kras^{G12D}$  and  $Kras^{G12D};Egfr^{KO}$  mice. (B) Confocal analysis of EGFR and KRAS localization in pancreata of 3 months old  $Kras^{G12D}$  mice depicts clear colocalization (arrowhead). (C) KRAS and EGFR can be immunoprecipitated in  $Kras^{G12D}$  derived tumor cell lines. IgG: negative control precipitated with isotype IgG; whole cell lysate served as positive control for the western blot. Numbers represent two different  $Kras^{G12D}$  cell lines. (D) Confocal analysis of KRAS localization in acinar epithelial explants from  $Kras^{G12D}$  and  $Kras^{G12D};Egfr^{KO}$  mice on day 2 in culture shows no difference in KRAS localization between the genotypes. All scale bars represent 10  $\mu$ m. (E,F) relative expression levels of *Egf* (E) and *Tgfa* (F) in whole pancreatic lysates from  $Kras^{G12D}$  and  $Kras^{G12D};Egfr^{KO}$  mice at 7 days of age.

### 3.3.6 EGFR-dependent ERK activation is required for pancreatic tumorigenesis

Pancreatic tumorigenesis is dependent on several molecules that have been associated with the EGFR signaling, including STAT3 activation [80, 133]. IHC for active phospho-STAT3 in  $Kras^{G12D}$  and  $Kras^{G12D};Egfr^{KO}$  pancreata showed



substantial focal regions of highly elevated levels of staining, resembling the staining pattern for active EGFR, and no quantitative difference by western blot compared to *Kras*<sup>G12D</sup> controls.

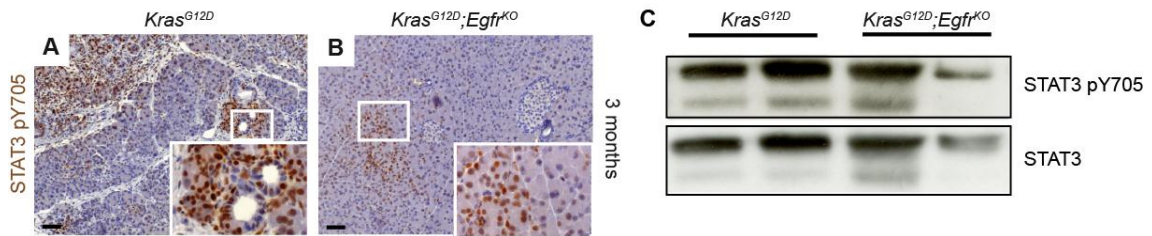


**Figure 3-25**  
**STAT3 activity is not changed in *Kras*<sup>G12D</sup>;*Egfr*<sup>KO</sup> pancreata.** (A,B) Staining for STAT3 pY705 depicts high STAT3 activity in *Kras*<sup>G12D</sup> mice centered in PanINs and surrounding acinar cells (A) and also focal areas of high activity in *Kras*<sup>G12D</sup>;*Egfr*<sup>KO</sup> mice (B). Scale bars represent 50  $\mu$ m. (C) Western Blot analysis for active and total STAT3 illustrated no substantial differences in pancreatic lysates of 4 week old *Kras*<sup>G12D</sup> and *Kras*<sup>G12D</sup>;*Egfr*<sup>KO</sup> mice.

Next it was explored if there were any differences on the activity levels of pathways that contribute to the transforming potential of unregulated KRAS signaling, including RAC1, PI3K/AKT (pAKT) and MAPK (pERK1/2). While RAC1 is an appealing target known to contribute to pancreatic tumorigenesis [134], no significant differences in the levels of active RAC1 in *Kras*<sup>G12D</sup> and *Kras*<sup>G12D</sup>;*Egfr*<sup>KO</sup> lysates were found and no evidence of F-actin reorganization associated with the *Kras*<sup>G12D</sup>;*Rac1*<sup>KO</sup> model as shown by previous work from our lab [134] could be detected (Figure 3-26).

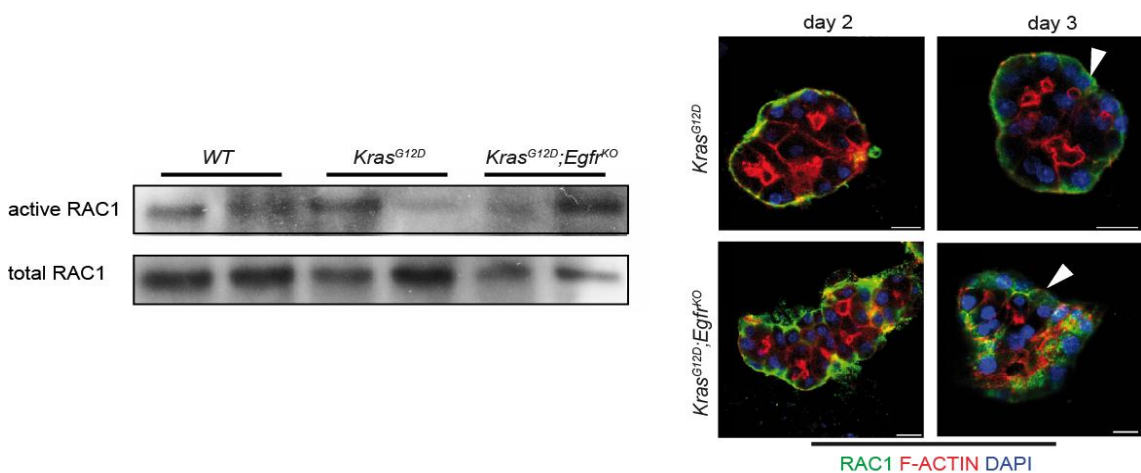


**Figure 3-26**  
**RAC1 activity is not different in *Kras*<sup>G12D</sup>;*Egfr*<sup>KO</sup> pancreata.** RAC1 activity assay (left side) shows no difference between *Kras*<sup>G12D</sup> and *Kras*<sup>G12D</sup>;*Egfr*<sup>KO</sup> mice. Also staining for RAC1 and F-



actin in acinar epithelial explants of *Kras*<sup>G12D</sup> (right side, upper panel) and *Kras*<sup>G12D</sup>;*Egfr*<sup>KO</sup> mice (right side, lower panel) depicts typical apical (arrowhead) and no basal localization of F-actin and comparable levels of RAC1 after two or three days in culture. Scale bars equal 10 μm.

*Kras*<sup>G12D</sup>;*Egfr*<sup>KO</sup> mice showed no diminution of active AKT compared to control *Kras*<sup>G12D</sup> mice (Figure 3-27), suggesting no difference in PI3K activity. In contrast, approximately 2-fold lower levels of pERK in 3 months old *Kras*<sup>G12D</sup>;*Egfr*<sup>KO</sup> pancreatic lysates were observed. Since this difference may be an indirect effect of enhanced pERK levels in tumors that form only in *Kras*<sup>G12D</sup> controls, a similar loss of pERK in 4-week-old pancreatic lysates, prior to substantial transformation was confirmed (Figure 3-27).

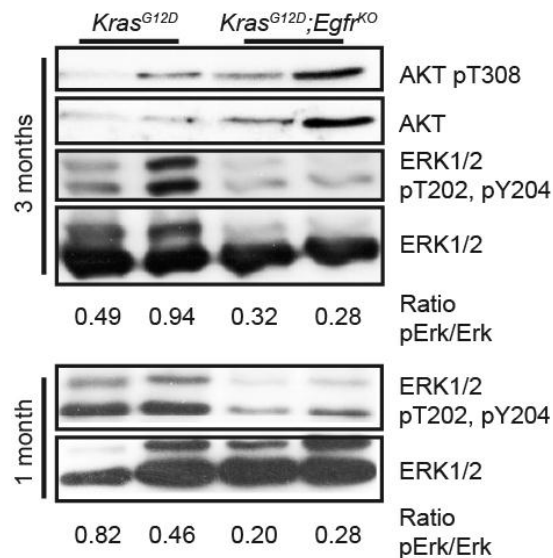


**Figure 3-27**

**Levels of active ERK are reduced in *Kras*<sup>G12D</sup>;*Egfr*<sup>KO</sup> pancreata.** Western Blot analysis of whole pancreatic lysates exhibits no significant change in AKT signaling in *Kras*<sup>G12D</sup>;*Egfr*<sup>KO</sup> mice in comparison to *Kras*<sup>G12D</sup> controls (upper panels) but reduced levels of ERK pT202,pY204 in 3 months old mice (middle panels) and even in only 1 month old (lower panels) *Kras*<sup>G12D</sup>;*Egfr*<sup>KO</sup> mice. Numbers indicate ratio of pERK/total ERK densitometric quantitation.

To assess if the effect of EGFR on ERK activation, even in the context of constitutive active KRAS, is also maintained in tumor cells, primary murine cell lines of PDAC from two *Kras*<sup>G12D</sup>;*p53*<sup>KO</sup> and two *Kras*<sup>G12D</sup>;*p53*<sup>KO</sup>;*Egfr*<sup>KO</sup> were isolated and taken into culture. Already the basic levels of pERK were reduced in *Kras*<sup>G12D</sup>;*p53*<sup>KO</sup>;*Egfr*<sup>KO</sup> cell lines in comparison to control *Kras*<sup>G12D</sup>;*p53*<sup>KO</sup> lines. After stimulation with full medium or EGF, pERK levels were also clearly lower.

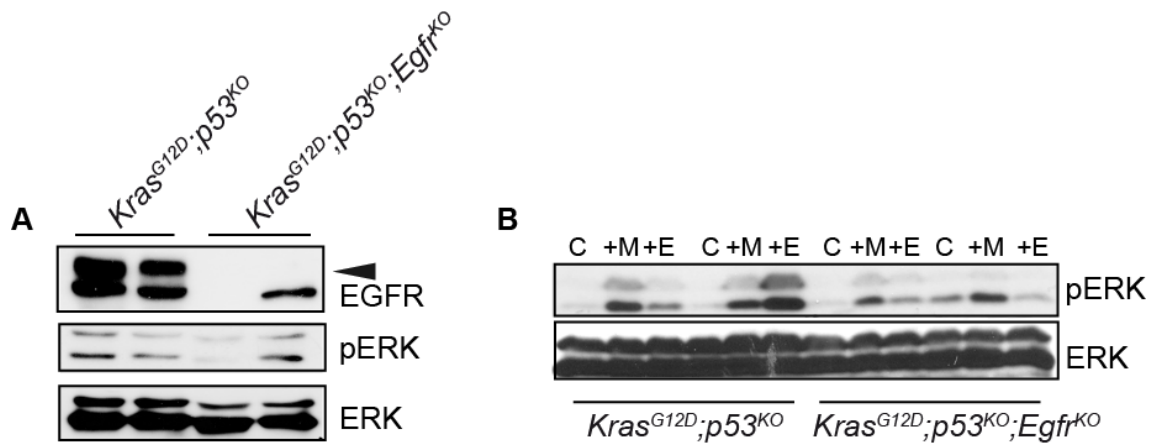


**Figure 3-28**

**ERK activity in  $Kras^{G12D};p53^{KO}$  and  $Kras^{G12D};p53^{KO};Egfr^{KO}$  primary murine cell lines.** (A) Primary murine  $Kras^{G12D};p53^{KO};Egfr^{KO}$  cell lines have lower basic ERK activity than cell lines isolated from  $Kras^{G12D};p53^{KO}$  pancreata. (B) Also upon stimulation with EGF (+E) or full medium (+M) cell lines from  $Egfr$ -KO tumors show less ERK activation.

To test if MAPK activity was critical for ADM and pancreatic tumorigenesis *in vitro* and *in vivo* the allosteric MEK1/2 inhibitor BAY 86-9766 was employed [135]. BAY 86-9766 treatment of acinar explants isolated from  $Kras^{G12D}$  mice revealed a strong dose-dependent block in acinar cell transdifferentiation (Figure 3-29 A, B). To verify the effect of MEK inhibition *in vivo* 6-week old  $Kras^{G12D}$  mice were treated with cerulein as before to induce pancreatitis. Concomitant with pancreatitis induction and continuing for 3 weeks after, mice were additionally treated daily with 25 mg/kg BAY86-9766 or vehicle by oral gavage (for schematic see Figure 3-29 C). As expected, vehicle-treated  $Kras^{G12D}$  mice developed fibrotic, inflamed tissue with the majority of the epithelia replaced by metaplasia and PanIN (Figure 3-29 E&F). In striking contrast, BAY86-9766-treated mice retained phenotypically normal tissue with only rare MUC5AC<sup>+</sup> PanINs (Figure 3-29 G-I). Western blot analysis confirmed reduced levels of active ERK in BAY86-9766-treated mice (Figure 3-29 D).

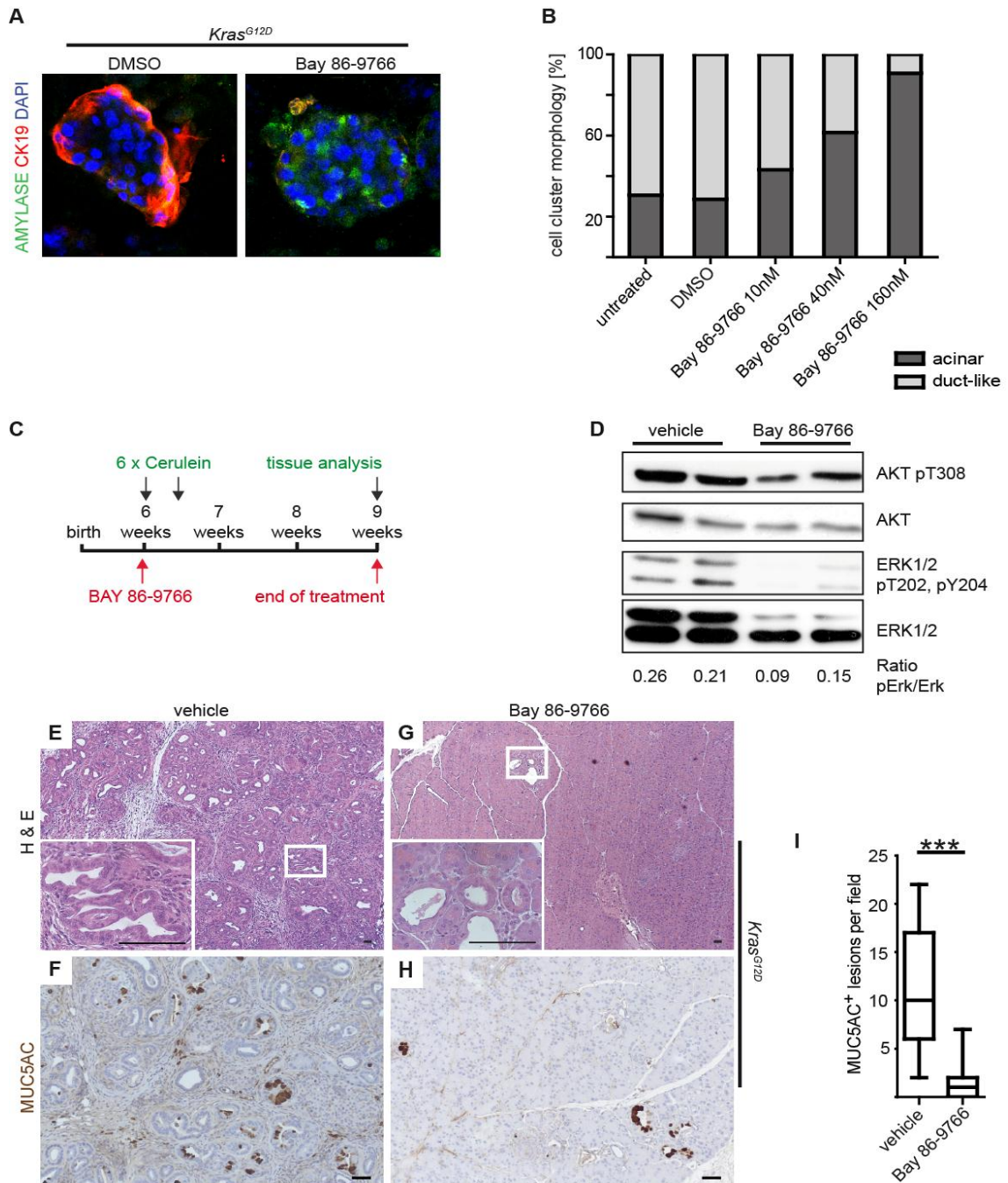


**Figure 3-29**

**EGFR-dependent ERK activation is required for pancreatic tumorigenesis.** (A-B) Staining for CK19 and amylase in acinar epithelial explants of *Kras<sup>G12D</sup>* mice (A) and phenotypical quantitation (B) shows inhibition of ADM upon treatment with the MEK inhibitor BAY 86-9766. Quantitation is representative of 3 independent experiments. (C) Schematic illustration of pancreatitis induction in *Kras<sup>G12D</sup>* mice and parallel treatment with the MEK inhibitor BAY 86-9766. In 6 week old *Kras<sup>G12D</sup>* mice acute pancreatitis was induced by 6 hourly injections with 50 µg/kg cerulein on two consecutive days. Additionally, mice were treated either with a single dose of BAY 86-9766 or vehicle for 6 days per week for in total 3 weeks. (D) Western blot analysis displays reduced levels of active ERK in BAY 86-9766 treated mice in comparison to controls (lower panels) but no difference in AKT activation (upper panels). Numbers indicate ratio of pERK/total ERK densitometric quantitation. (E-H) Histological analysis (E,G) and staining

for the PanIN marker MUC5AC (F,H) depicts induction of ADM and PanIN development as expected in the vehicle treated control group (E,F) whereas BAY 86-9766 treated mice exhibit mostly phenotypically normal pancreatic tissue and only rare PanIN induction (G,H) (n = 3). Scale bars represent 50  $\mu\text{m}$ . (I) Quantitation of MUC5AC<sup>+</sup> lesions shows a marked reduction in PanIN development in BAY 86-9766 treated mice in comparison to controls (\*\**p* < 0.001).

## 4 Discussion

Pancreatic ductal adenocarcinoma is a highly lethal disease with its incidence equaling its mortality with a median survival rate below 5 %. This is due to its late detection as well as to its high intrinsic resistance to any therapeutic approach. Despite huge efforts and achievements in basic pancreatic cancer research no significant improvement in patient survival could be accomplished and the death rates did not change during the last 20 years [18]. Still, it is of pivotal importance to improve our knowledge of every aspect of this fatal disease to finally obtain an enhancement in the diagnosis and treatment. As a contribution to the overall goal, aim of this thesis was to investigate a new possibility for biomarker detection for earlier diagnosis (3.1 and 4.1), to analyze drug distribution in PDAC for understanding delivery of existing therapies (3.2 and 4.2) and also to get better understanding of the molecular mechanisms causing PDAC for novel target identification (3.3 and 4.3).

### 4.1 MALDI imaging mass spectrometry for *in situ* proteomic analysis of preneoplastic lesions in pancreatic cancer

Because of the ongoing failure of therapeutic approaches to improve survival in PDAC patients, early detection is of key importance for better outcome in this otherwise fatal disease. In the first project of this thesis, MALDI Imaging Mass Spectrometry (MALDI-IMS) was applied with spatial resolution for *in situ* proteomic analysis of preneoplastic lesions of the pancreas in GEM with endogenous PDAC. Specifically, the question was addressed whether it is possible to identify proteins or peptides that can discriminate between morphologically normal pancreatic tissue, PanIN/IPMN precursor lesions and PDAC.

While the need for early detection of PDAC, ideally in a preinvasive state, is of obvious importance, proteomic analysis in humans are hindered by inherent interindividual and intratumoral genetic variations as well as confounding factors including environmental and nutritional conditions. Also, obtaining pancreatic

tissue with preneoplastic PanIN or IPMN lesions is not feasible for obvious reasons. Thus, GEM recapitulating human pancreatic carcinogenesis provide an excellent study platform and have already been utilized for the detection of serum biomarkers using SELDI-TOF analysis [26]. In another study, *Pdx1-Cre;Kras<sup>+G12D</sup>;Ink4a/Arf<sup>lox/lox</sup>* mice were used for plasma proteomic analysis and candidates were validated in the blood of patients with PDAC [136]. A recent study from Taguchi and colleagues compared plasma protein profiles of four mouse models of lung cancer with profiles of models of pancreatic, ovarian, colon, prostate, and breast cancer and two models of inflammation. They showed relevance to human lung cancer of the protein signatures identified on the basis of mouse models [137]. Therefore it was hypothesized that these GEM are a suitable platform for biomarker identification using MALDI-IMS.

MALDI-IMS is a rapidly developing approach for molecular tissue analysis with high potential for clinically relevant questions including identification of biomarkers, tumor classification, therapy response monitoring and drug imaging [102, 104, 105, 138-141]. In comparison to conventional mass spectrometry, a major advantage of this technique is the possibility of histology-directed tissue profiling with localization of identified *m/z*-species to specific tissue compartments such as preneoplastic lesions. While plasma proteomic approaches so far seem to be promising [142, 143], they did not yet accomplish the task to find clinically useful biomarkers for PDAC. In comparison to conventional laser-capture microdissection of PanIN lesions and subsequent conventional LC-MS/MS analysis, MALDI IMS allows to conduct proteomic analysis on the tissue while retaining the information about the spatial distribution of different analytes. Also this approach was not yet successful in identifying clinically applicable biomarkers [144]. Furthermore, laser captured microdissection is a targeted approach while MALDI IMS allows the parallel analysis of all different tissue types and morphologies present on the measured section. The spatial resolution of 70  $\mu\text{m}$  as used in this study allowed the analysis of small PanIN lesions, enabling to identify *m/z*-species selectively expressed in the respective compartments, although it is also a limiting factor of the methodology since this resolution cannot compete with the resolution

achieved in conventional histological and light-microscopical analyses. The spatial resolution of the measurements, which currently can go down to 50  $\mu\text{m}$ , is mostly restricted by the matrix application step because of the size of the matrix crystals [145]. Furthermore the balance between laser beam size and ion yield has to be optimized but reduces either spatial resolution or number of obtainable ions.

Among the differentially expressed  $m/z$  species,  $m/z$  2790, 2812 and 2829 were found to be highly specific for PanIN lesions. This enrichment was validated in an independent test sample of pancreatic tissue with PanIN-bearing vs. normal pancreatic tissue, demonstrating the discriminatory ability of the identified peaks. This proves that the applied method of MALDI-IMS is a suitable approach for label-free detection of biomarkers.

Identification of respective proteins from the masses measured by MALDI-IMS is a limiting and technically difficult task lacking standardized protocols. The approach used in this study for peptide/protein identification was specially established and is not yet described elsewhere. It was based on the assumption that since the discriminative  $m/z$  species obviously co-crystallized to the matrix, taking the matrix and bring it to subsequent analysis should serve as a pre-cleaning step and reduce the LC-MS/MS number of confounding peptides, proteins and other molecules as much as possible. Especially the content of ions, that are normally present in buffers when doing regular protein extraction from tissue, is almost completely avoided and therefore did not disturb the MS/MS identification.

Identification yielded two proteins, ALB1 and TMSB4X. Both candidates were validated by quantitative RT-PCR in total pancreatic lysates, demonstrating a significant upregulation of the transcripts of these proteins in *Kras*<sup>G12D</sup> mice in a preneoplastic state. Although the presence of mRNA may not directly correlate with increased protein expression, this transcriptional upregulation nevertheless supports the MALDI-IMS findings and the principle utility of the method to identify potential biomarkers even from small amounts of tissue such as PanIN lesions. Furthermore identification was confirmed on protein level, either via western blot analysis or specific immunohistological staining.

ALB1 has previously been identified to be present in pancreatic tumor tissue sections by direct MALDI-IMS-MS/MS [146]. Its identification in PanIN lesions may be due to several reasons. Of potential confounding factor, ALB1 may be attracted and bound by the mucinous content of PanIN lesions as has been described for the transepithelial transport of serum proteins to the intestinal mucus [147]. However, this is an unlikely scenario since already *Alb1* expression upregulation on the transcriptional level could be shown, and western blot depicted clear upregulation on protein level. While identification of murine ALB1 rules out contamination by fetal calf serum, serum ALB1 from blood vessels may potentially be recruited or associate with PanINs. Nevertheless, this seems to be implausibly especially since *m/z* 2790 was not detectable in blood vessels. Alternative possibilities include expression of ALB1 from quiescent pancreatic stellate cells [148], located in the stroma surrounding the PanIN lesions. However, ALB1 expression was not detected by re-visualization or by immunohistochemistry in the PanIN-surrounding stromal tissue. Detecting ALB1 specifically in PanIN lesions may therefore suggest a regulatory mechanism that warrants further investigation. Previous reports have shown that pancreatic exocrine cells can transdifferentiate to hepatocytes and that hepatic foci can be found in adult pancreas and in PDAC [112-115]. The transdifferentiated hepatocyte-like cells express a variety of proteins normally present in mature hepatocytes among which are ALB1, acute phase proteins and the liver-specific markers Transferrin, Alpha-Fetoprotein and Apolipoprotein A4 [149-151]. Recently, MacDonald and colleagues provided evidence that acinar cells start to express liver-restricted genes after modulation of the acinar cell specifying complex PTF1 [152]. Thus, activation of oncogenic KRAS<sup>G12D</sup> in acinar cells may lead to downregulation of PTF1 activity and subsequent expression of liver-restricted genes. Also in this study it could be shown that liver-specific genes and the hepatocyte marker HepPar1 were expressed and point to hepatic transdifferentiation processes as a likely scenario in the carcinogenic pancreas of GEM and therefore a plausible explanation for ALB1 expression in PanINs. Although HepPar1 was only detectable in 2 out of 4 hPanIN3 lesions this can be explained by the fact that this marker is known to



be expressed by hepatocytes [116] and since transdifferentiation processes might not be completed also may not necessarily be detectable in all PanIN3 lesions. Providing more functional evidence was beyond the scope of the study but shall be followed in more detail in future experiments. Taken together, ALB1 identification shows applicability of the MALDI-IMS approach also as starting point for understanding biological processes during PDAC development.

The second identified protein was TMSB4X, a protein known to be upregulated in human PDAC cells [153, 154] and in the developing pancreas [155]. Recent functional and expression studies suggest an important role of this protein during organogenesis and in many cellular processes including wound healing [156] and progenitor cell regulation [157, 158]. While also in this case functional analysis was beyond the scope of the study, TMSB4X may play a role in early preneoplastic and/or progenitor cell transformation under oncogenic stress. Interestingly, it has been identified in proteomic screens in various diseases and tissues, probably because of its small size, cleavage and high expression levels.

The confirmation of increased TMSB4X expression in sera from mice harboring preneoplastic lesions verifies the principal ability of MALDI-IMS and subsequent LC-MS/MS analysis to identify the respective proteins or peptides from peaks measured *in situ*. However, the subsequent approach of its utility as human serum biomarker for PDAC identification failed. Thus, it represents an imperfect biomarker and the transferability to the human system was not possible. So far, the approach has not achieved to demonstrate principle applicability for human biomarker discovery, but future work will focus on identifying additional proteins from the identified masses and then hopefully more clinically meaningful and transferable biomarkers.

Obviously, clinically useful biomarkers need to be measured distantly, i.e. in serum or pancreatic juice, since those body fluids are far more easily accessible, especially for potential screening diagnosis. ALB1 is no suitable candidate for obvious reasons, while TMSB4X is a protein that has been identified in a variety of pathological conditions, potentially arguing against this protein as specific enough within the aimed clinical context. Both candidates are

among the more abundant proteins, showing that the method is highly specific but not very sensitive. This is already visible when the number of total peaks measured in the detectable range between 2500 and 25000 Da is considered. In this mass range for sure more than the approximately 150  $m/z$  species that could be measured in total are present in the tissue. Data clarity suffers for masses below 500 Da [159], while masses bigger than 25 kDa are seldomly detected during MALDI-IMS. These restrictions exclude a great amount of interesting proteins. Additionally, restrictions due to the matrix are likely. The analytes are extracted from the underlying tissue when the solvent evaporates and co-crystallize with the matrix. Dependent on the chosen matrix, not all analytes have the same affinity with the matrix and a potential pre-selection of possibly detectable  $m/z$  species is likely [93, 96].

While this may be the case, the identification of many lesion-specific peaks of yet unknown proteins may hopefully lead to the detection of clinically meaningful biomarkers. In addition, with the advantage of an unbiased proteomic approach, this method is suitable to define a protein signature, which is of the subject of future studies. The approach as a proof-of-concept study may be valuable for several reasons: (i) it is one of the very few studies that have identified proteins from masses; (ii) there have been identified several and in some instances a long list of significant discriminating peaks when comparing the various lesion subtypes and disease conditions, enabling the future identification of potentially more suitable biomarker candidates; (iii) while PanIN- or IPMN-specific proteins may not be detectable in peripheral blood, they may nevertheless be detectable in other compartments such as pancreatic juice or cyst fluid helping to identify patients at risk for harboring preneoplastic pancreatic lesions. As such MALDI-IMS on sections from endogenous mouse models of PDAC should be considered as a suitable approach for potential biomarker discovery.

## **4.2 Analysis of erlotinib distribution in PDAC *in vivo***

The second project of this thesis aimed to investigate delivery and distribution of erlotinib in PDAC tissue and to analyze factors that might contribute to it using

genetically engineered mice. Underlying evidence for this approach stems from recent studies reporting that PDAC shows low vascularization and drug delivery [44, 160, 161]. PDAC is a highly lethal disease (the 4<sup>th</sup> leading cause of cancer deaths) although it is only the 10<sup>th</sup> most common cause of cancer in the western world [13]. To date, the only opportunity for improved survival is complete surgical resection for those with localized disease. However, this is only achievable for < 15 % of patients [14]. For patients with locally advanced or metastatic pancreatic cancer, gemcitabine treatment remains the best option, but with response rate of only 24 % and a median survival of 5.9 months [18, 162]. The only approved targeted chemotherapy is to date the small molecule receptor tyrosine kinase domain inhibitor erlotinib, which specifically inhibits the downstream signaling of the epidermal growth factor receptor (EGFR) upon ligand induced activation. The combination therapy with gemcitabine improves the median survival of patients significantly but only somewhat for about 10 days [18]. This is surprising insofar that in cell culture and xenograft models erlotinib and also other drugs currently in preclinical studies seem to be very efficient [163-166]. Additionally a subgroup of patients that developed a grade 2 rash as side effect in erlotinib plus gemcitabine therapy had a significantly prolonged survival compared to those with grade 1 or 0 rash (10.5 months, 5.8 months, and 5.3 months, respectively [ $p = 0.037$ ] [18]). Therefore it seems likely that additional factors co-determine therapy response in PDAC. Besides multiple molecular resistance mechanisms [90, 167], inefficient drug delivery is discussed as a main reason for poor treatment response [160, 161]. In a recent study Olive and colleagues investigated drug delivery in a GEM model of PDAC, the  $Kras^{G12D};p53^{KO}$  model, and in three distinct tumor transplantation models utilizing high resolution ultrasound and dynamic contrast enhanced magnetic resonance imaging [44]. They found tumors of the three transplantation models to be highly responsive for gemcitabine treatment but not tumors in the  $Kras^{G12D};p53^{KO}$  model due to low perfusion and high desmoplastic tumor microenvironment in the latter. Indeed, it was already shown that human pancreatic ductal adenocarcinomas are poorly perfused utilizing contrast enhanced endoscopic ultrasound and that this feature

distinguishes PDAC from endocrine tumors and inflammatory diseases of the pancreas [168, 169]. In this thesis MALDI Imaging mass spectrometry was applied on a GEM model of PDAC, the same as used by Olive and colleagues. As already discussed above (4.1) GEM are a suitable model platform for investigation of PDAC properties because they resemble the human disease very precisely. *Kras*<sup>G12D</sup>;*p53*<sup>KO</sup> mice develop the same desmoplastic reaction and microenvironment as found in human PDAC and show the same impaired treatment response as humans, as already shown by Olive et al. [170]. However, unlike Olive and colleagues, in this study it was not possible to correlate erlotinib distribution with the percentage of CD31-positive blood vessels in the tumors. On the contrary, percentage of CD31-positive vessels and relative intensities of erlotinib and its metabolite were absolutely independent. Still, it is possible to argue that CD31 as a marker for blood vessels is not sufficient to assess the percentage of functional vessels since especially in tumors impaired vessel formation can take place [171]. In living animals it is possible to assess functional blood perfusion using for example contrast enhanced endoscopic ultrasound. Since this was not possible in this study as mice had to be sacrificed for MALDI Imaging, staining for CD31 remained the best option. Clearly, better ways to assess functional perfusion in this experimental setting have to be established until absolute statements can be made. So far however, in this study it was not possible to detect any correlation between erlotinib distribution and vessel density.

On the other hand, there was a slight but significant correlation between the relative mass intensity of demethylated erlotinib and both proliferation and differentiation of the tumor. The correlation of drug intensity with proliferation seems reasonably logical insofar that higher proliferation is accompanied with higher metabolic turnover. Therefore not only substances necessary for metabolism and multiplication might be transported to the proliferative cells but also drugs and their metabolites. This result is quite controversial since a high proliferation rate in tumors is associated with poor outcome. It might on the other hand explain why the relative intensity of the metabolite but not erlotinib itself correlates with tumor proliferation. Since these tumor regions show an

increase in metabolism the turnover of erlotinib is enhanced as well. The chosen time point for analysis, one hour after drug application, seems to be sufficient to transform most of the applied drug to its metabolite. But although the increase in metabolism might imply that also the depletion of the drug is increased that does not seem to be the case. In *WT* mice four hours after application the relative intensity of erlotinib is already back to initial levels, but the level of the active metabolite is still high. Although this was only shown in healthy but not in PDAC tissue it gives at least a clear hint how and in which timelines turnover of erlotinib might take place.

Next to proliferation, higher metabolite intensity was also correlated with better differentiation of the tumor. This could be due to better accessibility of differentiated duct-like structures in comparison to dense, stroma-rich undifferentiated tumor regions. Additionally, undifferentiated tumors consist only of a very small amount of epithelial cells. The majority of undifferentiated tumors are comprised of stromal and inflammatory cells. This result could at least in part explain why poorly differentiated tumors have a poor prognosis. Also in general more erlotinib and metabolite could be detected in healthy acinar tissue than in tumor regions. Sure, healthy pancreatic tissue is comprised of more than 90 % exocrine cells whereas tumor regions consist of epithelial tumor cells and stroma. These different cell types might have a different affinity with erlotinib per se. Furthermore, in healthy tissues fluids are removed through a network of lymphatic vessels as well as the veins. Solid tumors lack or have fewer functional lymph vessels than normal tissues [172] which contribute to the increased interstitial fluid pressure in tumors [173-175]. It was shown that this increase in interstitial fluid pressure inhibits the distribution of larger molecules by convection [175-178]. The fact that erlotinib and its metabolite follow in their tissue distribution the flow of fluids in lymph nodes supports this potential explanation for lower drug levels. Additionally, hypoxia and acidity are different in tumor tissue. Hypoxia is a common feature of tumors as a result of impaired vessel formation and temporary disruption of functional vessels [179, 180]. Lower pH is an indirect result of this temporary hypoxia since due to impaired O<sub>2</sub> delivery glycolysis is increased to substitute the reduced energy supply. The

decreased clearance and increased production of CO<sub>2</sub> and carbonic acid lowers the interstitial pH, making acidity characteristic for solid tumors [181]. All these features of tumors as well as yet unknown characteristics might contribute to lower erlotinib and metabolite levels in overall tumor compared to normal tissue and also in poor differentiated in comparison to well differentiated tumor regions. What the results already definitely show is that preclinical studies with healthy animals do not represent suitable model systems for evaluation of drug distribution and response. The GEM used here are far more fitting for these kinds of studies.

Applying MALDI-IMS for monitoring of drug distribution is a novel approach that allows the direct correlation of drug distribution with morphology *in vivo*. First studies demonstrated the opportunity to detect not only the distribution of the drug itself, but also the simultaneous distribution of its individual metabolites, even in whole-body tissue sections [106, 182]. MALDI-IMS of drugs does not require isotope labeling of analytes, it is able to characterize drug and metabolites simultaneously and quantitate their single contributions and it can provide rapid and sensitive analysis. First applications provided good correlation to traditional autoradiography results [183-185] but disclosed also the current limitations of MALDI-IMS for small molecule imaging because of signal suppression, ionization deficiency and ion separability [106, 186]. Another challenge in drug imaging is the absolute quantification of MALDI-IMS data. Different approaches have been used, for example spotting a dilution series of the compound of interest directly on the tissue sections or carrier to obtain a linear standard curve [184, 187], or combining liquid chromatography coupled with MS/MS for the quantification and confirmation of molecular species in tissue sections [107, 140, 185, 188]. However, absolute quantification of MALDI-IMS data is still a technical challenge, due to missing appropriate calibration and internal standards, and novel approaches have been tried [189]. Because these approaches for quantification represent complete studies in themselves, in this thesis project the absolute quantification was replaced by the easier to assess relative quantification, since it was not aim of the study to

investigate drug concentration but rather relative drug distribution in different morphological compartments.

Despite these current challenges, MALDI-IMS has so far been successfully applied in several studies for analyzing pharmaceutical compounds in lung diseases [107, 187, 188], brain diseases [182, 184, 189] and cancer [170, 190, 191]. For example, Atkinson and colleagues detected reduced banoxatrone in hypoxic regions of human tumor xenografts in mice [190]. Bouslimani et al. detected almost exclusive presence of oxaliplatin and its metabolites in the cortex of rat kidneys, although the applied heat-treatment should increase the uptake of the drug into the kidney medulla [191]. However, so far no complex study combining GEM models of cancer with MALDI-IMS investigating not only drug distribution but also possible reasons for that was performed. This is the first study that demonstrates applicability of MALDI drug imaging on GEM for cancer in a clinically highly relevant setting. Sample numbers are representative unlike in former erlotinib MALDI-IMS studies, where for each time point one rat was analyzed [185]. In another study, human tissue was spotted with erlotinib after surgical resection [170], therefore not absolutely ensuring biological distribution. In this study mice were administered orally with erlotinib, resembling the administration form applied to PDAC patients. For the first time it was shown that (i) relative erlotinib and metabolite levels are higher in normal than in PDAC tissue, that (ii) at least in this study there was no correlation of intensity levels with tumor perfusion, that (iii) differentiation grade and proliferation rate of the tumor correlate with relative intensity levels of the biologically active O-demethylated metabolite of erlotinib and that (iv) the combination of GEM with MALDI drug imaging provides an excellent approach to study in more detail how and why chemotherapeutics distribute in tumor tissue and in what way these processes can be influenced and optimized for better treatment response in patients.

### **4.3 EGFR is essential for RAS-driven pancreatic carcinogenesis**

In the third and main project of this thesis, an essential role for EGFR in both spontaneous and pancreatitis-induced PanIN formation in mice expressing oncogenic KRAS was identified and characterized. EGFR has been implicated in the pathogenesis of several epithelial cancers, as evidenced by its common upregulation and activation [48]. Inappropriate EGFR activation can result from mutation or overexpression. Its contribution to tumor progression is presumably through its cooperation with other parallel oncogenic pathways. Interestingly, upregulation of EGFR and its ligands have been reported in PDAC [192] but because the majority of pancreatic cancers harbor oncogenic KRAS mutations, EGFR activity is presumed to be largely redundant, and certainly irrelevant for the KRAS-driven tumorigenesis process. However, several studies show that constitutive RAS signaling alone is not sufficient to compensate for EGFR activity. EGFR is necessary for the growth [193] and survival [194] of RAS-initiated cutaneous squamous cell carcinoma and maintains the stem-cell like nature of transformed keratinocytes [195]. In H-RAS initiated melanoma, an EGFR autocrine loop is required for tumor cell maintenance and survival [196]. In PDAC cell lines, the unique activities of EGFR promote cell proliferation and invasion even when KRAS is mutated [197-200]. Overall, the majority of studies support models where the unique activities of EGFR in RAS-mutated tumors are limited to post-transformation functions. Two studies provide notable exceptions where, *in vitro*, RAS transformation of otherwise normal immortalized cells requires EGFR activity [194, 201]. In addition, concomitant pancreatic activation of oncogenic KRAS and EGFR signaling leads to accelerated formation of high-grade preneoplastic lesions and PDAC, suggesting that EGFR signaling can substantially enhance RAS-induced oncogenicity [27].

Clinical data in colorectal cancer reinforce the view that EGFR signaling and KRAS mutations are functionally redundant [202]. However, the relationship between *Ras* mutations and EGFR-directed therapy is not as clear in lung and



pancreatic cancers. In PDAC patients as a whole, use of anti-EGFR therapy has a modest survival effect, at best. However subgroups of patients with a therapy-induced rash have a significantly improved survival [18]. A recent study analyzing EGFR-targeted therapy in PDAC directly xenografted at the time of surgery found high EGFR expression, but not KRAS mutations, to correlate with response to EGFR-directed treatment [203]. There have been mixed results regarding the relationship between KRAS mutations and patient response to gemcitabine and erlotinib in clinical trials [204, 205]. Collisson et al. defined different PDAC subtypes based on transcription profiles that correlated with specific responses to gemcitabine and erlotinib treatment [206]. Notably, KRAS mutations were no predictor of sensitivity to EGFR-targeted therapy, suggesting other ill-defined factors are involved.

The predictably reproducible tumor onset and progression in the *Kras*<sup>G12D</sup> PDAC model has allowed to explore the *in vivo* functions of EGFR that affect the transition of truly normal epithelia to preneoplastic and neoplastic lesions. It was found that KRAS expressing acinar cells upregulate EGFR in distinct, phenotypically normal acinar clusters prior to the formation of metaplasia and PanINs. This pattern of upregulation becomes more widespread over time, particularly in areas adjacent to metaplasia and PanINs, suggesting a propagation of the signal emanating from the aberrant epithelia. Upregulated expression of the main EGFR ligands *Tgfa* and *Egf* was also not changed in the pancreata of 7 day old *Kras*<sup>G12D</sup>; *Egfr*<sup>KO</sup> mice. Most importantly, it could be shown that blocking EGFR activity pharmacologically or genetically effectively eliminates KRAS-initiated pancreatic tumorigenesis, with or without pancreatitis induction, due to its critical role in amplifying ERK activation within the pancreas. It was found that EGFR is necessary for the transdifferentiation of transformation-resistant, terminally differentiated cells to a transformation-sensitive, progenitor cell-like, metaplastic duct phenotype. Thus, it can be proposed that EGFR's major role in pancreatic tumorigenesis lies in its control of cellular differentiation of the neoplastic precursors. Taken as a whole, the observations in this study show that EGFR pathway regulation is a crucial early

event in KRAS' hijacking of the pro-tumorigenic wound healing process proposed by Hebrok and colleagues [111].

Several possible downstream signaling pathways could be responsible for this important role of EGFR in pancreatic carcinogenesis. First, KRAS activity or localization itself could have been affected. But here it was shown that neither activity nor localization of KRAS were affected in EGFR-KO pancreata. Secondly, differences in RAC1 activity could be excluded as possible explanation for the striking phenotype observed. STAT3 and PI3K/AKT pathways also did not show substantial distinctions. The only considerable difference could be found in ERK activity.

The dependency of robust KRAS-induced ERK activity on EGFR was unexpected and may be mediated through several mechanisms. EGFR is known to localize both RAS [207] and RAF kinases [208], the typical mediators of the MEK/ERK cascade, to the plasma membrane, promoting their interaction. Similarly, relocalization of specific scaffold proteins [209] may promote RAS/RAF interaction. Alternative mechanisms include the regulation of the amount of total phosphorylated ERK by inhibiting the downstream terminators of ERK signaling, such as the ERK phosphatases. Whatever the precise mechanism of its regulation by EGFR signaling may be, blocking ERK activation by treating mice with the MEK selective inhibitor BAY 86-9766 demonstrates the absolutely critical role of this classic arm of RAS downstream effectors in pancreatic tumorigenesis. As such, EGFR enhancement of ERK activity in acinar cells is proposed to be critical for the initial steps of their transformation *in vivo*.

Much has been made recently of experimental pancreatitis being required for the transformation of oncogenic KRAS expressing acinar cells [10, 11, 126, 210]. In the prevailing model, cerulein induces intracellular activation of digestive enzymes, leading to cellular stress and necrosis. Necrotic cells attract pro-tumorigenic inflammatory cells, which cooperate with oncogenic KRAS signaling in the epithelia to induce tumor formation, in part by overcoming cellular senescence [210, 211]. While this model provides a satisfying connection between PDAC and one of its primary risk factors, this thesis' data

show that KRAS induces transdifferentiation of acinar cells *in vitro*, demonstrating that this aspect of the pathology can be initiated cell-autonomously. The protection from metaplastic and neoplastic duct formation when EGFR activity is ablated *in vivo* suggests that this cell autonomous signal is required and largely precedes the inflammatory response.

In summary, in this thesis a critical role for EGFR activity in KRAS' reprogramming of the pancreatic epithelia en route to tumorigenesis has been identified. EGFR activation in this context results in a substantial amplification of MEK signaling. KRAS mutation alone is not sufficient to induce PDAC but needs signaling of its upstream pathway member EGFR. The EGFR/MEK signaling axis is critical for some of the fundamental pathologies associated with PDAC risk, such as the formation of metaplastic ducts in pancreatitis suggesting that there may be benefit in targeting the pathway in these at-risk patients, to restore homeostasis and thereby reduce the chance of tumorigenesis. As a more general point, these results show that linear pathway signaling is not as clear as it was thought to be and that constitutive activation of a downstream effector does not make the function of upstream molecules redundant.

## 5 Summary

Aim of this thesis was the close investigation of different aspects of pancreatic ductal adenocarcinoma (PDAC) on the basis of and with the use of genetically engineered mouse models (GEM). PDAC is a fatal disease with very low median survival and high mortality mostly due to its late detection, early metastasis and high intrinsic resistance to any chemotherapy. Using GEM, all stages of the disease – early preneoplastic lesions as well as end stage cancer – are addressable at defined time points.

In the first project of this thesis GEM were subjected to the novel method of matrix assisted laser desorption/ionization imaging mass spectrometry (MALDI IMS) to evaluate the possibility for potential new biomarker detection for earlier diagnosis. MALDI IMS allows the label-free proteomic analysis of tissue with spatial resolution while keeping morphological information. Pancreatic sections of GEM with preneoplastic lesions as well as wild type and PDAC tissue were measured with MALDI IMS and many differentially expressed *m/z* species could be detected. Two masses could be identified using liquid chromatography and tandem mass spectrometry (LC-MS/MS). Murine serum albumin (ALB1) was verified using western blot and immunohistochemistry and was found to be associated with hepatic transdifferentiation of PDAC tissue. Thymosin beta 4 (TMSB4X) was upregulated in PanIN and PDAC and also in serum of GEM in comparison to wild type. Both proteins are no suitable candidates for a potential useful biomarker but the results presented in this thesis show the principle applicability of MALDI IMS on the basis of GEM to investigate the peptidome/proteome of cancer tissue.

In the second project of this thesis MALDI IMS was utilized to investigate the delivery and distribution of erlotinib, a small tyrosine kinase inhibitor and to date the only approved targeted chemotherapy for PDAC. Erlotinib was orally applied to GEM with PDAC and its distribution, as well as the distribution of its active metabolite, was measured. It could be shown that relative levels of erlotinib and its metabolite were highest one hour after application in wild type pancreata and that they were significantly lower in PDAC tissue. The distribution and relative levels in the tumor did not correlate with the percentage of CD31 positive

vessels but instead a significant positive correlation between the relative levels of the active metabolite and proliferation as well as differentiation of the tumor could be observed.

In the third and main project of this thesis the role of the epidermal growth factor receptor (EGFR) in PDAC development in the background of the well-established *Kras*<sup>G12D</sup> mouse model was evaluated. It was shown that oncogenic KRAS upregulates EGFR expression and activation. Genetic ablation or pharmacological inhibition of EGFR effectively eliminates KRAS-driven tumorigenesis *in vivo*, with EGFR activity being necessary for the formation of transformation-sensitive metaplastic ducts. In addition, EGFR is necessary for high level activation of ERK, which is critical for pancreatic tumorigenesis, especially for transdifferentiation of acinar to ductal cells, even in the context of pancreatitis-induced PanIN formation in *Kras*<sup>G12D</sup> mice. These novel and provoking results allow new insight into the molecular basics of cancer formation and might change the thinking of linear pathway signaling.

## 6 References

1. Pan, F.C. and C. Wright, *Pancreas organogenesis: from bud to plexus to gland*. Dev Dyn, 2011. 240(3): p. 530-65.
2. Edlund, H., *Pancreatic organogenesis--developmental mechanisms and implications for therapy*. Nat Rev Genet, 2002. 3(7): p. 524-32.
3. Rohen J.W. and Lütjen-Drecoll E., *Funktionelle Anatomie des Menschen*. 10 ed. 2001: Schattauer.
4. Kopp, J.L., C.L. Dubois, E. Hao, F. Thorel, P.L. Herrera, and M. Sander, *Progenitor cell domains in the developing and adult pancreas*. Cell Cycle, 2011. 10(12): p. 1921-7.
5. Willemer, S., H.P. Elsasser, and G. Adler, *Hormone-induced pancreatitis*. Eur Surg Res, 1992. 24 Suppl 1: p. 29-39.
6. Yoo, B.M., T.Y. Oh, Y.B. Kim, M. Yeo, J.S. Lee, Y.J. Surh, B.O. Ahn, W.H. Kim, S. Sohn, J.H. Kim, and K.B. Hahm, *Novel antioxidant ameliorates the fibrosis and inflammation of cerulein-induced chronic pancreatitis in a mouse model*. Pancreatology, 2005. 5(2-3): p. 165-76.
7. Thrower, E., S. Husain, and F. Gorelick, *Molecular basis for pancreatitis*. Curr Opin Gastroenterol, 2008. 24(5): p. 580-5.
8. Siveke, J.T., C. Lubeseder-Martellato, M. Lee, P.K. Mazur, H. Nakhai, F. Radtke, and R.M. Schmid, *Notch signaling is required for exocrine regeneration after acute pancreatitis*. Gastroenterology, 2008. 134(2): p. 544-55.
9. Michalski, C.W., A. Gorbachevski, M. Erkan, C. Reiser, S. Deucker, F. Bergmann, T. Giese, M. Weigand, N.A. Giese, H. Friess, and J. Kleeff, *Mononuclear cells modulate the activity of pancreatic stellate cells which in turn promote fibrosis and inflammation in chronic pancreatitis*. J Transl Med, 2007. 5: p. 63.
10. Carriere, C., A.L. Young, J.R. Gunn, D.S. Longnecker, and M. Korc, *Acute pancreatitis markedly accelerates pancreatic cancer progression in mice expressing oncogenic Kras*. Biochem Biophys Res Commun, 2009. 382(3): p. 561-5.
11. Guerra, C., A.J. Schuhmacher, M. Canamero, P.J. Grippo, L. Verdaguer, L. Perez-Gallego, P. Dubus, E.P. Sandgren, and M. Barbacid, *Chronic pancreatitis is essential for induction of pancreatic ductal adenocarcinoma by K-Ras oncogenes in adult mice*. Cancer Cell, 2007. 11(3): p. 291-302.
12. Mulkeen, A.L., P.S. Yoo, and C. Cha, *Less common neoplasms of the pancreas*. World J Gastroenterol, 2006. 12(20): p. 3180-5.
13. Siegel, R., D. Naishadham, and A. Jemal, *Cancer statistics, 2012*. CA Cancer J Clin, 2012. 62(1): p. 10-29.
14. Sohn, T.A., C.J. Yeo, J.L. Cameron, L. Koniaris, S. Kaushal, R.A. Abrams, P.K. Sauter, J. Coleman, R.H. Hruban, and K.D. Lillemoe, *Resected adenocarcinoma of the pancreas-616 patients: results, outcomes, and prognostic indicators*. J Gastrointest Surg, 2000. 4(6): p. 567-79.
15. Schneider, G., J.T. Siveke, F. Eckel, and R.M. Schmid, *Pancreatic cancer: basic and clinical aspects*. Gastroenterology, 2005. 128(6): p. 1606-25.
16. Mazur, P.K. and J.T. Siveke, *Genetically engineered mouse models of pancreatic cancer: unravelling tumour biology and progressing translational oncology*. Gut, 2011.
17. Morris, J.P.t., S.C. Wang, and M. Hebrok, *KRAS, Hedgehog, Wnt and the twisted developmental biology of pancreatic ductal adenocarcinoma*. Nat Rev Cancer, 2010. 10(10): p. 683-95.

18. Moore, M.J., D. Goldstein, J. Hamm, A. Figer, J.R. Hecht, S. Gallinger, H.J. Au, P. Murawa, D. Walde, R.A. Wolff, D. Campos, R. Lim, K. Ding, G. Clark, T. Voskoglou-Nomikos, M. Ptasynski, and W. Parulekar, *Erlotinib plus gemcitabine compared with gemcitabine alone in patients with advanced pancreatic cancer: a phase III trial of the National Cancer Institute of Canada Clinical Trials Group*. *J Clin Oncol*, 2007. 25(15): p. 1960-6.
19. Yeh, J.J. and C.J. Der, *Targeting signal transduction in pancreatic cancer treatment*. *Expert Opin Ther Targets*, 2007. 11(5): p. 673-94.
20. Melstrom L.G. and Grippo P. J., *Models of pancreatic cancer: understanding disease*. 2008: Springer.
21. Ulrich, A.B., B.M. Schmieid, J. Standop, M.B. Schneider, and P.M. Pour, *Pancreatic cell lines: a review*. *Pancreas*, 2002. 24(2): p. 111-20.
22. Grippo, P.J. and E.P. Sandgren, *Modeling pancreatic cancer in animals to address specific hypotheses*. *Methods Mol Med*, 2005. 103: p. 217-43.
23. Mazur, P.K., B.M. Gruner, H. Nakhai, B. Sipos, U. Zimmer-Strobl, L.J. Strobl, F. Radtke, R.M. Schmid, and J.T. Siveke, *Identification of epidermal Pdx1 expression discloses different roles of Notch1 and Notch2 in murine Kras(G12D)-induced skin carcinogenesis in vivo*. *PLoS One*, 2010. 5(10): p. e13578.
24. Obata, J., M. Yano, H. Mimura, T. Goto, R. Nakayama, Y. Mibu, C. Oka, and M. Kawaichi, *p48 subunit of mouse PTF1 binds to RBP-Jkappa/CBF-1, the intracellular mediator of Notch signalling, and is expressed in the neural tube of early stage embryos*. *Genes Cells*, 2001. 6(4): p. 345-60.
25. Sandgren, E.P., N.C. Luetetteke, R.D. Palmiter, R.L. Brinster, and D.C. Lee, *Overexpression of TGF alpha in transgenic mice: induction of epithelial hyperplasia, pancreatic metaplasia, and carcinoma of the breast*. *Cell*, 1990. 61(6): p. 1121-35.
26. Hingorani, S.R., E.F. Petricoin, A. Maitra, V. Rajapakse, C. King, M.A. Jacobetz, S. Ross, T.P. Conrads, T.D. Veenstra, B.A. Hitt, Y. Kawaguchi, D. Johann, L.A. Liotta, H.C. Crawford, M.E. Putt, T. Jacks, C.V. Wright, R.H. Hruban, A.M. Lowy, and D.A. Tuveson, *Preinvasive and invasive ductal pancreatic cancer and its early detection in the mouse*. *Cancer Cell*, 2003. 4(6): p. 437-50.
27. Siveke, J.T., H. Einwachter, B. Sipos, C. Lubeseder-Martellato, G. Kloppel, and R.M. Schmid, *Concomitant pancreatic activation of Kras(G12D) and Tgfa results in cystic papillary neoplasms reminiscent of human IPMN*. *Cancer Cell*, 2007. 12(3): p. 266-79.
28. Wagner, M., F.R. Greten, C.K. Weber, S. Koschnick, T. Mattfeldt, W. Deppert, H. Kern, G. Adler, and R.M. Schmid, *A murine tumor progression model for pancreatic cancer recapitulating the genetic alterations of the human disease*. *Genes Dev*, 2001. 15(3): p. 286-93.
29. Aguirre, A.J., N. Bardeesy, M. Sinha, L. Lopez, D.A. Tuveson, J. Horner, M.S. Redston, and R.A. DePinho, *Activated Kras and Ink4a/Arf deficiency cooperate to produce metastatic pancreatic ductal adenocarcinoma*. *Genes Dev*, 2003. 17(24): p. 3112-26.
30. Bardeesy, N., A.J. Aguirre, G.C. Chu, K.H. Cheng, L.V. Lopez, A.F. Hezel, B. Feng, C. Brennan, R. Weissleder, U. Mahmood, D. Hanahan, M.S. Redston, L. Chin, and R.A. Depinho, *Both p16(Ink4a) and the p19(Arf)-p53 pathway constrain progression of pancreatic adenocarcinoma in the mouse*. *Proc Natl Acad Sci U S A*, 2006. 103(15): p. 5947-52.
31. Hingorani, S.R., L. Wang, A.S. Multani, C. Combs, T.B. Deramaudt, R.H. Hruban, A.K. Rustgi, S. Chang, and D.A. Tuveson, *Trp53R172H and KrasG12D*

- cooperate to promote chromosomal instability and widely metastatic pancreatic ductal adenocarcinoma in mice.* *Cancer Cell*, 2005. 7(5): p. 469-83.
32. Mazur, P.K., H. Einwachter, M. Lee, B. Sipos, H. Nakhai, R. Rad, U. Zimmer-Strobl, L.J. Strobl, F. Radtke, G. Kloppel, R.M. Schmid, and J.T. Siveke, *Notch2 is required for progression of pancreatic intraepithelial neoplasia and development of pancreatic ductal adenocarcinoma.* *Proc Natl Acad Sci U S A*, 2010. 107(30): p. 13438-43.
  33. Hanlon, L., J.L. Avila, R.M. Demarest, S. Troutman, M. Allen, F. Ratti, A.K. Rustgi, B.Z. Stanger, F. Radtke, V. Adsay, F. Long, A.J. Capobianco, and J.L. Kissil, *Notch1 functions as a tumor suppressor in a model of K-ras-induced pancreatic ductal adenocarcinoma.* *Cancer Res*, 2010. 70(11): p. 4280-6.
  34. Bardeesy, N., K.H. Cheng, J.H. Berger, G.C. Chu, J. Pahler, P. Olson, A.F. Hezel, J. Horner, G.Y. Lauwers, D. Hanahan, and R.A. DePinho, *Smad4 is dispensable for normal pancreas development yet critical in progression and tumor biology of pancreas cancer.* *Genes Dev*, 2006. 20(22): p. 3130-46.
  35. Kojima, K., S.M. Vickers, N.V. Adsay, N.C. Jhala, H.G. Kim, T.R. Schoeb, W.E. Grizzle, and C.A. Klug, *Inactivation of Smad4 accelerates Kras(G12D)-mediated pancreatic neoplasia.* *Cancer Res*, 2007. 67(17): p. 8121-30.
  36. Izeradjene, K., C. Combs, M. Best, A. Gopinathan, A. Wagner, W.M. Grady, C.X. Deng, R.H. Hruban, N.V. Adsay, D.A. Tuveson, and S.R. Hingorani, *Kras(G12D) and Smad4/Dpc4 haploinsufficiency cooperate to induce mucinous cystic neoplasms and invasive adenocarcinoma of the pancreas.* *Cancer Cell*, 2007. 11(3): p. 229-43.
  37. Hezel, A.F., A.C. Kimmelman, B.Z. Stanger, N. Bardeesy, and R.A. Depinho, *Genetics and biology of pancreatic ductal adenocarcinoma.* *Genes Dev*, 2006. 20(10): p. 1218-49.
  38. Bardeesy, N. and R.A. DePinho, *Pancreatic cancer biology and genetics.* *Nat Rev Cancer*, 2002. 2(12): p. 897-909.
  39. Soto, J.L., V.M. Barbera, M. Saceda, and A. Carrato, *Molecular biology of exocrine pancreatic cancer.* *Clin Transl Oncol*, 2006. 8(5): p. 306-12.
  40. Goldstein, A.M., M.C. Fraser, J.P. Struewing, C.J. Hussussian, K. Ranade, D.P. Zimetkin, L.S. Fontaine, S.M. Organic, N.C. Dracopoli, W.H. Clark, Jr., and et al., *Increased risk of pancreatic cancer in melanoma-prone kindreds with p16INK4 mutations.* *N Engl J Med*, 1995. 333(15): p. 970-4.
  41. Agarwal, M.L., W.R. Taylor, M.V. Chernov, O.B. Chernova, and G.R. Stark, *The p53 network.* *J Biol Chem*, 1998. 273(1): p. 1-4.
  42. Singh, P., J.D. Wig, and R. Srinivasan, *The Smad family and its role in pancreatic cancer.* *Indian J Cancer*, 2011. 48(3): p. 351-60.
  43. Nakhai, H., J.T. Siveke, B. Klein, L. Mendoza-Torres, P.K. Mazur, H. Algul, F. Radtke, L. Strobl, U. Zimmer-Strobl, and R.M. Schmid, *Conditional ablation of Notch signaling in pancreatic development.* *Development*, 2008. 135(16): p. 2757-65.
  44. Olive, K.P., M.A. Jacobetz, C.J. Davidson, A. Gopinathan, D. McIntyre, D. Honess, B. Madhu, M.A. Goldgraben, M.E. Caldwell, D. Allard, K.K. Frese, G. Denicola, C. Feig, C. Combs, S.P. Winter, H. Ireland-Zecchini, S. Reichelt, W.J. Howat, A. Chang, M. Dhara, L. Wang, F. Ruckert, R. Grutzmann, C. Pilarsky, K. Izeradjene, S.R. Hingorani, P. Huang, S.E. Davies, W. Plunkett, M. Egorin, R.H. Hruban, N. Whitebread, K. McGovern, J. Adams, C. Iacobuzio-Donahue, J. Griffiths, and D.A. Tuveson, *Inhibition of Hedgehog signaling enhances delivery of chemotherapy in a mouse model of pancreatic cancer.* *Science*, 2009. 324(5933): p. 1457-61.
  45. Wells, A., *EGF receptor.* *Int J Biochem Cell Biol*, 1999. 31(6): p. 637-43.



46. Gschwind, A., O.M. Fischer, and A. Ullrich, *The discovery of receptor tyrosine kinases: targets for cancer therapy*. Nat Rev Cancer, 2004. 4(5): p. 361-70.
47. Jansson, M., L. Philipson, and B. Vennstrom, *Isolation and characterization of multiple human genes homologous to the oncogenes of avian erythroblastosis virus*. EMBO J, 1983. 2(4): p. 561-5.
48. Normanno, N., A. De Luca, C. Bianco, L. Strizzi, M. Mancino, M.R. Maiello, A. Carotenuto, G. De Feo, F. Caponigro, and D.S. Salomon, *Epidermal growth factor receptor (EGFR) signaling in cancer*. Gene, 2006. 366(1): p. 2-16.
49. Yarden, Y. and M.X. Sliwkowski, *Untangling the ErbB signalling network*. Nat Rev Mol Cell Biol, 2001. 2(2): p. 127-37.
50. Olayioye, M.A., R.M. Neve, H.A. Lane, and N.E. Hynes, *The ErbB signaling network: receptor heterodimerization in development and cancer*. EMBO J, 2000. 19(13): p. 3159-67.
51. Guy, P.M., J.V. Platko, L.C. Cantley, R.A. Cerione, and K.L. Carraway, 3rd, *Insect cell-expressed p180erbB3 possesses an impaired tyrosine kinase activity*. Proc Natl Acad Sci U S A, 1994. 91(17): p. 8132-6.
52. Mitsudomi, T. and Y. Yatabe, *Epidermal growth factor receptor in relation to tumor development: EGFR gene and cancer*. FEBS J, 2009. 277(2): p. 301-8.
53. Cohen, S., *Isolation of a mouse submaxillary gland protein accelerating incisor eruption and eyelid opening in the new-born animal*. J Biol Chem, 1962. 237: p. 1555-62.
54. Cohen, S., *The stimulation of epidermal proliferation by a specific protein (EGF)*. Dev Biol, 1965. 12(3): p. 394-407.
55. Carpenter, G., K.J. Lembach, M.M. Morrison, and S. Cohen, *Characterization of the binding of 125-I-labeled epidermal growth factor to human fibroblasts*. J Biol Chem, 1975. 250(11): p. 4297-304.
56. Singh, A.B. and R.C. Harris, *Autocrine, paracrine and juxtacrine signaling by EGFR ligands*. Cell Signal, 2005. 17(10): p. 1183-93.
57. Zhao, J., H. Chen, Y.L. Wang, and D. Warburton, *Abrogation of tumor necrosis factor-alpha converting enzyme inhibits embryonic lung morphogenesis in culture*. Int J Dev Biol, 2001. 45(4): p. 623-31.
58. Sunnarborg, S.W., C.L. Hinkle, M. Stevenson, W.E. Russell, C.S. Raska, J.J. Peschon, B.J. Castner, M.J. Gerhart, R.J. Paxton, R.A. Black, and D.C. Lee, *Tumor necrosis factor-alpha converting enzyme (TACE) regulates epidermal growth factor receptor ligand availability*. J Biol Chem, 2002. 277(15): p. 12838-45.
59. Borrell-Pages, M., F. Rojo, J. Albanell, J. Baselga, and J. Arribas, *TACE is required for the activation of the EGFR by TGF-alpha in tumors*. EMBO J, 2003. 22(5): p. 1114-24.
60. Sahin, U., G. Weskamp, K. Kelly, H.M. Zhou, S. Higashiyama, J. Peschon, D. Hartmann, P. Saftig, and C.P. Blobel, *Distinct roles for ADAM10 and ADAM17 in ectodomain shedding of six EGFR ligands*. J Cell Biol, 2004. 164(5): p. 769-79.
61. Dempsey, P.J., K. Garton, and E.W. Raines, *Emerging roles of TACE as a key protease in ErbB ligand shedding*. Mol Interv, 2002. 2(3): p. 136-41.
62. Schneider, M.R. and E. Wolf, *The epidermal growth factor receptor ligands at a glance*. J Cell Physiol, 2009. 218(3): p. 460-6.
63. Sigismund, S., E. Argenzio, D. Tosoni, E. Cavallaro, S. Polo, and P.P. Di Fiore, *Clathrin-mediated internalization is essential for sustained EGFR signaling but dispensable for degradation*. Dev Cell, 2008. 15(2): p. 209-19.
64. Joazeiro, C.A., S.S. Wing, H. Huang, J.D. Levenson, T. Hunter, and Y.C. Liu, *The tyrosine kinase negative regulator c-Cbl as a RING-type, E2-dependent ubiquitin-protein ligase*. Science, 1999. 286(5438): p. 309-12.

65. Levkowitz, G., H. Waterman, S.A. Ettenberg, M. Katz, A.Y. Tsygankov, I. Alroy, S. Lavi, K. Iwai, Y. Reiss, A. Ciechanover, S. Lipkowitz, and Y. Yarden, *Ubiquitin ligase activity and tyrosine phosphorylation underlie suppression of growth factor signaling by c-Cbl/Sli-1*. *Mol Cell*, 1999. 4(6): p. 1029-40.
66. Goh, L.K., F. Huang, W. Kim, S. Gygi, and A. Sorkin, *Multiple mechanisms collectively regulate clathrin-mediated endocytosis of the epidermal growth factor receptor*. *J Cell Biol*, 2010. 189(5): p. 871-83.
67. Reddy, C.C., A. Wells, and D.A. Lauffenburger, *Receptor-mediated effects on ligand availability influence relative mitogenic potencies of epidermal growth factor and transforming growth factor alpha*. *J Cell Physiol*, 1996. 166(3): p. 512-22.
68. Avraham, R. and Y. Yarden, *Feedback regulation of EGFR signalling: decision making by early and delayed loops*. *Nat Rev Mol Cell Biol*, 2011. 12(2): p. 104-17.
69. Wheeler, D.L., E.F. Dunn, and P.M. Harari, *Understanding resistance to EGFR inhibitors-impact on future treatment strategies*. *Nat Rev Clin Oncol*, 2010. 7(9): p. 493-507.
70. Yoon, S. and R. Seger, *The extracellular signal-regulated kinase: multiple substrates regulate diverse cellular functions*. *Growth Factors*, 2006. 24(1): p. 21-44.
71. Sibililia, M., R. Kroismayr, B.M. Lichtenberger, A. Natarajan, M. Hecking, and M. Holcman, *The epidermal growth factor receptor: from development to tumorigenesis*. *Differentiation*, 2007. 75(9): p. 770-87.
72. Sibililia, M. and E.F. Wagner, *Strain-dependent epithelial defects in mice lacking the EGF receptor*. *Science*, 1995. 269(5221): p. 234-8.
73. Threadgill, D.W., A.A. Dlugosz, L.A. Hansen, T. Tennenbaum, U. Lichti, D. Yee, C. LaMantia, T. Mourton, K. Herrup, R.C. Harris, and et al., *Targeted disruption of mouse EGF receptor: effect of genetic background on mutant phenotype*. *Science*, 1995. 269(5221): p. 230-4.
74. Miettinen, P.J., J.E. Berger, J. Meneses, Y. Phung, R.A. Pedersen, Z. Werb, and R. Derynck, *Epithelial immaturity and multiorgan failure in mice lacking epidermal growth factor receptor*. *Nature*, 1995. 376(6538): p. 337-41.
75. Miettinen, P.J. and K. Heikinheimo, *Transforming growth factor-alpha (TGF-alpha) and insulin gene expression in human fetal pancreas*. *Development*, 1992. 114(4): p. 833-40.
76. Miettinen, P.J., M. Huotari, T. Koivisto, J. Ustinov, J. Palgi, S. Rasilainen, E. Lehtonen, J. Keski-Oja, and T. Otonkoski, *Impaired migration and delayed differentiation of pancreatic islet cells in mice lacking EGF-receptors*. *Development*, 2000. 127(12): p. 2617-27.
77. Tobita, K., H. Kijima, S. Dowaki, H. Kashiwagi, Y. Ohtani, Y. Oida, H. Yamazaki, M. Nakamura, Y. Ueyama, M. Tanaka, S. Inokuchi, and H. Makuuchi, *Epidermal growth factor receptor expression in human pancreatic cancer: Significance for liver metastasis*. *Int J Mol Med*, 2003. 11(3): p. 305-9.
78. Ueda, S., S. Ogata, H. Tsuda, N. Kawarabayashi, M. Kimura, Y. Sugiura, S. Tamai, O. Matsubara, K. Hatsuse, and H. Mochizuki, *The correlation between cytoplasmic overexpression of epidermal growth factor receptor and tumor aggressiveness: poor prognosis in patients with pancreatic ductal adenocarcinoma*. *Pancreas*, 2004. 29(1): p. e1-8.
79. Ji, H., X. Zhao, Y. Yuza, T. Shimamura, D. Li, A. Protopopov, B.L. Jung, K. McNamara, H. Xia, K.A. Glatt, R.K. Thomas, H. Sasaki, J.W. Horner, M. Eck, A. Mitchell, Y. Sun, R. Al-Hashem, R.T. Bronson, S.K. Rabindran, C.M. Discafani, E. Maher, G.I. Shapiro, M. Meyerson, and K.K. Wong, *Epidermal growth factor*

- receptor variant III mutations in lung tumorigenesis and sensitivity to tyrosine kinase inhibitors.* Proc Natl Acad Sci U S A, 2006. 103(20): p. 7817-22.
80. Lesina, M., M.U. Kurkowski, K. Ludes, S. Rose-John, M. Treiber, G. Kloppel, A. Yoshimura, W. Reindl, B. Sipos, S. Akira, R.M. Schmid, and H. Algul, *Stat3/Socs3 activation by IL-6 transsignaling promotes progression of pancreatic intraepithelial neoplasia and development of pancreatic cancer.* Cancer Cell, 2011. 19(4): p. 456-69.
  81. Weihua, Z., R. Tsan, W.C. Huang, Q. Wu, C.H. Chiu, I.J. Fidler, and M.C. Hung, *Survival of cancer cells is maintained by EGFR independent of its kinase activity.* Cancer Cell, 2008. 13(5): p. 385-93.
  82. Dittmann, K., C. Mayer, B. Fehrenbacher, M. Schaller, R. Kehlbach, and H.P. Rodemann, *Nuclear EGFR shuttling induced by ionizing radiation is regulated by phosphorylation at residue Thr654.* FEBS Lett, 2010. 584(18): p. 3878-84.
  83. Khan, E.M., J.M. Heidinger, M. Levy, M.P. Lisanti, T. Ravid, and T. Goldkorn, *Epidermal growth factor receptor exposed to oxidative stress undergoes Src- and caveolin-1-dependent perinuclear trafficking.* J Biol Chem, 2006. 281(20): p. 14486-93.
  84. Dittmann, K., C. Mayer, and H.P. Rodemann, *Nuclear EGFR as novel therapeutic target: insights into nuclear translocation and function.* Strahlenther Onkol, 2009. 186(1): p. 1-6.
  85. Wang, S.C., Y. Nakajima, Y.L. Yu, W. Xia, C.T. Chen, C.C. Yang, E.W. McIntush, L.Y. Li, D.H. Hawke, R. Kobayashi, and M.C. Hung, *Tyrosine phosphorylation controls PCNA function through protein stability.* Nat Cell Biol, 2006. 8(12): p. 1359-68.
  86. Hanada, N., H.W. Lo, C.P. Day, Y. Pan, Y. Nakajima, and M.C. Hung, *Co-regulation of B-Myb expression by E2F1 and EGF receptor.* Mol Carcinog, 2006. 45(1): p. 10-7.
  87. Hung, L.Y., J.T. Tseng, Y.C. Lee, W. Xia, Y.N. Wang, M.L. Wu, Y.H. Chuang, C.H. Lai, and W.C. Chang, *Nuclear epidermal growth factor receptor (EGFR) interacts with signal transducer and activator of transcription 5 (STAT5) in activating Aurora-A gene expression.* Nucleic Acids Res, 2008. 36(13): p. 4337-51.
  88. Lin, S.Y., K. Makino, W. Xia, A. Matin, Y. Wen, K.Y. Kwong, L. Bourguignon, and M.C. Hung, *Nuclear localization of EGF receptor and its potential new role as a transcription factor.* Nat Cell Biol, 2001. 3(9): p. 802-8.
  89. Lo, H.W., S.C. Hsu, M. Ali-Seyed, M. Gunduz, W. Xia, Y. Wei, G. Bartholomeusz, J.Y. Shih, and M.C. Hung, *Nuclear interaction of EGFR and STAT3 in the activation of the iNOS/NO pathway.* Cancer Cell, 2005. 7(6): p. 575-89.
  90. Faller, B.A. and B. Burtness, *Treatment of pancreatic cancer with epidermal growth factor receptor-targeted therapy.* Biologics, 2009. 3: p. 419-28.
  91. Caprioli, R.M., T.B. Farmer, and J. Gile, *Molecular imaging of biological samples: localization of peptides and proteins using MALDI-TOF MS.* Anal Chem, 1997. 69(23): p. 4751-60.
  92. Seeley, E.H. and R.M. Caprioli, *MALDI imaging mass spectrometry of human tissue: method challenges and clinical perspectives.* Trends Biotechnol, 2011. 29(3): p. 136-43.
  93. Balluff, B., C. Schone, H. Hofler, and A. Walch, *MALDI imaging mass spectrometry for direct tissue analysis: technological advancements and recent applications.* Histochem Cell Biol, 2011. 136(3): p. 227-44.
  94. Schwamborn, K. and R.M. Caprioli, *Molecular imaging by mass spectrometry--looking beyond classical histology.* Nat Rev Cancer, 2010. 10(9): p. 639-46.

95. Walch, A., S. Rauser, S.O. Deininger, and H. Hofler, *MALDI imaging mass spectrometry for direct tissue analysis: a new frontier for molecular histology*. *Histochem Cell Biol*, 2008. 130(3): p. 421-34.
96. Castellino, S., M.R. Groseclose, and D. Wagner, *MALDI imaging mass spectrometry: bridging biology and chemistry in drug development*. *Bioanalysis*, 2011. 3(21): p. 2427-41.
97. Pierson, J., J.L. Norris, H.R. Aerni, P. Svenningsson, R.M. Caprioli, and P.E. Andren, *Molecular profiling of experimental Parkinson's disease: direct analysis of peptides and proteins on brain tissue sections by MALDI mass spectrometry*. *J Proteome Res*, 2004. 3(2): p. 289-95.
98. Stoeckli, M., D. Staab, M. Staufienbiel, K.H. Wiederhold, and L. Signor, *Molecular imaging of amyloid beta peptides in mouse brain sections using mass spectrometry*. *Anal Biochem*, 2002. 311(1): p. 33-9.
99. Balluff, B., M. Elsner, A. Kowarsch, S. Rauser, S. Meding, C. Schuhmacher, M. Feith, K. Herrmann, C. Rocken, R.M. Schmid, H. Hofler, A. Walch, and M.P. Ebert, *Classification of HER2/neu status in gastric cancer using a breast-cancer derived proteome classifier*. *J Proteome Res*, 2010. 9(12): p. 6317-22.
100. Rauser, S., C. Marquardt, B. Balluff, S.O. Deininger, C. Albers, E. Belau, R. Hartmer, D. Suckau, K. Specht, M.P. Ebert, M. Schmitt, M. Aubele, H. Hofler, and A. Walch, *Classification of HER2 receptor status in breast cancer tissues by MALDI imaging mass spectrometry*. *J Proteome Res*, 2010. 9(4): p. 1854-63.
101. Schwamborn, K., R.C. Krieg, P. Jirak, G. Ott, R. Knuchel, A. Rosenwald, and A. Wellmann, *Application of MALDI imaging for the diagnosis of classical Hodgkin lymphoma*. *J Cancer Res Clin Oncol*. 136(11): p. 1651-5.
102. Lemaire, R., S.A. Menguellat, J. Stauber, V. Marchaudon, J.P. Lucot, P. Collinet, M.O. Farine, D. Vinatier, R. Day, P. Ducoroy, M. Salzet, and I. Fournier, *Specific MALDI imaging and profiling for biomarker hunting and validation: fragment of the 11S proteasome activator complex, Reg alpha fragment, is a new potential ovary cancer biomarker*. *J Proteome Res*, 2007. 6(11): p. 4127-34.
103. Schwartz, S.A., R.J. Weil, R.C. Thompson, Y. Shyr, J.H. Moore, S.A. Toms, M.D. Johnson, and R.M. Caprioli, *Proteomic-based prognosis of brain tumor patients using direct-tissue matrix-assisted laser desorption ionization mass spectrometry*. *Cancer Res*, 2005. 65(17): p. 7674-81.
104. Yanagisawa, K., Y. Shyr, B.J. Xu, P.P. Massion, P.H. Larsen, B.C. White, J.R. Roberts, M. Edgerton, A. Gonzalez, S. Nadaf, J.H. Moore, R.M. Caprioli, and D.P. Carbone, *Proteomic patterns of tumour subsets in non-small-cell lung cancer*. *Lancet*, 2003. 362(9382): p. 433-9.
105. Reyzer, M.L., R.L. Caldwell, T.C. Dugger, J.T. Forbes, C.A. Ritter, M. Guix, C.L. Arteaga, and R.M. Caprioli, *Early changes in protein expression detected by mass spectrometry predict tumor response to molecular therapeutics*. *Cancer Res*, 2004. 64(24): p. 9093-100.
106. Stoeckli, M., D. Staab, A. Schweitzer, J. Gardiner, and D. Seebach, *Imaging of a beta-peptide distribution in whole-body mice sections by MALDI mass spectrometry*. *J Am Soc Mass Spectrom*, 2007. 18(11): p. 1921-4.
107. Manier, M.L., M.L. Reyzer, A. Goh, V. Dartois, L.E. Via, C.E. Barry, 3rd, and R.M. Caprioli, *Reagent precoated targets for rapid in-tissue derivatization of the anti-tuberculosis drug isoniazid followed by MALDI imaging mass spectrometry*. *J Am Soc Mass Spectrom*, 2011. 22(8): p. 1409-19.
108. Marino, S., M. Vooijs, H. van Der Gulden, J. Jonkers, and A. Berns, *Induction of medulloblastomas in p53-null mutant mice by somatic inactivation of Rb in the external granular layer cells of the cerebellum*. *Genes Dev*, 2000. 14(8): p. 994-1004.

109. Nakhai, H., S. Sel, J. Favor, L. Mendoza-Torres, F. Paulsen, G.I. Duncker, and R.M. Schmid, *Ptf1a is essential for the differentiation of GABAergic and glycinergic amacrine cells and horizontal cells in the mouse retina*. Development, 2007. 134(6): p. 1151-60.
110. Natarajan, A., B. Wagner, and M. Sibilio, *The EGF receptor is required for efficient liver regeneration*. Proc Natl Acad Sci U S A, 2007. 104(43): p. 17081-6.
111. Morris, J.P.t., D.A. Cano, S. Sekine, S.C. Wang, and M. Hebrok, *Beta-catenin blocks Kras-dependent reprogramming of acini into pancreatic cancer precursor lesions in mice*. J Clin Invest, 2010. 120(2): p. 508-20.
112. Cingolani, N., R. Shaco-Levy, A. Farruggio, D.S. Klimstra, and J. Rosai, *Alpha-fetoprotein production by pancreatic tumors exhibiting acinar cell differentiation: study of five cases, one arising in a mediastinal teratoma*. Hum Pathol, 2000. 31(8): p. 938-44.
113. Reddy, J.K., M.S. Rao, S.A. Qureshi, M.K. Reddy, D.G. Scarpelli, and N.D. Lalwani, *Induction and origin of hepatocytes in rat pancreas*. J Cell Biol, 1984. 98(6): p. 2082-90.
114. Dabeva, M.D., E. Hurston, and D.A. Shafritz, *Transcription factor and liver-specific mRNA expression in facultative epithelial progenitor cells of liver and pancreas*. Am J Pathol, 1995. 147(6): p. 1633-48.
115. Paner, G.P., K.S. Thompson, and C.V. Reyes, *Hepatoid carcinoma of the pancreas*. Cancer, 2000. 88(7): p. 1582-9.
116. Minervini, M.I., A.J. Demetris, R.G. Lee, B.I. Carr, J. Madariaga, and M.A. Nalesnik, *Utilization of hepatocyte-specific antibody in the immunocytochemical evaluation of liver tumors*. Mod Pathol, 1997. 10(7): p. 686-92.
117. Han, T., Y. Liu, H. Liu, Z.Y. Zhu, Y. Li, S.X. Xiao, Z. Guo, and Z.G. Zhao, *Serum thymosin beta4 levels in patients with hepatitis B virus-related liver failure*. World J Gastroenterol, 2010. 16(5): p. 625-30.
118. Weller, F.E., M.G. Mutchnick, A.L. Goldstein, and P.H. Naylor, *Enzyme immunoassay measurement of thymosin beta 4 in human serum*. J Biol Response Mod, 1988. 7(1): p. 91-6.
119. Gerdes, J., H. Lemke, H. Baisch, H.H. Wacker, U. Schwab, and H. Stein, *Cell cycle analysis of a cell proliferation-associated human nuclear antigen defined by the monoclonal antibody Ki-67*. J Immunol, 1984. 133(4): p. 1710-5.
120. Fjallskog, M.L., M.H. Lejonklou, K.E. Oberg, B.K. Eriksson, and E.T. Janson, *Expression of molecular targets for tyrosine kinase receptor antagonists in malignant endocrine pancreatic tumors*. Clin Cancer Res, 2003. 9(4): p. 1469-73.
121. Korc, M., H. Friess, Y. Yamanaka, M.S. Kobrin, M. Buchler, and H.G. Beger, *Chronic pancreatitis is associated with increased concentrations of epidermal growth factor receptor, transforming growth factor alpha, and phospholipase C gamma*. Gut, 1994. 35(10): p. 1468-73.
122. Zhao, S., Y. Wang, L. Cao, M.M. Ouellette, and J.W. Freeman, *Expression of oncogenic K-ras and loss of Smad4 cooperate to induce the expression of EGFR and to promote invasion of immortalized human pancreas ductal cells*. International journal of cancer. Journal international du cancer, 2010. 127(9): p. 2076-87.
123. Jaganathan, S., P. Yue, and J. Turkson, *Enhanced sensitivity of pancreatic cancer cells to concurrent inhibition of aberrant signal transducer and activator of transcription 3 and epidermal growth factor receptor or Src*. The Journal of pharmacology and experimental therapeutics, 2010. 333(2): p. 373-81.
124. Larbouret, C., B. Robert, I. Navarro-Teulon, S. Thezenas, M.Z. Ladjemi, S. Morisseau, E. Campigna, F. Bibeau, J.P. Mach, A. Pelegrin, and D. Azria, *In*

- vivo therapeutic synergism of anti-epidermal growth factor receptor and anti-HER2 monoclonal antibodies against pancreatic carcinomas.* Clinical cancer research : an official journal of the American Association for Cancer Research, 2007. 13(11): p. 3356-62.
125. Pino, M.S., M. Shrader, C.H. Baker, F. Cognetti, H.Q. Xiong, J.L. Abbruzzese, and D.J. McConkey, *Transforming growth factor alpha expression drives constitutive epidermal growth factor receptor pathway activation and sensitivity to gefitinib (Iressa) in human pancreatic cancer cell lines.* Cancer research, 2006. 66(7): p. 3802-12.
  126. Gidekel Friedlander, S.Y., G.C. Chu, E.L. Snyder, N. Girnius, G. Dibelius, D. Crowley, E. Vasile, R.A. DePinho, and T. Jacks, *Context-dependent transformation of adult pancreatic cells by oncogenic K-Ras.* Cancer Cell, 2009. 16(5): p. 379-89.
  127. De Lisle, R.C. and C.D. Logsdon, *Pancreatic acinar cells in culture: expression of acinar and ductal antigens in a growth-related manner.* Eur J Cell Biol, 1990. 51(1): p. 64-75.
  128. Miyamoto, Y., A. Maitra, B. Ghosh, U. Zechner, P. Argani, C.A. Iacobuzio-Donahue, V. Sriuranpong, T. Iso, I.M. Meszoely, M.S. Wolfe, R.H. Hruban, D.W. Ball, R.M. Schmid, and S.D. Leach, *Notch mediates TGF alpha-induced changes in epithelial differentiation during pancreatic tumorigenesis.* Cancer Cell, 2003. 3(6): p. 565-76.
  129. Selander, L. and H. Edlund, *Nestin is expressed in mesenchymal and not epithelial cells of the developing mouse pancreas.* Mech Dev, 2002. 113(2): p. 189-92.
  130. Ji, B., L. Tsou, H. Wang, S. Gaiser, D.Z. Chang, J. Daniluk, Y. Bi, T. Grote, D.S. Longnecker, and C.D. Logsdon, *Ras activity levels control the development of pancreatic diseases.* Gastroenterology, 2009. 137(3): p. 1072-82, 1082 e1-6.
  131. Basu, T., P.H. Warne, and J. Downward, *Role of Shc in the activation of Ras in response to epidermal growth factor and nerve growth factor.* Oncogene, 1994. 9(12): p. 3483-91.
  132. Gale, N.W., S. Kaplan, E.J. Lowenstein, J. Schlessinger, and D. Bar-Sagi, *Grb2 mediates the EGF-dependent activation of guanine nucleotide exchange on Ras.* Nature, 1993. 363(6424): p. 88-92.
  133. Fukuda, A., S.C. Wang, J.P.t. Morris, A.E. Folias, A. Liou, G.E. Kim, S. Akira, K.M. Boucher, M.A. Firpo, S.J. Mulvihill, and M. Hebrok, *Stat3 and MMP7 contribute to pancreatic ductal adenocarcinoma initiation and progression.* Cancer Cell, 2011. 19(4): p. 441-55.
  134. Heid, I., C. Lubeseder-Martellato, B. Sipos, P.K. Mazur, M. Lesina, R.M. Schmid, and J.T. Siveke, *Early requirement of Rac1 in a mouse model of pancreatic cancer.* Gastroenterology, 2011. 141(2): p. 719-30, 730 e1-7.
  135. Iverson, C., G. Larson, C. Lai, L.T. Yeh, C. Dadson, P. Weingarten, T. Appleby, T. Vo, A. Maderna, J.M. Vernier, R. Hamatake, J.N. Miner, and B. Quart, *RDEA119/BAY 869766: a potent, selective, allosteric inhibitor of MEK1/2 for the treatment of cancer.* Cancer Res, 2009. 69(17): p. 6839-47.
  136. Faca, V.M., K.S. Song, H. Wang, Q. Zhang, A.L. Krasnoselsky, L.F. Newcomb, R.R. Plentz, S. Gurumurthy, M.S. Redston, S.J. Pitteri, S.R. Pereira-Faca, R.C. Ireton, H. Katayama, V. Glukhova, D. Phanstiel, D.E. Brenner, M.A. Anderson, D. Misek, N. Scholler, N.D. Urban, M.J. Barnett, C. Edelstein, G.E. Goodman, M.D. Thornquist, M.W. McIntosh, R.A. DePinho, N. Bardeesy, and S.M. Hanash, *A mouse to human search for plasma proteome changes associated with pancreatic tumor development.* PLoS Med, 2008. 5(6): p. e123.
  137. Taguchi, A., K. Politi, S.J. Pitteri, W.W. Lockwood, V.M. Faca, K. Kelly-Spratt, C.H. Wong, Q. Zhang, A. Chin, K.S. Park, G. Goodman, A.F. Gazdar, J. Sage,

- D.M. Dinulescu, R. Kucherlapati, R.A. Depinho, C.J. Kemp, H.E. Varmus, and S.M. Hanash, *Lung cancer signatures in plasma based on proteome profiling of mouse tumor models*. *Cancer Cell*, 2011. 20(3): p. 289-99.
138. Meistermann, H., J.L. Norris, H.R. Aerni, D.S. Cornett, A. Friedlein, A.R. Erskine, A. Augustin, M.C. De Vera Mudry, S. Ruepp, L. Suter, H. Langen, R.M. Caprioli, and A. Ducret, *Biomarker discovery by imaging mass spectrometry: transthyretin is a biomarker for gentamicin-induced nephrotoxicity in rat*. *Mol Cell Proteomics*, 2006. 5(10): p. 1876-86.
139. Schwartz, S.A., R.J. Weil, M.D. Johnson, S.A. Toms, and R.M. Caprioli, *Protein profiling in brain tumors using mass spectrometry: feasibility of a new technique for the analysis of protein expression*. *Clin Cancer Res*, 2004. 10(3): p. 981-7.
140. Reyzer, M.L., Y. Hsieh, K. Ng, W.A. Korfmacher, and R.M. Caprioli, *Direct analysis of drug candidates in tissue by matrix-assisted laser desorption/ionization mass spectrometry*. *J Mass Spectrom*, 2003. 38(10): p. 1081-92.
141. Caprioli, R.M., *Deciphering protein molecular signatures in cancer tissues to aid in diagnosis, prognosis, and therapy*. *Cancer Res*, 2005. 65(23): p. 10642-5.
142. Pan, S., R. Chen, R.E. Brand, S. Hawley, Y. Tamura, P.R. Gafken, B.P. Milless, D.R. Goodlett, J. Rush, and T.A. Brentnall, *Multiplex Targeted Proteomic Assay for Biomarker Detection in Plasma: A Pancreatic Cancer Biomarker Case Study*. *J Proteome Res*, 2012.
143. Pan, S., R. Chen, D.A. Crispin, D. May, T. Stevens, M.W. McIntosh, M.P. Bronner, A. Ziogas, H. Anton-Culver, and T.A. Brentnall, *Protein alterations associated with pancreatic cancer and chronic pancreatitis found in human plasma using global quantitative proteomics profiling*. *J Proteome Res*, 2011. 10(5): p. 2359-76.
144. Ohuchida, K., K. Mizumoto, Y. Miyasaka, J. Yu, L. Cui, H. Yamaguchi, H. Toma, S. Takahata, N. Sato, E. Nagai, K. Yamaguchi, M. Tsuneyoshi, and M. Tanaka, *Over-expression of S100A2 in pancreatic cancer correlates with progression and poor prognosis*. *J Pathol*, 2007. 213(3): p. 275-82.
145. Jaskolla, T.W., M. Karas, U. Roth, K. Steinert, C. Menzel, and K. Reihls, *Comparison between vacuum sublimed matrices and conventional dried droplet preparation in MALDI-TOF mass spectrometry*. *J Am Soc Mass Spectrom*, 2009. 20(6): p. 1104-14.
146. Djidja, M.C., E. Claude, M.F. Snel, P. Scriven, S. Francese, V. Carolan, and M.R. Clench, *MALDI-ion mobility separation-mass spectrometry imaging of glucose-regulated protein 78 kDa (Grp78) in human formalin-fixed, paraffin-embedded pancreatic adenocarcinoma tissue sections*. *J Proteome Res*, 2009. 8(10): p. 4876-84.
147. Lukie, B.E., *Serum protein content of rat small-intestinal mucus*. *Dig Dis Sci*, 1986. 31(1): p. 73-8.
148. Kim, N., W. Yoo, J. Lee, H. Kim, H. Lee, Y.S. Kim, D.U. Kim, and J. Oh, *Formation of vitamin A lipid droplets in pancreatic stellate cells requires albumin*. *Gut*, 2009. 58(10): p. 1382-90.
149. Lardon, J., S. De Breuck, I. Rooman, L. Van Lommel, M. Kruhoffer, T. Orntoft, F. Schuit, and L. Bouwens, *Plasticity in the adult rat pancreas: transdifferentiation of exocrine to hepatocyte-like cells in primary culture*. *Hepatology*, 2004. 39(6): p. 1499-507.
150. Shen, C.N., J.R. Seckl, J.M. Slack, and D. Tosh, *Glucocorticoids suppress beta-cell development and induce hepatic metaplasia in embryonic pancreas*. *Biochem J*, 2003. 375(Pt 1): p. 41-50.
151. Shen, C.N., J.M. Slack, and D. Tosh, *Molecular basis of transdifferentiation of pancreas to liver*. *Nat Cell Biol*, 2000. 2(12): p. 879-87.

152. Masui, T., G.H. Swift, T. Deering, C. Shen, W.S. Coats, Q. Long, H.P. Elsassser, M.A. Magnuson, and R.J. MacDonald, *Replacement of Rbpj with Rbpjl in the PTF1 complex controls the final maturation of pancreatic acinar cells.* Gastroenterology, 2010. 139(1): p. 270-80.
153. Zhang, Y., L.W. Feurino, Q. Zhai, H. Wang, W.E. Fisher, C. Chen, Q. Yao, and M. Li, *Thymosin Beta 4 is overexpressed in human pancreatic cancer cells and stimulates proinflammatory cytokine secretion and JNK activation.* Cancer Biol Ther, 2008. 7(3): p. 419-23.
154. Paciucci, R., G. Berrozpe, M. Tora, E. Navarro, A. Garcia de Herreros, and F.X. Real, *Isolation of tissue-type plasminogen activator, cathepsin H, and non-specific cross-reacting antigen from SK-PC-1 pancreas cancer cells using subtractive hybridization.* FEBS Lett, 1996. 385(1-2): p. 72-6.
155. Nemolato, S., T. Cabras, F. Cau, M.U. Fanari, D. Fanni, B. Manconi, I. Messana, M. Castagnola, and G. Faa, *Different thymosin Beta 4 immunoreactivity in foetal and adult gastrointestinal tract.* PLoS One, 2010. 5(2): p. e9111.
156. Goldstein, A.L., E. Hannappel, G. Sosne, and H.K. Kleinman, *Thymosin beta4: a multi-functional regenerative peptide. Basic properties and clinical applications.* Expert Opin Biol Ther. 12(1): p. 37-51.
157. Smart, N., C.A. Risebro, A.A. Melville, K. Moses, R.J. Schwartz, K.R. Chien, and P.R. Riley, *Thymosin beta4 induces adult epicardial progenitor mobilization and neovascularization.* Nature, 2007. 445(7124): p. 177-82.
158. Spurney, C.F., H.J. Cha, A. Sali, G.S. Pandey, E. Pistilli, A.D. Guerron, H. Gordish-Dressman, E.P. Hoffman, and K. Nagaraju, *Evaluation of skeletal and cardiac muscle function after chronic administration of thymosin beta-4 in the dystrophin deficient mouse.* PLoS One, 2010. 5(1): p. e8976.
159. Watrous, J.D., T. Alexandrov, and P.C. Dorrestein, *The evolving field of imaging mass spectrometry and its impact on future biological research.* J Mass Spectrom, 2011. 46(2): p. 209-22.
160. Minchinton, A.I. and I.F. Tannock, *Drug penetration in solid tumours.* Nat Rev Cancer, 2006. 6(8): p. 583-92.
161. Tredan, O., C.M. Galmarini, K. Patel, and I.F. Tannock, *Drug resistance and the solid tumor microenvironment.* J Natl Cancer Inst, 2007. 99(19): p. 1441-54.
162. Burris, H.A., 3rd, M.J. Moore, J. Andersen, M.R. Green, M.L. Rothenberg, M.R. Modiano, M.C. Cripps, R.K. Portenoy, A.M. Storniolo, P. Tarassoff, R. Nelson, F.A. Dorr, C.D. Stephens, and D.D. Von Hoff, *Improvements in survival and clinical benefit with gemcitabine as first-line therapy for patients with advanced pancreas cancer: a randomized trial.* J Clin Oncol, 1997. 15(6): p. 2403-13.
163. Shimamura, T., R.E. Royal, M. Kioi, A. Nakajima, S.R. Husain, and R.K. Puri, *Interleukin-4 cytotoxin therapy synergizes with gemcitabine in a mouse model of pancreatic ductal adenocarcinoma.* Cancer Res, 2007. 67(20): p. 9903-12.
164. Harsha, H.C., A. Jimeno, H. Molina, A.B. Mihalas, M.G. Goggins, R.H. Hruban, R.D. Schulick, U. Kamath, A. Maitra, M. Hidalgo, and A. Pandey, *Activated epidermal growth factor receptor as a novel target in pancreatic cancer therapy.* J Proteome Res, 2008. 7(11): p. 4651-8.
165. Bruns, C.J., M. Shrader, M.T. Harbison, C. Portera, C.C. Solorzano, K.W. Jauch, D.J. Hicklin, R. Radinsky, and L.M. Ellis, *Effect of the vascular endothelial growth factor receptor-2 antibody DC101 plus gemcitabine on growth, metastasis and angiogenesis of human pancreatic cancer growing orthotopically in nude mice.* Int J Cancer, 2002. 102(2): p. 101-8.
166. Verma, A., S. Guha, P. Diagaradjane, A.B. Kunnumakkara, A.M. Sanguino, G. Lopez-Berestein, A.K. Sood, B.B. Aggarwal, S. Krishnan, J.G. Gelovani, and K.



- Mehta, *Therapeutic significance of elevated tissue transglutaminase expression in pancreatic cancer*. Clin Cancer Res, 2008. 14(8): p. 2476-83.
167. Zahorowska, B., P.J. Crowe, and J.L. Yang, *Combined therapies for cancer: a review of EGFR-targeted monotherapy and combination treatment with other drugs*. J Cancer Res Clin Oncol, 2009. 135(9): p. 1137-48.
  168. Sofuni, A., H. Iijima, F. Moriyasu, D. Nakayama, M. Shimizu, K. Nakamura, F. Itokawa, and T. Itoi, *Differential diagnosis of pancreatic tumors using ultrasound contrast imaging*. J Gastroenterol, 2005. 40(5): p. 518-25.
  169. Sakamoto, H., M. Kitano, Y. Suetomi, K. Maekawa, Y. Takeyama, and M. Kudo, *Utility of contrast-enhanced endoscopic ultrasonography for diagnosis of small pancreatic carcinomas*. Ultrasound Med Biol, 2008. 34(4): p. 525-32.
  170. Marko-Varga, G., T.E. Fehniger, M. Rezeli, B. Dome, T. Laurell, and A. Vegvari, *Drug localization in different lung cancer phenotypes by MALDI mass spectrometry imaging*. J Proteomics, 2011. 74(7): p. 982-92.
  171. Weis, S.M. and D.A. Cheresh, *Tumor angiogenesis: molecular pathways and therapeutic targets*. Nat Med, 2011. 17(11): p. 1359-70.
  172. Leu, A.J., D.A. Berk, A. Lymboussaki, K. Alitalo, and R.K. Jain, *Absence of functional lymphatics within a murine sarcoma: a molecular and functional evaluation*. Cancer Res, 2000. 60(16): p. 4324-7.
  173. Milosevic, M.F., A.W. Fyles, R. Wong, M. Pintilie, M.C. Kavanagh, W. Levin, L.A. Manchul, T.J. Keane, and R.P. Hill, *Interstitial fluid pressure in cervical carcinoma: within tumor heterogeneity, and relation to oxygen tension*. Cancer, 1998. 82(12): p. 2418-26.
  174. Stohrer, M., Y. Boucher, M. Stangassinger, and R.K. Jain, *Oncotic pressure in solid tumors is elevated*. Cancer Res, 2000. 60(15): p. 4251-5.
  175. Heldin, C.H., K. Rubin, K. Pietras, and A. Ostman, *High interstitial fluid pressure - an obstacle in cancer therapy*. Nat Rev Cancer, 2004. 4(10): p. 806-13.
  176. Netti, P.A., L.M. Hamberg, J.W. Babich, D. Kierstead, W. Graham, G.J. Hunter, G.L. Wolf, A. Fischman, Y. Boucher, and R.K. Jain, *Enhancement of fluid filtration across tumor vessels: implication for delivery of macromolecules*. Proc Natl Acad Sci U S A, 1999. 96(6): p. 3137-42.
  177. Pluen, A., Y. Boucher, S. Ramanujan, T.D. McKee, T. Gohongi, E. di Tomaso, E.B. Brown, Y. Izumi, R.B. Campbell, D.A. Berk, and R.K. Jain, *Role of tumor-host interactions in interstitial diffusion of macromolecules: cranial vs. subcutaneous tumors*. Proc Natl Acad Sci U S A, 2001. 98(8): p. 4628-33.
  178. Salnikow, A.V., V.V. Iversen, M. Koisti, C. Sundberg, L. Johansson, L.B. Stuhr, M. Sjoquist, H. Ahlstrom, R.K. Reed, and K. Rubin, *Lowering of tumor interstitial fluid pressure specifically augments efficacy of chemotherapy*. FASEB J, 2003. 17(12): p. 1756-8.
  179. Chaplin, D.J., M.J. Trotter, R.E. Durand, P.L. Olive, and A.I. Minchinton, *Evidence for intermittent radiobiological hypoxia in experimental tumour systems*. Biomed Biochim Acta, 1989. 48(2-3): p. S255-9.
  180. Durand, R.E. and N.E. LePard, *Contribution of transient blood flow to tumour hypoxia in mice*. Acta Oncol, 1995. 34(3): p. 317-23.
  181. Helmlinger, G., F. Yuan, M. Dellian, and R.K. Jain, *Interstitial pH and pO<sub>2</sub> gradients in solid tumors in vivo: high-resolution measurements reveal a lack of correlation*. Nat Med, 1997. 3(2): p. 177-82.
  182. Khatib-Shahidi, S., M. Andersson, J.L. Herman, T.A. Gillespie, and R.M. Caprioli, *Direct molecular analysis of whole-body animal tissue sections by imaging MALDI mass spectrometry*. Anal Chem, 2006. 78(18): p. 6448-56.
  183. Trim, P.J., C.M. Henson, J.L. Avery, A. McEwen, M.F. Snel, E. Claude, P.S. Marshall, A. West, A.P. Princivalle, and M.R. Clench, *Matrix-assisted laser*

- desorption/ionization-ion mobility separation-mass spectrometry imaging of vinblastine in whole body tissue sections.* Anal Chem, 2008. 80(22): p. 8628-34.
184. Hsieh, Y., R. Casale, E. Fukuda, J. Chen, I. Knemeyer, J. Wingate, R. Morrison, and W. Korfmacher, *Matrix-assisted laser desorption/ionization imaging mass spectrometry for direct measurement of clozapine in rat brain tissue.* Rapid Commun Mass Spectrom, 2006. 20(6): p. 965-72.
  185. Signor, L., E. Varesio, R.F. Staack, V. Starke, W.F. Richter, and G. Hopfgartner, *Analysis of erlotinib and its metabolites in rat tissue sections by MALDI quadrupole time-of-flight mass spectrometry.* J Mass Spectrom, 2007. 42(7): p. 900-9.
  186. Sugiura, Y. and M. Setou, *Imaging mass spectrometry for visualization of drug and endogenous metabolite distribution: toward in situ pharmacometabolomes.* J Neuroimmune Pharmacol, 2010. 5(1): p. 31-43.
  187. Nilsson, A., T.E. Fehniger, L. Gustavsson, M. Andersson, K. Kenne, G. Marko-Varga, and P.E. Andren, *Fine mapping the spatial distribution and concentration of unlabeled drugs within tissue micro-compartments using imaging mass spectrometry.* PLoS One, 2010. 5(7): p. e11411.
  188. Prideaux, B., V. Dartois, D. Staab, D.M. Weiner, A. Goh, L.E. Via, C.E. Barry, 3rd, and M. Stoeckli, *High-sensitivity MALDI-MRM-MS imaging of moxifloxacin distribution in tuberculosis-infected rabbit lungs and granulomatous lesions.* Anal Chem, 2011. 83(6): p. 2112-8.
  189. Koeniger, S.L., N. Talaty, Y. Luo, D. Ready, M. Voorbach, T. Seifert, S. Cepa, J.A. Fagerland, J. Bouska, W. Buck, R.W. Johnson, and S. Spanton, *A quantitation method for mass spectrometry imaging.* Rapid Commun Mass Spectrom, 2011. 25(4): p. 503-10.
  190. Atkinson, S.J., P.M. Loadman, C. Sutton, L.H. Patterson, and M.R. Clench, *Examination of the distribution of the bioreductive drug AQ4N and its active metabolite AQ4 in solid tumours by imaging matrix-assisted laser desorption/ionisation mass spectrometry.* Rapid Commun Mass Spectrom, 2007. 21(7): p. 1271-6.
  191. Bouslimani, A., N. Bec, M. Glueckmann, C. Hirtz, and C. Larroque, *Matrix-assisted laser desorption/ionization imaging mass spectrometry of oxaliplatin derivatives in heated intraoperative chemotherapy (HIPEC)-like treated rat kidney.* Rapid Commun Mass Spectrom, 2010. 24(4): p. 415-21.
  192. Friess, H., P. Berberat, M. Schilling, J. Kunz, M. Korc, and M.W. Buchler, *Pancreatic cancer: the potential clinical relevance of alterations in growth factors and their receptors.* J Mol Med (Berl), 1996. 74(1): p. 35-42.
  193. Dlugosz, A.A., L. Hansen, C. Cheng, N. Alexander, M.F. Denning, D.W. Threadgill, T. Magnuson, R.J. Coffey, Jr., and S.H. Yuspa, *Targeted disruption of the epidermal growth factor receptor impairs growth of squamous papillomas expressing the v-ras(Ha) oncogene but does not block in vitro keratinocyte responses to oncogenic ras.* Cancer Res, 1997. 57(15): p. 3180-8.
  194. Sibilica, M., A. Fleischmann, A. Behrens, L. Stingl, J. Carroll, F.M. Watt, J. Schlessinger, and E.F. Wagner, *The EGF receptor provides an essential survival signal for SOS-dependent skin tumor development.* Cell, 2000. 102(2): p. 211-20.
  195. Hansen, L.A., R.L. Woodson, 2nd, S. Holbus, K. Strain, Y.C. Lo, and S.H. Yuspa, *The epidermal growth factor receptor is required to maintain the proliferative population in the basal compartment of epidermal tumors.* Cancer Res, 2000. 60(13): p. 3328-32.
  196. Bardeesy, N., M. Kim, J. Xu, R.S. Kim, Q. Shen, M.W. Bosenberg, W.H. Wong, and L. Chin, *Role of epidermal growth factor receptor signaling in RAS-driven melanoma.* Mol Cell Biol, 2005. 25(10): p. 4176-88.

197. Jaganathan, S., P. Yue, and J. Turkson, *Enhanced sensitivity of pancreatic cancer cells to concurrent inhibition of aberrant signal transducer and activator of transcription 3 and epidermal growth factor receptor or Src*. *J Pharmacol Exp Ther*, 2010. 333(2): p. 373-81.
198. Larbouret, C., B. Robert, I. Navarro-Teulon, S. Thezenas, M.Z. Ladjemi, S. Morisseau, E. Campigna, F. Bibeau, J.P. Mach, A. Pelegrin, and D. Azria, *In vivo therapeutic synergism of anti-epidermal growth factor receptor and anti-HER2 monoclonal antibodies against pancreatic carcinomas*. *Clin Cancer Res*, 2007. 13(11): p. 3356-62.
199. Pino, M.S., M. Shrader, C.H. Baker, F. Cognetti, H.Q. Xiong, J.L. Abbruzzese, and D.J. McConkey, *Transforming growth factor alpha expression drives constitutive epidermal growth factor receptor pathway activation and sensitivity to gefitinib (Iressa) in human pancreatic cancer cell lines*. *Cancer Res*, 2006. 66(7): p. 3802-12.
200. Zhao, S., Y. Wang, L. Cao, M.M. Ouellette, and J.W. Freeman, *Expression of oncogenic K-ras and loss of Smad4 cooperate to induce the expression of EGFR and to promote invasion of immortalized human pancreas ductal cells*. *Int J Cancer*, 2010. 127(9): p. 2076-87.
201. Gangarosa, L.M., N. Sizemore, R. Graves-Deal, S.M. Oldham, C.J. Der, and R.J. Coffey, *A raf-independent epidermal growth factor receptor autocrine loop is necessary for Ras transformation of rat intestinal epithelial cells*. *J Biol Chem*, 1997. 272(30): p. 18926-31.
202. Barton, S., N. Starling, and C. Swanton, *Predictive molecular markers of response to epidermal growth factor receptor(EGFR) family-targeted therapies*. *Curr Cancer Drug Targets*, 2010. 10(8): p. 799-812.
203. Jimeno, A., A.C. Tan, J. Coffa, N.V. Rajeshkumar, P. Kulesza, B. Rubio-Viqueira, J. Wheelhouse, B. Diosdado, W.A. Messersmith, C. Iacobuzio-Donahue, A. Maitra, M. Varella-Garcia, F.R. Hirsch, G.A. Meijer, and M. Hidalgo, *Coordinated epidermal growth factor receptor pathway gene overexpression predicts epidermal growth factor receptor inhibitor sensitivity in pancreatic cancer*. *Cancer Res*, 2008. 68(8): p. 2841-9.
204. da Cunha Santos, G., N. Dhani, D. Tu, K. Chin, O. Ludkovski, S. Kamel-Reid, J. Squire, W. Parulekar, M.J. Moore, and M.S. Tsao, *Molecular predictors of outcome in a phase 3 study of gemcitabine and erlotinib therapy in patients with advanced pancreatic cancer: National Cancer Institute of Canada Clinical Trials Group Study PA.3*. *Cancer*. 116(24): p. 5599-607.
205. Kim, S.T., H. Lim do, K.T. Jang, T. Lim, J. Lee, Y.L. Choi, H.L. Jang, J.H. Yi, K.K. Baek, S.H. Park, Y.S. Park, H.Y. Lim, W.K. Kang, and J.O. Park, *Impact of KRAS mutations on clinical outcomes in pancreatic cancer patients treated with first-line gemcitabine-based chemotherapy*. *Mol Cancer Ther*, 2011. 10(10): p. 1993-9.
206. Collisson, E.A., A. Sadanandam, P. Olson, W.J. Gibb, M. Truitt, S. Gu, J. Cooc, J. Weinkle, G.E. Kim, L. Jakkula, H.S. Feiler, A.H. Ko, A.B. Olshen, K.L. Danenberg, M.A. Tempero, P.T. Spellman, D. Hanahan, and J.W. Gray, *Subtypes of pancreatic ductal adenocarcinoma and their differing responses to therapy*. *Nat Med*, 2011. 17(4): p. 500-3.
207. Zhao, C., G. Du, K. Skowronek, M.A. Frohman, and D. Bar-Sagi, *Phospholipase D2-generated phosphatidic acid couples EGFR stimulation to Ras activation by Sos*. *Nat Cell Biol*, 2007. 9(6): p. 706-12.
208. Zhang, L., M. Bewick, and R.M. Lafrenie, *EGFR and ErbB2 differentially regulate Raf-1 translocation and activation*. *Lab Invest*, 2002. 82(1): p. 71-8.
209. Casar, B., I. Arozarena, V. Sanz-Moreno, A. Pinto, L. Agudo-Ibanez, R. Marais, R.E. Lewis, M.T. Berciano, and P. Crespo, *Ras subcellular localization defines*

- extracellular signal-regulated kinase 1 and 2 substrate specificity through distinct utilization of scaffold proteins*. Mol Cell Biol, 2009. 29(5): p. 1338-53.
210. Guerra, C., M. Collado, C. Navas, A.J. Schuhmacher, I. Hernandez-Porrás, M. Canamero, M. Rodríguez-Justo, M. Serrano, and M. Barbacid, *Pancreatitis-induced inflammation contributes to pancreatic cancer by inhibiting oncogene-induced senescence*. Cancer Cell, 2011. 19(6): p. 728-39.
211. Lee, K.E. and D. Bar-Sagi, *Oncogenic KRas suppresses inflammation-associated senescence of pancreatic ductal cells*. Cancer Cell, 2010. 18(5): p. 448-58.

## 7 Supplementary material

### 7.1.1 Supplementary Tables 7-1 to 7-12

Each table lists all discriminating  $m/z$ -species (mass) for the in the table title indicated comparison, the corresponding  $p$  value with Wilcoxon rank-sum test with Benjamini-Hochberg correction (PWKW) and the average relative intensity (AVE) of this mass within the two groups. For reasons of clarity and comprehensibility  $p$  values were rounded according to standard mathematical rules.

**Table 7-1**  
Significant  $m/z$ -species from comparison PanIN vs IPMN

Mass	PWKW	Ave IPMN	Ave PanIN
2813.18	<0.05	5.33	7.83
2830.11	<0.05	5.49	7.71
3789.68	<0.05	3.79	5.68
7219.74	<0.05	2.1	3.69
7418.39	<0.05	2.2	3.72
2791.08	<0.05	18.1	27.56

**Table 7-2**  
Significant  $m/z$ -species from comparison PanIN vs PDAC

Mass	PWKW	Ave PanIN	Ave PDAC
4936.62	<0.001	4.28	12.28
3473.41	<0.001	6.63	3.88
3438.84	<0.001	5.21	3.46
3789.66	<0.01	5.66	3.42
7219.74	<0.01	3.71	1.9
7180.42	<0.01	2.14	1.64
7418.46	<0.01	3.75	1.89
6223.02	<0.01	3.35	4.61
5836.12	<0.05	3.68	2.29
3531.57	<0.05	4.99	3.86
4747.02	<0.05	3.66	6.67
4334.14	<0.05	7.35	5.16
9959.11	<0.05	1.44	2.82
6274.23	<0.05	3.53	4.89

3514.79	<0.05	4.57	3.74
4165.71	<0.05	4.33	3.51
14034.25	<0.05	0.92	1.73
11300.51	<0.05	0.99	1.47
6257.68	<0.05	2.39	2.89
4319.12	<0.05	4.05	3.24
4236.97	<0.05	4.29	3.63
8425.64	<0.05	1.54	1.83
4963.06	<0.05	17.2	37.17
5800.84	<0.05	6.24	2.54
11337.21	<0.05	0.98	1.31
3455.95	<0.05	5.03	4.03
14001.79	<0.05	0.96	1.57
6242.88	<0.05	2.63	3.16
6170.3	<0.05	2.4	2.69
4984.01	<0.05	7.81	13.05

**Table 7-3**  
Significant *m/z*-species from comparison PDAC vs IPMN

Mass	PWKW	Ave PDAC	Ave IPMN
4936.53	< 0.01	12.3	4.51
3456.02	< 0.01	4.03	5.89
3423.61	< 0.01	3.7	4.5
3514.57	< 0.01	3.74	4.74
3530.81	< 0.05	3.83	5.04
3473.17	< 0.05	3.84	5.37
3439.16	< 0.05	3.49	4.97
9958.4	< 0.05	2.83	1.39
5765.04	< 0.05	2.07	2.93

**Table 7-4**  
Significant *m/z*-species from comparison PDAC vs Lesion (PanIN and IPMN)

Mass	PWKW	Ave Lesion	Ave PDAC
4936.44	< 0.001	4.31	12.28
3424.45	< 0.01	4.58	3.72
3473.09	< 0.01	5.64	3.87
3439.43	< 0.01	4.82	3.48
3530.74	< 0.01	5.04	3.84
7417.9	< 0.05	3.12	1.89

3789.51	< 0.05	5.01	3.42
5835.38	< 0.05	3.49	2.22
9958.48	< 0.05	1.49	2.85
7219.16	< 0.05	3.1	1.91
3455.73	< 0.05	5.19	4.03
3514.25	< 0.05	4.57	3.74
4962.82	< 0.05	17.85	37.17
4746.61	< 0.05	4.02	6.68
14033.43	< 0.05	1.01	1.73
5800.94	< 0.05	5.66	2.44

**Table 7-5**  
**Significant *m/z*-species from comparison wild type vs PDAC**

<b>Mass</b>	<b>PWKW</b>	<b>Ave WT</b>	<b>Ave PDAC</b>
6646.03	< 0.001	19.9	4.77
6683.87	< 0.001	5.33	2.13
6604.23	< 0.001	3.68	2.13
6310.97	< 0.001	3.75	2.41
6571.18	< 0.001	2.55	2
3454.92	< 0.001	7.91	4.11
6118.98	< 0.001	3.62	2.35
2791.7	< 0.001	5.83	29.41
4936.6	< 0.001	3.48	12.29
6274.16	< 0.001	10.71	4.9
6222.46	< 0.001	9.07	4.62
6142.17	< 0.001	2.86	2.19
6189.29	< 0.001	3.98	2.61
3002.06	< 0.001	3.76	5.01
6851.29	< 0.001	2.32	1.8
6168.87	< 0.01	3.47	2.59
9959.63	< 0.01	1.31	2.86
11138.33	< 0.01	1.22	0.91
12537.43	< 0.01	0.94	0.69
2813.75	< 0.01	3.78	7.16
10502.28	< 0.01	2.28	1.24
3322.95	< 0.01	4.65	3.59
3039.79	< 0.01	3.54	5.32
4962.96	< 0.01	13.03	37.17

4983.85	< 0.01	5.33	13.06
2830.6	< 0.01	4.01	7.25
4333.38	< 0.01	3.02	5.16
5168.85	< 0.01	2.93	4.54
7639.3	< 0.01	1.61	1.32
4540.4	< 0.01	2.68	3.66
3440	< 0.01	4.27	3.42
17451.23	< 0.01	0.58	0.42
20689.06	< 0.01	0.46	0.35
4746.93	< 0.05	3.44	6.67
4278.44	< 0.05	3.08	4.01
10579.88	< 0.05	1.36	1.06
24759.57	< 0.05	0.44	0.32
20975.94	< 0.05	0.46	0.35
11099.96	< 0.05	1.03	0.86
5022.15	< 0.05	3.7	6.37
4836.74	< 0.05	5.02	3.42
4919.44	< 0.05	2.86	3.53
11170.36	< 0.05	1.05	0.89
7003.99	< 0.05	2.21	1.94
11055.96	< 0.05	1.14	0.97
14403.69	< 0.05	0.8	0.65
5060.07	< 0.05	2.93	3.96
20734.74	< 0.05	0.43	0.35

**Table 7-6**  
**Significant *m/z*-species from comparison wild type vs IPMN**

<b>Mass</b>	<b>PWKW</b>	<b>Ave WT</b>	<b>Ave IPMN</b>
3530.62	< 0.001	3.7	4.92
6604.28	< 0.001	3.66	2.44
6645.81	< 0.001	19.76	6.04
4334.02	< 0.001	3.06	5.06
4239.16	< 0.001	3.21	4.4
4165.67	< 0.001	3.12	4.23
6274.04	< 0.001	10.67	4.63
6222.09	< 0.001	9.03	4.53
6683.78	< 0.001	5.23	2.42
4541.08	< 0.001	2.79	3.72



3513.67	< 0.001	3.87	4.66
14001.34	< 0.001	1.96	1.11
6167.9	< 0.001	3.95	2.87
4277.83	< 0.001	3.07	4.1
3492.48	< 0.001	4.82	8.31
6118.91	< 0.001	3.66	2.57
3001.32	< 0.01	3.86	4.99
6311.13	< 0.01	3.75	2.69
11137.79	< 0.01	1.22	0.92
2790.78	< 0.01	5.81	17.64
10501.63	< 0.01	2.26	1.29
6141.25	< 0.01	2.8	2.25
2829.5	< 0.01	4	5.45
14409.62	< 0.01	0.78	0.6
11056.09	< 0.01	1.06	0.85
17456.17	< 0.01	0.5	0.38
2813	< 0.01	3.8	5.3
3058.99	< 0.01	3.75	4.61
11102.19	< 0.01	1	0.82
21788.64	< 0.01	0.43	0.33
2928.46	< 0.01	3.72	4.63
6570.16	< 0.01	2.86	2.26
12535.09	< 0.01	0.94	0.73
6850.56	< 0.05	2.33	1.99
10639.75	< 0.05	1.08	0.86
6722.7	< 0.05	2.45	1.84
3423.34	< 0.05	3.91	4.44
11035.48	< 0.05	0.97	0.82
12060.97	< 0.05	0.85	0.71
11213.27	< 0.05	1.02	0.86
3454.89	< 0.05	7.93	5.93
4983.7	< 0.05	5.24	8.12
4746.48	< 0.05	3.42	4.38
5764.58	< 0.05	2.36	3.2
11001.87	< 0.05	1.03	0.91
15186.74	< 0.05	0.65	0.55

**Table 7-7**  
**Significant *m/z*-species from comparison wild type vs PanIN**

<b>Mass</b>	<b>PWKW</b>	<b>Ave WT</b>	<b>Ave PanIN</b>
6645.57	< 0.000001	19.88	3.88
2812.81	< 0.000001	3.78	7.77
6683.46	< 0.000001	5.32	2.24
6189.01	< 0.000001	3.91	2.38
6604.32	< 0.000001	3.68	2.23
6310.84	< 0.000001	3.83	2.41
2790.74	< 0.000001	5.83	27.36
6273.78	< 0.000001	10.71	3.56
6222.05	< 0.000001	9.06	3.4
4334.21	< 0.000001	3.02	7.21
2829.86	< 0.000001	4	7.68
6165.7	< 0.000001	3.45	2.29
4165.53	< 0.000001	3.1	4.36
6138.83	< 0.000001	2.8	2.09
6118.58	< 0.000001	3.63	2.4
6573.03	< 0.000001	2.67	2.04
11138.83	< 0.0001	1.23	0.88
4319.57	< 0.0001	2.93	4.14
3789.22	< 0.0001	3.26	5.67
3533.02	< 0.0001	3.71	4.93
11080.49	< 0.0001	0.95	0.73
7418.34	< 0.001	1.83	3.71
4277.76	< 0.001	3.13	4.13
14000.87	< 0.001	1.98	1.06
10501.7	< 0.001	2.27	1.24
12538.25	< 0.001	0.93	0.71
4542.17	< 0.001	2.73	3.85
3576.52	< 0.001	3.36	5.28
3000.49	< 0.001	3.88	5.01
11102.36	< 0.001	0.98	0.78
6721.28	< 0.001	2.61	1.97
7219.48	< 0.001	1.94	3.69
15695.28	< 0.001	0.62	0.46
6975.7	< 0.001	2.22	1.91
5341.74	< 0.001	2.31	2.92

14395.28	< 0.001	0.69	0.52
11211.78	< 0.01	0.96	0.77
15191.66	< 0.01	0.65	0.52
3454.71	< 0.01	7.89	5.09
6549.13	< 0.01	3.01	2.52
12506.55	< 0.01	0.79	0.61
11056.61	< 0.01	1.13	0.94
10394.43	< 0.01	1.08	0.88
14973.3	< 0.01	0.79	0.62
10366.15	< 0.01	1.13	0.93
14445.38	< 0.01	0.74	0.56
3473.73	< 0.01	4.49	6.59
3428.85	< 0.01	3.93	4.75
11004.75	< 0.01	1.01	0.86
14615.2	< 0.01	0.63	0.49
14798.83	< 0.01	0.63	0.5
14314.19	< 0.01	0.73	0.56
15614.77	< 0.01	0.63	0.49
4046.56	< 0.01	3.32	4.23
14743.51	< 0.01	0.61	0.49
14845.83	< 0.01	0.58	0.46
17446.51	< 0.01	0.53	0.41
4836.38	< 0.01	5.02	3.47
17012.19	< 0.01	0.49	0.39
22155.52	< 0.01	0.43	0.36
5078.23	< 0.01	2.72	3.2
10893.48	< 0.01	0.96	0.83
5059.92	< 0.05	2.92	3.46
11537.97	< 0.05	1.01	0.85
8943.89	< 0.05	1.34	1.18
13642.93	< 0.05	0.63	0.53
16152.94	< 0.05	0.54	0.44
3513.89	< 0.05	3.78	4.57
6850.39	< 0.05	2.33	2.07
14771.67	< 0.05	0.64	0.51
17160.36	< 0.05	0.49	0.4
14931.5	< 0.05	0.65	0.51
10976.4	< 0.05	0.95	0.83

15430.26	< 0.05	0.61	0.51
3949.53	< 0.05	4.79	6.87
13697.54	< 0.05	0.73	0.63
15272.36	< 0.05	0.65	0.53
13615.66	< 0.05	0.67	0.59
20735.67	< 0.05	0.42	0.34
18586.18	< 0.05	0.45	0.38
5168.06	< 0.05	2.92	3.4
16980.38	< 0.05	0.49	0.41
21785.11	< 0.05	0.49	0.42
22075.49	< 0.05	0.43	0.35
4983.43	< 0.05	5.29	7.71
5021.31	< 0.05	3.7	4.63
11596.16	< 0.05	1.05	0.92
18667.48	< 0.05	0.48	0.4
20684.92	< 0.05	0.46	0.38
13842.09	< 0.05	0.73	0.61
10935.39	< 0.05	1.16	1.02
10872.07	< 0.05	0.9	0.82

**Table 7-8**  
**Significant *m/z*-species from comparison wild type vs Lesion (PanIN and IPMN)**

<b>Mass</b>	<b>PWKW</b>	<b>Ave WT</b>	<b>Ave Lesion</b>
6604.52	< 0.000001	3.65	2.32
6645.95	< 0.00001	19.72	4.91
6222.22	< 0.00001	9.02	3.96
6684.08	< 0.00001	5.25	2.43
4334.15	< 0.00001	3.02	5.91
6189.79	< 0.00001	3.91	2.57
6274.22	< 0.00001	10.67	4.24
6140.21	< 0.00001	2.81	2.18
2813.03	< 0.00001	3.74	6.76
4237.05	< 0.00001	3.21	4.16
2790.95	< 0.0001	5.83	22.79
4165	< 0.0001	3.11	4.09
3531.69	< 0.0001	3.72	5
6166.41	< 0.0001	3.43	2.48
3576.44	< 0.0001	3.35	4.85

6311.16	< 0.0001	3.73	2.56
6118.92	< 0.0001	3.64	2.58
4541.56	< 0.0001	2.74	3.78
14001.39	< 0.0001	1.96	1.12
3789.62	< 0.0001	3.26	5.03
4319.84	< 0.0001	2.82	3.79
2829.68	< 0.0001	4.01	6.92
3000.78	< 0.0001	4	5.02
4278.29	< 0.0001	3.16	4.08
10502.19	< 0.001	2.27	1.29
11137.94	< 0.001	1.22	0.92
11079.85	< 0.001	0.94	0.75
6572.86	< 0.001	2.66	2.17
6721.56	< 0.001	2.8	2.07
14408.88	< 0.001	0.73	0.56
14207.26	< 0.001	1.02	0.78
3454.83	< 0.01	7.88	5.22
3513.74	< 0.01	3.8	4.55
10576.87	< 0.01	1.29	0.96
7418.57	< 0.01	1.89	3.16
12537.58	< 0.01	0.98	0.77
11101.77	< 0.01	1	0.82
17455.45	< 0.01	0.59	0.45
7219.52	< 0.01	1.99	3.15
11056.67	< 0.01	1.12	0.93
13161.19	< 0.01	0.68	0.56
10391.13	< 0.01	1.09	0.91
11211.99	< 0.01	1.01	0.84
14746.9	< 0.01	0.64	0.52
15618.42	< 0.01	0.65	0.52
15654.28	< 0.01	0.6	0.48
6975.77	< 0.01	2.21	1.97
15186.81	< 0.01	0.69	0.58
3493.38	< 0.01	4.81	8.03
15696.38	< 0.01	0.66	0.52
8944.05	< 0.01	1.31	1.18
14791.57	< 0.01	0.74	0.61
11004.05	< 0.01	0.97	0.84

3425.45	< 0.01	3.95	4.55
14975.31	< 0.01	0.73	0.59
10363.87	< 0.01	1.13	0.99
24841.63	< 0.01	0.42	0.35
11236.49	< 0.05	0.9	0.79
4046.81	< 0.05	3.19	3.88
5168.19	< 0.05	2.95	3.45
3473.85	< 0.05	4.49	5.68
2850.6	< 0.05	3.73	4.55
20668.61	< 0.05	0.44	0.37
6850.77	< 0.05	2.32	2.05
13359.43	< 0.05	0.73	0.64
5078.18	< 0.05	2.72	3.15
13236.04	< 0.05	0.73	0.64
12236.23	< 0.05	0.87	0.78
13637.89	< 0.05	0.63	0.55
21880.76	< 0.05	0.54	0.46
5060.18	< 0.05	2.92	3.42
20962.1	< 0.05	0.43	0.36
4983.54	< 0.05	5.27	7.47
13405.54	< 0.05	0.75	0.66
4937.09	< 0.05	3.42	4.21
8363.86	< 0.05	1.38	1.27

**Table 7-9**  
Significant *m/z*-species from comparison PanIN vs CP

Mass	PWKW	Ave PanIN	Ave CP
2791.02	< 0.0001	27.86	3.83
6272.28	< 0.0001	3.55	16.42
4334.2	< 0.0001	7.3	2.64
2813.27	< 0.0001	7.88	3.42
2830.01	< 0.0001	7.74	3.49
4165.67	< 0.0001	4.37	2.69
4319.55	< 0.0001	4.13	2.61
4277.4	< 0.0001	4.13	2.65
11084.9	< 0.0001	0.77	1.12
6220.09	< 0.0001	3.41	10.84
6681.29	< 0.0001	2.2	5.51

6116.98	< 0.0001	2.36	4.68
6643.31	< 0.001	3.88	21.26
6309.16	< 0.001	2.38	4.48
3789.61	< 0.001	5.71	3.08
13996.35	< 0.001	0.98	2.84
4542	< 0.001	3.89	2.42
6660.91	< 0.001	2.33	4.94
8806.15	< 0.001	1.24	1.76
11172.41	< 0.001	0.84	1.14
4046.89	< 0.001	4.23	2.77
3532.03	< 0.001	4.94	3.54
11052.44	< 0.001	0.95	1.31
11214.97	< 0.001	0.79	1.08
3576.76	< 0.001	5.28	3.26
11250.51	< 0.01	0.83	1.04
7418.38	< 0.01	3.72	1.73
3427.35	< 0.01	4.74	3.44
11000.84	< 0.01	0.87	1.07
10501.61	< 0.01	1.18	2.57
3002.16	< 0.01	4.99	3.85
8976.56	< 0.01	1.18	1.66
11297.32	< 0.01	1	1.36
6700.88	< 0.01	1.86	2.8
11335.12	< 0.01	1.01	1.37
7219.33	< 0.01	3.71	1.95
7454.34	< 0.01	2.1	1.5
8941.9	< 0.01	1.19	1.6
6080.47	< 0.01	2.2	2.51
6973.63	< 0.01	1.97	2.3
6182.4	< 0.01	2.54	3.9
6139.36	< 0.01	2.06	2.8
10577.29	< 0.01	0.99	1.27
9362.89	< 0.05	1.07	1.32
6602.32	< 0.05	2.33	3.18
3345	< 0.05	3.99	4.77
5077.84	< 0.05	3.24	2.68
6093.45	< 0.05	2.14	2.49
7015.17	< 0.05	2.18	2.41

6719.67	< 0.05	1.89	2.46
12317.17	< 0.05	0.73	0.98
14966.41	< 0.05	0.6	0.94
9280.88	< 0.05	1.43	1.59
5059.8	< 0.05	3.46	2.92
5167.91	< 0.05	3.41	2.93
15111.76	< 0.05	0.53	0.69
4983.31	< 0.05	7.76	5.24
3515.11	< 0.05	4.57	3.82
14367.25	< 0.05	0.53	0.7

**Table 7-10**  
**Significant *m/z*-species from comparison IPMN vs CP**

<b>Mass</b>	<b>PWKW</b>	<b>Ave IPMN</b>	<b>Ave CP</b>
2791.04	< 0.001	18.23	3.76
6271.83	< 0.001	4.72	16.29
4333.46	< 0.001	5.02	2.64
6116.68	< 0.001	2.47	4.66
2829.99	< 0.001	5.55	3.42
3530.67	< 0.001	5.17	3.51
4277.18	< 0.001	4.11	2.59
4238.21	< 0.001	4.39	2.87
4165.44	< 0.001	4.14	2.68
2813.57	< 0.001	5.45	3.41
13995.22	< 0.001	1.04	2.83
11051.53	< 0.01	0.91	1.29
3059.16	< 0.01	4.6	3.38
3423.14	< 0.01	4.44	3.41
3002.7	< 0.01	4.99	3.84
11134.15	< 0.01	0.94	1.37
11088.57	< 0.01	0.81	1.13
6219.81	< 0.01	4.58	10.72
8804.88	< 0.01	1.27	1.73
11214.91	< 0.01	0.83	1.06
3514.68	< 0.01	4.82	3.96
6078.73	< 0.01	2.22	2.5
6681.11	< 0.01	2.46	5.49
10499.87	< 0.01	1.27	2.59



11168.02	< 0.01	0.87	1.14
6643.22	< 0.05	6.14	21.12
8976.77	< 0.05	1.23	1.68
8442.76	< 0.05	1.5	1.27
6308.82	< 0.05	2.78	4.46
6700.68	< 0.05	1.93	2.82
4766.39	< 0.05	3.24	2.63
7417.42	< 0.05	2.14	1.66
3492.74	< 0.05	8.54	5.11
6661.96	< 0.05	2.68	4.82
8940.24	< 0.05	1.22	1.58
12366.52	< 0.05	0.66	0.95
11000.56	< 0.05	0.89	1.06
4983.08	< 0.05	8.03	5.12
12120.88	< 0.05	0.88	1.32
6719.8	< 0.05	1.79	2.38
6043.95	< 0.05	2.23	2.49
12310.05	< 0.05	0.78	1.02
11296.92	< 0.05	1.13	1.36
8425.23	< 0.05	1.47	1.38

**Table 7-11**  
**Significant *m/z*-species from comparison Lesion (PanIN and IPMN) vs CP**

<b>Mass</b>	<b>PWKW</b>	<b>Ave Lesion</b>	<b>Ave CP</b>
2791.04	< 0.0001	23.22	3.79
6272.76	< 0.0001	4.31	16.37
2830	< 0.0001	7.01	3.41
2813.39	< 0.0001	6.89	3.4
4333.86	< 0.0001	5.94	2.65
4277.35	< 0.0001	4.02	2.6
4165.31	< 0.0001	4.05	2.64
4319.47	< 0.0001	3.77	2.55
6117.72	< 0.0001	2.49	4.67
4541.61	< 0.0001	3.78	2.37
13997.18	< 0.0001	1.02	2.82
3576.67	< 0.0001	4.87	3.29
3789.69	< 0.001	5.01	2.9
3531.38	< 0.001	5.02	3.53

6681.98	< 0.001	2.31	5.51
11052.15	< 0.001	0.92	1.28
6220.71	< 0.001	3.98	10.77
7418.24	< 0.001	3.1	1.72
6644.07	< 0.001	4.98	21.18
3002.57	< 0.001	4.97	3.85
11085.05	< 0.001	1	1.42
6309.73	< 0.001	2.61	4.47
88036.18	< 0.001	1.28	1.73
8976.51	< 0.001	1.22	1.67
3424.62	< 0.01	4.53	3.46
10501.11	< 0.01	1.28	2.59
11168.21	< 0.01	0.89	1.15
8941.21	< 0.01	1.22	1.58
11217.95	< 0.01	0.83	1.06
7219.14	< 0.01	3.14	1.92
6701.45	< 0.01	2	2.87
6078.38	< 0.01	2.27	2.49
10999.51	< 0.01	0.9	1.06
12363.61	< 0.01	0.68	0.95
11298.16	< 0.05	1.06	1.34
11335.3	< 0.05	1.08	1.35
10577.5	< 0.05	1.05	1.28
6974.56	< 0.05	2.04	2.28
5168.2	< 0.05	3.41	2.9
6183.57	< 0.05	2.72	3.84
5078.05	< 0.05	3.14	2.62
6602.7	< 0.05	2.46	3.2

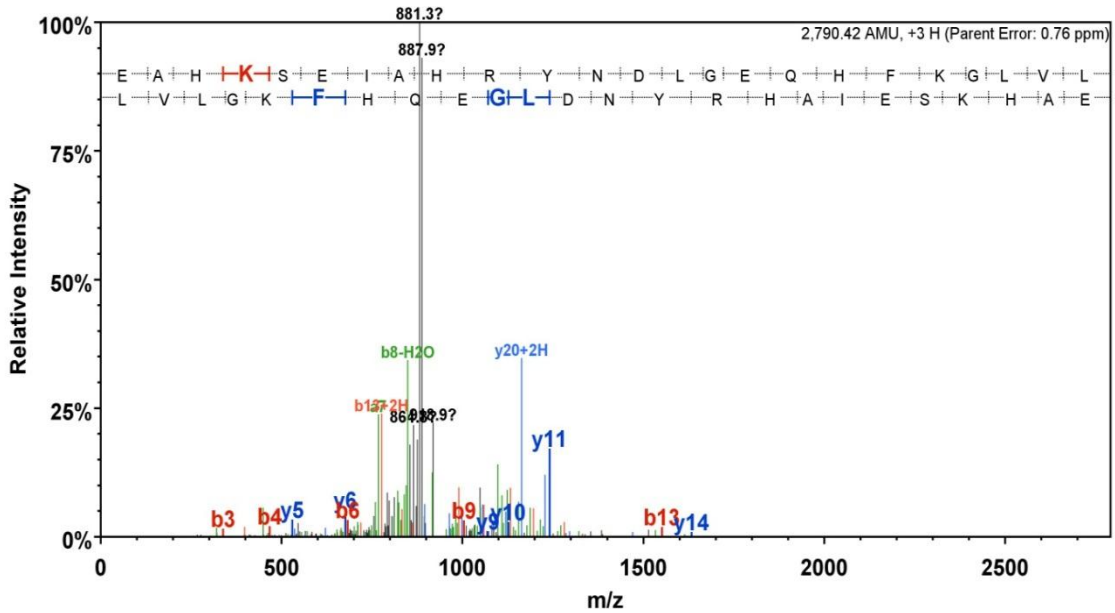
**Table 7-12**  
**Significant *m/z*-species from comparison PDAC vs CP**

<b>Mass</b>	<b>PWKW</b>	<b>Ave PDAC</b>	<b>Ave CP</b>
2791.67	< 0.01	29.37	3.75
6644.36	< 0.01	4.79	20.97
6272.81	< 0.01	4.95	16.31
2930.68	< 0.01	7.25	3.41
2813.94	< 0.01	7.18	3.4
4333.28	< 0.01	5.16	2.6

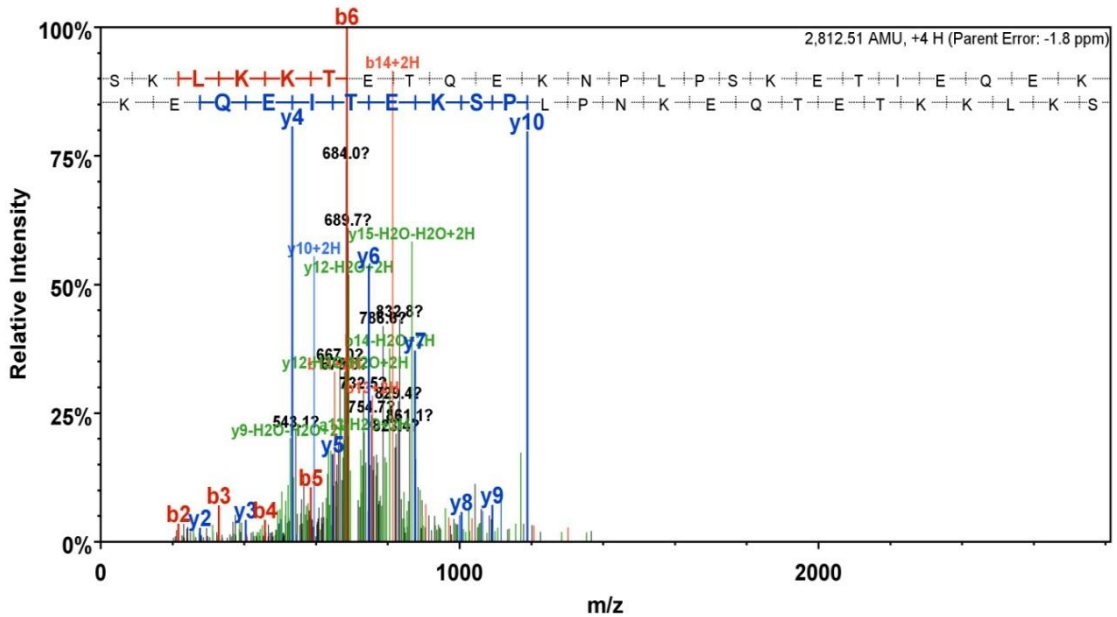
3039.5	< 0.01	5.33	3.29
4277.92	< 0.01	4.01	2.58
8806.15	< 0.01	1.12	1.68
6682.36	< 0.01	2.08	5.45
6663.38	< 0.01	2.23	4.79
3439.69	< 0.01	3.46	4.81
6702.27	< 0.01	1.75	2.82
6585.81	< 0.01	1.92	2.5
5798.16	< 0.01	2.45	14.3
4936.05	< 0.01	12.66	3.62
6220.97	< 0.01	4.62	10.72
6117.71	< 0.01	2.35	4.66
6309.92	< 0.01	2.37	4.41
4540.31	< 0.01	3.64	2.33
3324.37	< 0.01	3.55	4.76
3345.25	< 0.01	3.58	4.72
4983.42	< 0.01	13.12	5.2
6602.57	< 0.01	2.02	3.2
9957.9	< 0.05	2.85	1.27
10500.35	< 0.05	1.14	2.58
11053.19	< 0.05	0.94	1.27
11089.55	< 0.05	0.88	1.18
11169.75	< 0.05	0.86	1.12
4962.53	< 0.05	37.42	15.64
5835.08	< 0.05	2.13	5.02
5168.17	< 0.05	4.53	2.89
3002.57	< 0.05	5.02	3.81
4920.15	< 0.05	3.54	2.48
6080.27	< 0.05	2.29	2.6
5140.7	< 0.05	3.32	2.42
4737.02	< 0.05	4.9	2.6
3059.83	< 0.05	4.36	3.32
5871.12	< 0.05	1.98	2.93
6849.79	< 0.05	1.76	2.27
5059.6	< 0.05	3.94	2.87
9362.69	< 0.05	1.08	1.29
4746.32	< 0.05	6.48	3.37
2851.89	< 0.05	4.39	3.22

## 7.1.2 Annotated MS/MS spectra supporting the identification of ALB1 and TMSB4X

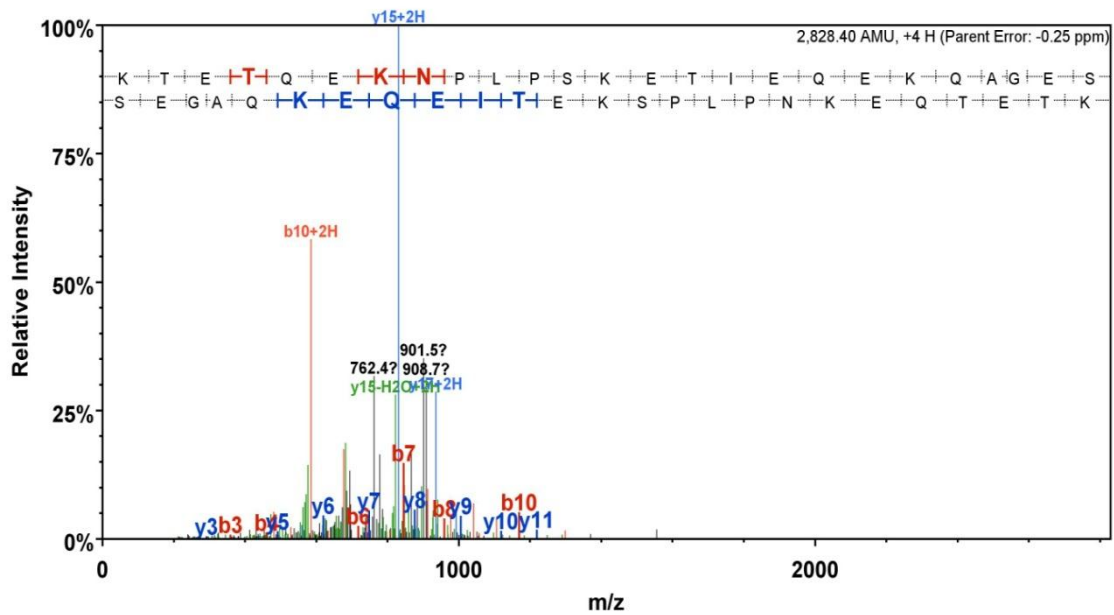
1. ALB1 EAHKSEIAHRYNDLGEQHFHFKGLVVL (parent  $m/z$  931.1487, Mascot ion score 65.2)



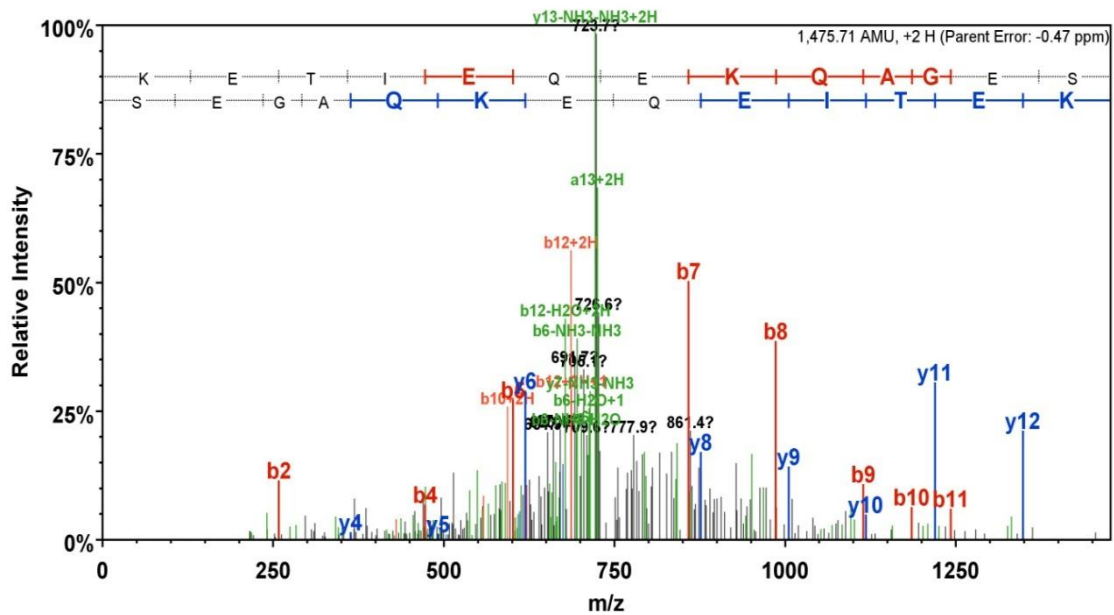
2. TMSB4X SKLKKTTETQEKNPPLPSKETEIQEK (parent  $m/z$  704.1362, Mascot ion score 32.5)



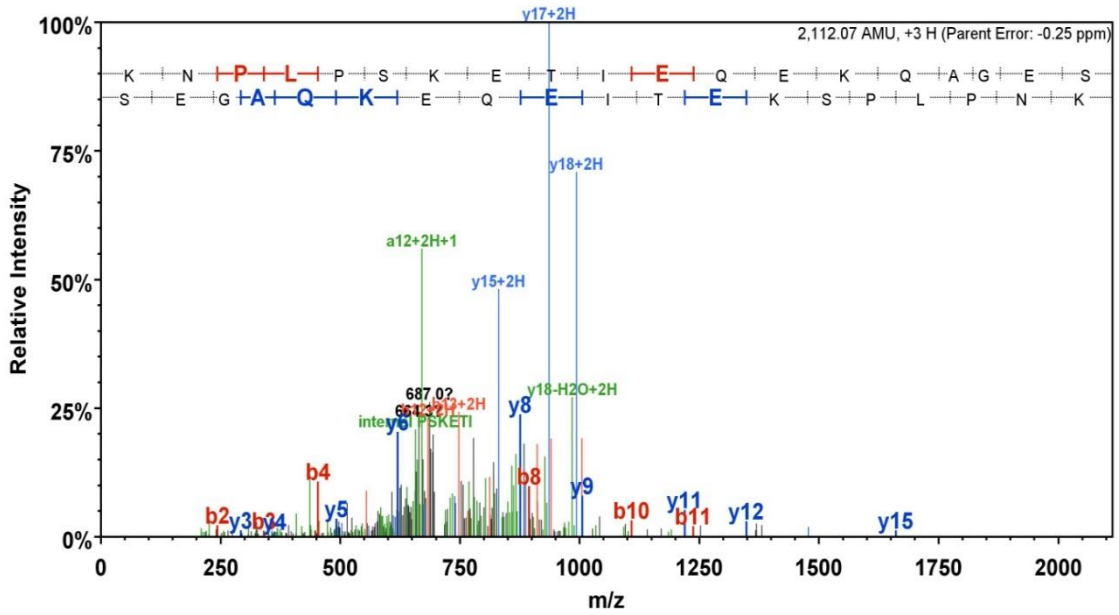
3. TMSB4X KTETQEKNPLPSKETIEQEKQAGES (parent m/z 708.1087, Mascot ion score 38.4)



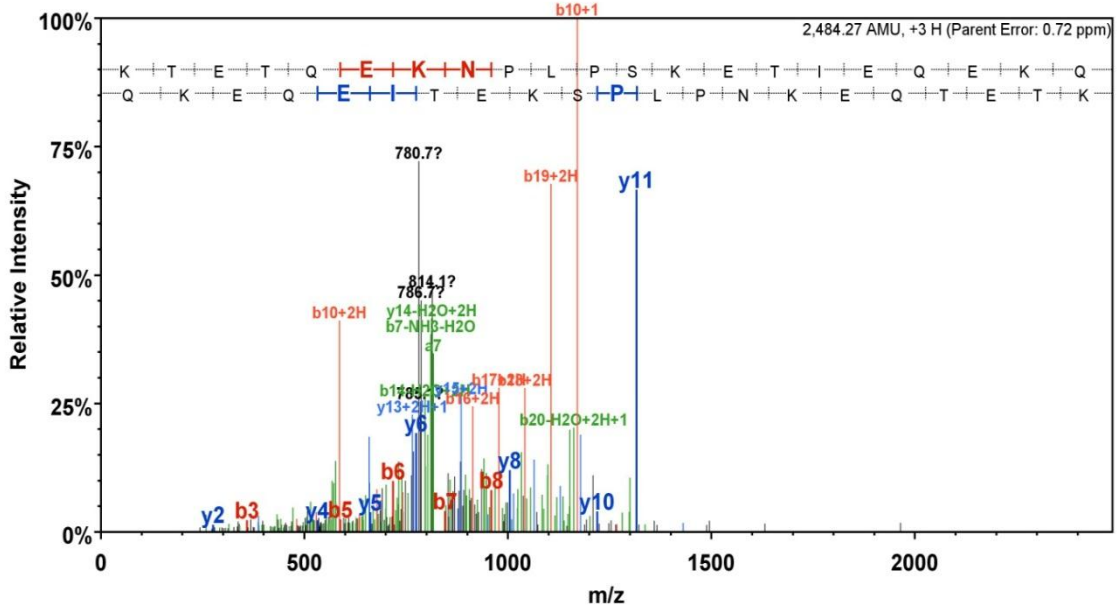
4. TMSB4X KETIEQEKQAGES (parent m/z 738.8627, Mascot ion score 47.0)



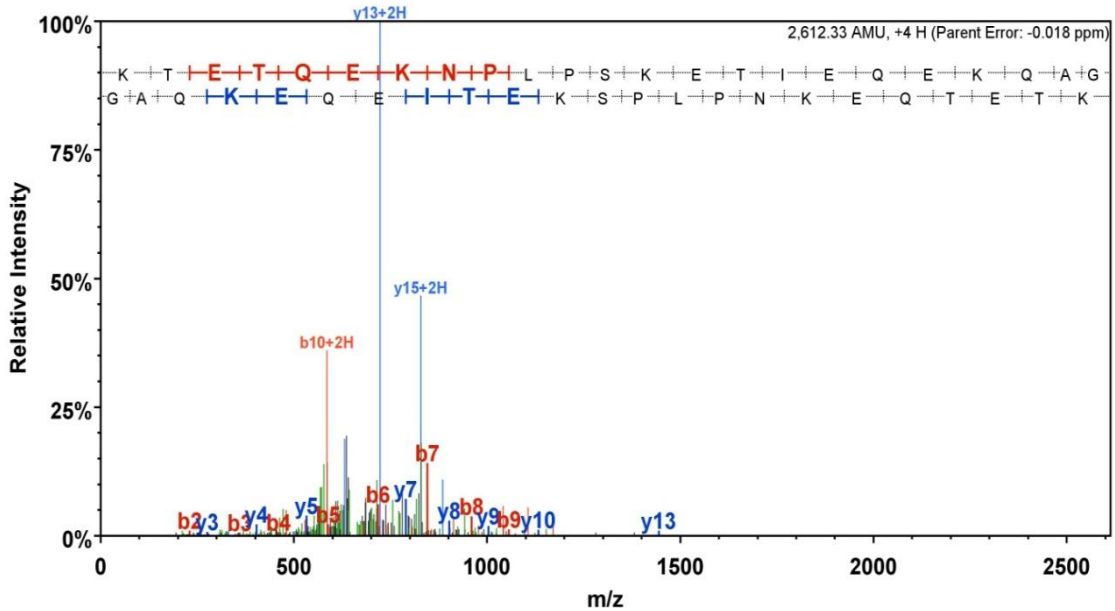
5. TMSB4X KNPLPSKETIEQEQAGES (parent m/z 705.0310, Mascot ion score 33.7)



6. TMSB4X KTETQEKNPLPSKETIEQEQ (parent m/z 829.0988, Mascot ion score 36.3)



7. TMSB4X KTETQKNPLPSKETIEQEKQAG (parent m/z 654.0902, Mascot ion score 41.1)



7.1.3 Sequence coverage of ALB1 and TMSB4X

Shaded in yellow are the identified peptide fragments in LC-MS/MS of the whole protein sequences belonging to ALB1 and TMSB4X.

IPI00131695 (91%), 68,692.9 Da  
 Serum albumin precursor  
 1 unique peptides, 1 unique spectra, 1 total spectra, 24/608 amino acids (4% coverage)

signal peptide	propeptide		
MKWVTFLLLL	FVSGSAFSRG	VFRREAHKSE	IAHRYNDLGE
FSQYLQKCSY	DEHAKLVQEV	TDFAKTCVAD	ESAANCDKSL
IPNLRENYGE	LADCCTKQEP	ERNECF LQHK	DDNPSLPPFE
FKENPTTFMG	HYLHEVARRH	PYFYAPELLY	YAEQYNEILT
CLTPKLDGVK	EKALVSSVRQ	RMKCSSMQKF	GERAFKAWAV
DFAEITKLAT	DLTKVNKECC	HGDLLLECADD	RAELAKYMCE
TCCDKPL LKK	AHCLSEVEHD	TMPADLPAIA	ADFVEDQEV
LGTFLY EYSR	RHPDYSVSL	LRLAKKYEAT	LEKCCAEANP
FQPLVEEPKN	LVKTNCDLYE	KLGEYGFQNA	ILVRYTQKAP
ARNLGRVGTK	CCTLPEDQRL	PCVEDYLSAI	LNRVCLLHEK
CSGSLVRRP	CFSALTVDET	YVPKEFKAET	FTFHSDICTL
TALAE L VKHK	PKATAEQLKT	VMDDFAQFLD	TCKKAADKDT
TRCKDALA			CFSTEGPNLV

IPI00115538 (100%), 5,679.8 Da  
 Isoform Long of Thymosin beta-4  
 3 unique peptides, 3 unique spectra, 3 total spectra, 25/50 amino acids (50% coverage)

MLLPATMSDK	PDMAEIEKFD	KSKL LK	KTETQ	EKNPLPSKET	IEQEKQAGES
------------	------------	---------	-------	------------	------------

## 8 Appendix

### 8.1 List of abbreviations

ADM	Acinar ductal metaplasia
AKT	v-akt murine thymoma viral oncogene homolog
ALB1	Albumin
bp	base pairs
CHCA	$\alpha$ -cyano-4-hydroxycinnamic acid
CK	Cytokeratin
CP	Chronic pancreatitis
Da	Dalton
EGFR	Epidermal growth factor receptor
EGF	Epidermal growth factor
ERK	Extracellular signal-related protein kinase
FFPE	Formalin-fixed, paraffin-embedded
GEM	Genetically engineered mice
H & E	Hematoxylin and eosin
IF	Immunofluorescence
IHC	Immunohistochemistry
IPMN	Intraductal papillary mucinous neoplasia
ITO	Indium-Tin-Oxide
KRAS	Kirsten-Ras
LC-MS/MS	Liquid chromatography and tandem mass spectrometry
LSL	Lox-Stop-Lox
MALDI-IMS	Matrix assisted laser desorption/ionization imaging mass spectrometry
MAPK	Mitogen activated protein kinase
MCN	Mucinous cystic neoplasia
MEK	Mitogen activated protein kinase kinase
<i>m/z</i>	mass over charge
PanIN	Pancreatic intraepithelial neoplasia



PDAC	Pancreatic ductal adenocarcinoma
PI3K	Phosphoinositid-3-Kinase
RAC1	RAS-related C3 botulinum substrate 1
RAF	Rat fibrosarcoma
RAS	Rat sarcoma
ROC	Receiver Operating Characteristics
ROI	Region of interest
RTK	Receptor tyrosine kinase
RT-PCR	Reverse transcription-Polymerase-chain reaction
SA	Sinapinic acid
SAM	Significance Analysis of Microarrays
TGFA	Transforming growth factor alpha
TMSB4X	Thymosin beta-4
WT	Wild type

## 8.2 Curriculum vitae

Name Barbara Maria Grüner  
Geburtsdatum 25. September 1983  
Geburtsort Pegnitz, Deutschland

### schulische Ausbildung

1990 – 1994 Grund- und Teilhauptschule Obertrubach  
1994 – 2003 Gymnasium Fränkische Schweiz Ebermannstadt  
Abschluss: Abitur 1,0

### Akademische Ausbildung

2003 -2008 Studium der Molekularen Medizin  
Friedrich-Alexander Universität Erlangen-Nürnberg  
Abschluss: Diplom in Molekularer Medizin 1,1  
Titel: Diplom-Molekularmedizinerin (Dipl. Mol.-Med.)  
2008 – 2012 Promotion zum Dr. rer. nat. am Klinikum rechts der Isar  
und am Wissenschaftszentrum Weihenstephan  
der Technischen Universität München  
im Rahmen der International Max Planck Research School  
for Molecular and Cellular Life Sciences (IMPRS-LS)

### Auszeichnungen und Preise

2002 Teilnahme am Ferienseminar für besonders begabte  
Gymnasiasten des Freistaates Bayern  
2003 Preis des Bayerischen Clubs für die beste Facharbeit  
Oberfrankens, verliehen im Bayerischen Landtag  
2003 – 2008 Hochbegabtenstipendium nach dem bayerischen  
Begabtenförderungsgesetz für die gesamte Studiendauer

### Konferenzen und Preise

10/2009 Tagung der Bayerischen Gesellschaft für Gastroenterologie  
- Posterpräsentation  
11/2010 Jahrestagung des Deutschen Pankreasclubs  
- Vortrag  
9/2011 AACR Conference “Frontiers in Basic Cancer Research”  
- Posterpräsentation  
- ausgewählter Vortrag

- Präsentation im Rahmen der AACR Pressekonferenz zu besonders neuen Erkenntnissen in der Tumorgrundlagenforschung
  - Reisekostenstipendium „scholar in training award“
- 11/2011 Munich Biomarker Conference
- Posterpräsentation
- 6/2012 AACR special conference „Pancreatic Cancer“
- Posterpräsentation

#### Veröffentlichungen

Falkowska-Hansen, B., J. Kollar, **B.M. Gruener**, M. Schanz, P. Boukamp, J. Siveke, A. Rethwilm, and M. Kirschner, *An inducible Tet-Off-H2B-GFP lentiviral reporter vector for detection and in vivo isolation of label-retaining cells*. Exp Cell Res, 2010. 316(11): p. 1885-95.

Mazur, P.K., **B.M. Gruener**, H. Nakhai, B. Sipos, U. Zimmer-Strobl, L.J. Strobl, F. Radtke, R.M. Schmid, and J.T. Siveke, *Identification of epidermal Pdx1 expression discloses different roles of Notch1 and Notch2 in murine Kras(G12D)-induced skin carcinogenesis in vivo*. PLoS One, 2010. 5(10): p. e13578.

**Gruener B.M.**, H. Hahne, P.K. Mazur, M. Trajkovic-Arsic, S. Maier, I. Esposito, C.W. Michalski, J. Kleeff, S. Rauser, R.M. Schmid, B. Kuester, A. Walch, and J.T. Siveke, *MALDI imaging mass spectrometry for in situ proteomic analysis of preneoplastic lesions in pancreatic cancer*. PLoS One, 2012;7(6):e39424. Epub 2012 Jun 26

Ardito C.M\*., **B.M. Gruener\***, C. Lubeseder-Martellato, K.K. Takeuchi, K.E. DelGiorno, E.S. Carpenter, C.J. Halbrook, D. Pal, J.C. Hall, P.K. Mazur, T. Briel, A. Herner, D.W. Threadgill, M. Sibilica, M.K. Washington, C.L. Wilson, R.M. Schmid, E.W. Raines, H.C. Crawford, and J.T. Siveke, *EGF Receptor is Required for Kras-induced Pancreatic Tumorigenesis*. Cancer Cell 2012, <http://dx.doi.org/10.1016/j.ccr.2012.07.024>

*\*both authors contributed equally to this work*

### **8.3 Acknowledgements - Danksagungen**

Mein besonderer Dank gilt Prof. Michael Schemann für die bereitwillige und hilfreiche Betreuung der Doktorarbeit am Wissenschaftszentrum Weihenstephan.

Bei Dr. Jens Siveke möchte ich mich ganz besonders herzlich für die Möglichkeit zu dieser Arbeit, die gute, verständnisvolle, motivierende und diskussionsfreudige Betreuung und die großartige Unterstützung während meiner Doktorarbeit bedanken.

Vielen Dank an die Mitglieder meines Thesis Advisory Committees Prof. Roland Schmid, Prof. Christoph Turck und Prof. Axel Walch für ihre Zeit und Mühe und die sehr hilfreichen Diskussionsbeiträge und Versuchsvorschläge. Bei Prof. Schmid möchte ich mich außerdem dafür bedanken, dass er mir die Teilnahme an der AACR Conference Pancreatic Cancer ermöglicht hat und für die netten Ausflüge zum Skifahren und Oktoberfest.

Mein großer Dank geht an die International Max Planck Research School for Molecular and Cellular Life Sciences (IMPRS-LS), in deren Rahmen ich diese Doktorarbeit machen konnte. Vielen Dank an das Coordination Office Dr. Hans-Jörg Schäffer, Dr. Ingrid Wolf und Maximiliane Reif für ihre Unterstützung und große Einsatzbereitschaft.

Bei Prof. Axel Walch und seiner Arbeitsgruppe möchte ich mich für die gute Zusammenarbeit und Hilfe beim Erlernen der MALDI IMS Methode bedanken, vor allem auch bei Benjamin Balluff, Mareike Elsner, Claudia-Mareike Pflüger und Stephan Meding für ihre bereitwillige und freundschaftliche Unterstützung.

Mein Dank gilt Prof. Bernhard Küster, Hannes Hahne und Stefan Meier für die Hilfe und Zusammenarbeit bei der Peptididentifikation.

Ganz herzlich möchte ich mich bei meiner gesamten Arbeitsgruppe bedanken. Pawel, Irina, Clara, Roxanne, Vicky, Marija, Mathilde, Silke, Thomas, Tobias, Nicole, Florian, Alex, Marcel und Katharina, und auch Patrick und Karen aus der Nachbargruppe, vielen Dank für die vielen netten Stunden im und außerhalb des Labors und für eure Unterstützung und Hilfe. Vor allem bei Pawel und Clara möchte ich mich für ihre bereitwillige Unterstützung und für die vielen hilfreichen Diskussionen bedanken.

Vor allem möchte ich mich bei meiner Familie bedanken: Bei meiner großen Schwester Kathrin, die mich immer unterstützt, bei meiner Oma für ihre wunderbare Fürsorge und bei meinen Eltern für ihre immerwährende liebevolle Unterstützung und Motivation. Danke Mama und Papa, dass ihr immer für mich da seid, mich liebt und an mich glaubt.